Synchronization Techniques for Femtocell Networks

Jinlin Peng

Submitted in accordance with the requirements for the degree of Doctor of Philosophy

THE UNIVERSITY OF LEEDS

SCHOOL OF ELECTRONIC AND ELECTRICAL ENGINEERING

September 2013

The candidate confirms that the work submitted is his own and appropriate references have been given to the work of others

Dedicated to my wife Yanqiong, my son Yibo, my Mom and Dad.

Contents

Acknowledgments **1**

Abstract **3**

List of Figures **8**

List of Tables **9**

Abbreviations **10**

1 Introduction **13**

1.1 Introduction to Femtocells 13

1.1.1 Why Femtocells? 13

1.1.2 What is a Femtocell? 15

1.1.3 Femtocell Attributes 17

1.1.4 Femtocell Applications 19

1.1.5 Benefits from Femtocell 20

1.1.6 Technical Challenges 23

1.2 Research Objectives 27

1.3 Major Contribution 28

1.4 Thesis Organization 30

1.5 List of Publications 32

2 Time Synchronization for Femtocells 34

2.1 Reasons for Femtocell Synchronization 34

2.2 Strict Accuracy Requirements Meet Stringent Cost Limits 37

2.3 Overview of Synchronization Methods for Femtocells 38

2.3.1 GPS 40

2.3.2 Synchronization via TV signals 41

2.3.3 Packet Timing via Backhaul 42

2.3.4 Neighbouring Cells Listening 44

2.4 Summary 46

3 An Improved IEEE 1588 Time Synchronization Scheme 48

3.1 Introduction 48

3.2 System Model 50

3.2.1 Femtocell IEEE 1588 Synchronization Scenario 50

3.2.2 Clock Model 50

3.3 Basic Mechanism of IEEE 1588 51

3.4 Related Works 54

3.4.1 An Enhanced IEEE 1588 with Buffering Time Control 54

3.4.2 IEEE 1588 Clock Synchronization Using Dual Slave Clocks in a Slave 55

3.4.3 An Enhanced IEEE 1588 using Block Burst Transmission 56

3.5 An Improved IEEE 1588 Scheme and Clock Offset Estimation 58

3.5.1 Clock Offset (ϕ) Estimation with a Gaussian Delay Model 61

3.5.2 Clock Offset (ϕ) Estimation with Exponential Delay Model . . . 63

3.5.3 Mean Squared Error Analysis 66

3.6 Performance Evaluation 69

3.7 Summary 71

4 Variable-Length IEEE 1588 Time Synchronization Scheme 73

4.1 Introduction . . . 73

4.2 Main Idea . . . 75

4.3 Clock Offset Estimation with No Clock Skew . . . 77

4.3.1 Clock Offset Estimation ($\hat{\phi}$) for Gaussian Delay Model . . . 77

4.3.2 Clock Offset Estimation ($\hat{\phi}$) for Exponential Delay Model . . . 79

4.3.3 Parameter Optimization . . . 81

4.3.4 Synchronization Performance Evaluation . . . 84

4.4 Multiple Linear Regression Based Clock Offset and Clock Skew Estimation 86

4.4.1 Normal Linear Regression Based Estimation . . . 88

4.4.2 Multiple Linear Regression Based Estimation . . . 91

4.4.3 Parameter Optimization . . . 94

4.4.4 Performance Evaluation . . . 97

4.5 Summary . . . 101

5 Receiver-Receiver Synchronization for Femtocells 103

5.1 Introduction . . . 103

5.2 Receiver-Receiver Synchronization for Wireless Networks . . . 104

5.2.1 Introduction to Wireless Sensor Network Synchronization . . . 104

5.2.2 Receiver-Receiver Synchronization . . . 106

5.2.3 Disadvantages of RBS . . . 108

5.3 Scheme 1: MS-Assisted Receiver-Receiver Synchronization for femtocells 109

5.3.1 Synchronization Scenario . . . 109

5.3.2 Proposed Scheme . . . 110

5.4 Scheme 2: A Novel RRS based scheme for femtocell networks . . . 112

5.4.1 Synchronization Scenario . . . 112

5.4.2 Proposed Scheme . . . 113

5.4.3 Performance Analysis 116
5.5 Simulation Results 117
5.6 Summary 118

6 A Hybrid Synchronization Scheme Based on Wireless IEEE 1588 and Receiver-Receiver Synchronization 120

6.1 Introduction 120
6.2 Synchronization Scenario 122
6.3 Hybrid Wireless IEEE 1588 and Receiver-Receiver Synchronization . . . 123
6.3.1 Conventional Wireless IEEE 1588 123
6.3.2 The Hybrid Synchronization Scheme Based on Wireless IEEE 1588 and RRS 125
6.4 Number of Transmitted Timing Messages 130
6.5 Robustness Study 134
6.6 Synchronization Accuracy 136
6.7 Summary 138

7 Dual Sources Synchronization for Femtocells 139

7.1 Introduction 139
7.2 Synchronization Scenario 141
7.3 A Two-Step Weighted Multiple Linear Regression Based Synchronization Scheme for Femtocells 142
7.3.1 Step 1: Normal Linear Regression Based Coarse Synchronization and Noise Variance Estimation 143
7.3.2 Step 2: Weighted Multiple Linear Regression Based Fine Synchronization 145
7.4 Performance Evaluation 148

7.5 Summary 151

8 Conclusions and Future Work **154**

8.1 Conclusions 154

8.2 Future Work 157

Bibliography **159**

Acknowledgments

To begin with, I would like to sincerely thank my first supervisor Dr. Li Zhang for her continuous support in my PhD course and during my life in UK. Her patient and professional guidance has really helped me in my research and writing up this thesis. She also offers me so much help in my daily life, especially when I was new to this country. For me, she is not only a wonderful supervisor for my research, but also a sincere friend.

I would like to express my gratitude to my second supervisor Dr. Des McLernon for always helping me with any problems in my research and encouraging me. I would also like to express my thanks to Pengfei, Ray, Chinazo, and other friends and colleagues at the School of Electronic and Electrical Engineering for making my time here one of the most memorable experience.

I would also like to thank my dear friends in Leeds: Bing, Daowei, Jihui, Yangwen, Pengfei, Faith and the many more who made my life in Leeds much more colourful.

Finally, I would like to thank the four most important people in my life: my wife Yanqiong, my son Yibo and my Mom and Dad. Their honest love and unconditional support gives me the most powerful motivation to finish both my PhD course and this thesis. They are all the best treasure that I could have in this world.

Abstract

Femtocells are small, low-cost and low-power cellular base stations optimized for providing wireless voice and broadband services to customers in a relatively small area. Femtocells are considered to be one of the most promising solutions for future wireless communication with all the advantages that they bring, such as better indoor coverage, higher spectrum efficiency and lower energy consumption to name but a few.

However time synchronization for femtocells is very challenging. Femtocells are expected to be equipped with cheap and less accurate crystal oscillators, which cannot satisfy the femtocell synchronization requirements. Moreover, femtocells are deployed in a variety of scenarios with different synchronization requirements and so different synchronization solutions are needed. Existing solutions for some of the femtocell synchronization scenarios either are unsuitable for that particular scenario or suffer serious performance degradation. Therefore, this thesis is focused on investigating the time synchronization problem for femtocells and proposing novel synchronization schemes.

This thesis mainly investigated two femtocell synchronization methods: synchronization via backhaul and synchronization via neighbouring cells listening. Femtocell synchronization using the IEEE 1588 protocol, which is seen as the major solution for femtocell synchronization via backhaul, suffers from both asymmetric and random delay problems. An 'improved IEEE 1588' scheme is firstly proposed, which utilizes additional packets with different sizes in every IEEE 1588 synchronization process to solve both of these problems. Although the simulation results show that the 'improved IEEE 1588'

scheme successfully overcomes both aforementioned limitations and yields much better synchronization accuracy than the conventional scheme, it also brings an additional undesirable overhead. Therefore, this thesis also presented a 'variable-length IEEE 1588' scheme, where the length of transmitted packets varies periodically. Simulation results show that the synchronization accuracy of the 'variable-length IEEE 1588' scheme is similar to the 'improved IEEE 1588' scheme but with the advantage of a significantly reduced number of transmitted messages.

For femtocell synchronization via neighbouring cells listening, listening to other synchronized femtocells is an important approach, especially for femtocells in SOHO (Small Office and Home Office) area where the femtocells overlap with each other and then form a wireless femtocell network. This thesis carefully examines the time synchronization in wireless femtocell networks. First, the receiver-receiver synchronization (RRS), which has proved efficient in WSNs (wireless sensor networks), is applied in wireless femtocell networks. Two new RRS based synchronization schemes are proposed for different scenarios to ensure better availability. Second, a hybrid synchronization scheme based on wireless IEEE 1588 and RRS is proposed for wireless femtocell networks. The synchronization accuracy and robustness of this hybrid scheme are then evaluated through simulations.

Finally, the synchronization scenario where the femtocell is connected to more than one synchronization sources is studied. The basic solution for this scenario is to simply select the best synchronization source when it is available. A two-step weighted multiple linear regression (WMLR) based synchronization scheme is proposed for this case, and it is proved via simulations that it provides better synchronization accuracy and better stability than the basic solution, especially when the two synchronization sources are comparable.

List of Figures

1.1 Traffic demand in North America [10]. 14

1.2 Typical femtocell deployment scenario [7]. 16

1.3 Examples of four stand-alone femtocells, manufactured by Samsung, Ubiqusys and Nokia Siemens Networks. 17

1.4 Femtocell market status [7]. 19

1.5 Femtocells help increase capacity and offload traffic from macrocells [8]. 21

1.6 A femtocell spectrum reuse scenario. 22

1.7 Cross-tier interference in a Macro/Femto scenario [10]. 24

2.1 Phase synchronization and frequency synchronization for the femtocell. . 35

2.2 Major Synchronization Sources for Femtocells [41]. 39

2.3 Femtocell synchronization using TV+GPS signals [45]. 42

2.4 IEEE 1588 Master-Slave hierarchy [46]. 43

3.1 Femtocell IEEE 1588 synchronization scenario. 50

3.2 IEEE 1588 PTP messaging timing diagram. 52

3.3 Enhanced IEEE 1588 with buffering time control [48]. 55

3.4 Schematic for the dual clocks generation [49]. 56

3.5 Block burst transmission for the asymmetric ratio calculation [56]. 57

3.6 The improved IEEE 1588 synchronization scheme. 59

3.7 MSEs of both MLEs in a Gaussian random delay environment ($\sigma = 1\mu s, \alpha = 2$). 67
3.8 MSEs of both MLEs in an exponential random delay environment ($\lambda = 1\mu s, \alpha = 2$). 68
3.9 MSEs of both MLEs of clock offset as a function of the packet length ratio α ($\sigma = 1\mu s$, $\lambda = 1\mu s$, $N = 10$). 69
3.10 Bias errors of the slave clock for different synchronization schemes as a function of the asymmetric ratio in a Gaussian random delay model ($\mu = 100\mu s$, $\sigma = 20\mu s$, $\alpha = 23.7$). 70
3.11 Bias errors of the slave clock for different synchronization schemes as a function of the asymmetric ratio in an exponential random delay model ($\lambda = 100\mu s$, $\alpha = 23.7$). 71

4.1 Comparison between conventional IEEE 1588 and the 'variable-length IEEE 1588' scheme. 76
4.2 Set Θ and the point (d,ϕ) that maximizes (4.21) and (4.22). 81
4.3 MSEs of the two estimators of clock offset ($\hat{\phi}$) as a function of the packet length ratio α ($\sigma = 1$, $\lambda = 1$, $N = 10$). 84
4.4 RMSEs of the slave clock offset estimate ($\hat{\phi}$) for different synchronization schemes as a function of asymmetric ratio with a Gaussian random delay model ($\mu = 100\mu s$, $\sigma = 20\mu s$, $N = 100$, $\alpha = 23.7$, $\beta = 24.7$). 85
4.5 RMSEs of the slave clock offset estimate ($\hat{\phi}$) for different synchronization schemes as a function of asymmetric ratio with an exponential random delay model ($\lambda = 100\mu s$, $N = 100$, $\alpha = 23.7$, $\beta = 9.25$). 86
4.6 Normal linear regression vs. the proposed multiple linear regression. . . . 94
4.7 RMSEs of proposed estimator for d_{asym} versus the number of synchronization processes (N) in variable length IEEE 1588. 98

4.8 MSEs of (4.70), (4.71) and (4.72) against the value of α in variable length IEEE 1588. 99

4.9 MSEs of (4.70), (4.71) and (4.72) against the value of β ($2 \leq \beta \leq 20$) in variable length IEEE 1588. 100

4.10 RMSEs of the slave clock for different synchronization schemes as a function of asymmetric ratio, with Gaussian random delay models (μ_1, σ_1^2) and (μ_2, σ_2^2). 101

5.1 Packet delay components. 105

5.2 The *b*th message exchange process in RBS. 106

5.3 Critical path comparison. In sender-receiver synchronization, 'critical path' contains all four parts of the packet delay components. In RBS, the Send Time and Access Time are eliminated from 'critical path'. . . . 108

5.4 MS-assisted femtocell synchronization scenario. 109

5.5 The *i*th synchronization process of Scheme 1. 110

5.6 Wireless femtocell network synchronization scenario. 113

5.7 The *i*th synchronization process of Scheme 2. 114

5.8 Average clock offset for RBS in a Macrocell after N synchronization processes. 118

5.9 Average clock offset after N synchronization processes in Scheme 1, parameterized on different receive time standard deviations. 119

5.10 Average clock offset after N synchronization processes in Scheme 2, parameterized on different receive time standard deviations. 119

6.1 The femtocell wireless network synchronization scenario. 122

6.2 Message exchanging of the conventional wireless IEEE 1588 in the *i*th synchronization cycle. 123

6.3 Message exchanging of the proposed hybrid scheme in the *i*th synchronization cycle. 126

6.4 Comparison of the required synchronization cycles (per femtocell) for the proposed hybrid scheme and the conventional wireless IEEE 1588 with $R1 = 1$, $R2 = 2$, $P1 = 0.95$, $P2 = 0.99$. 133

6.5 Comparison of the overall required synchronization messages for the proposed hybrid scheme and the conventional wireless IEEE 1588 with $R1 = 1$, $R2 = 2$, $P1 = 0.95$, $P2 = 0.99$. 134

6.6 Robustness comparison between different schemes in terms of the synchronization failure rate vs. packet loss rate (from 0 to 0.5) with $M = 2$ and $M = 16$. 136

6.7 RMSEs of the clock offset estimations of the proposed hybrid scheme in comparison with the conventional wireless IEEE 1588. 137

6.8 RMSEs of the clock skew estimations of the proposed hybrid scheme in comparison with the conventional wireless IEEE 1588. 138

7.1 Dual Synchronization Sources Scenario. 141

7.2 Flow chart of the proposed two-step WMLR based synchronization scheme. 147

7.3 Comparison of the RMSEs of the clock offset estimations. 149

7.4 Comparison of the RMSEs of the clock skew estimations. 150

7.5 Comparison of the RMSEs of the asymmetric error estimations. 151

7.6 The impact of the observation noise variance ratio ($\frac{\sigma_A^2}{\sigma_B^2}$) on the performance of WMLR in terms of the RMSEs of the clock skew estimation of different methods. 152

7.7 The impact of the observation number ratio ($\frac{N_A}{N_B}$) on the performance of WMLR in terms of the RMSEs of the clock skew estimation of different methods. 153

List of Tables

2.1 Clock Accuracy Requirements [2]. 37

2.2 Types of Crystal Oscillators [40]. 38

2.3 Four Major Single-source Femtocell Synchronization Methods. 47

6.1 Number of Required Timing Messages for the Three Schemes for the Scenario in Fig. 6.1. 131

Abbreviations

3GPP	**3**rd **G**eneration **P**artnership **P**roject
ADSL	**A**symmetric **D**igital **S**ubscriber **L**ine
AGPS	**A**ssisted **G**lobal **P**ositioning **S**ystem
BS	**B**ase **S**tation
CCI	**C**o-**C**hannel **I**nterference
CDMA	**C**ode **D**ivision **M**ultiple **A**ccess
CRLB	**C**ramér–**R**ao **L**ower **B**ound
DoS	**D**enial of **S**ervice
DSL	**D**igital **S**ubscriber **L**ine
FDD	**F**requency-**D**ivision **D**uplexing
FR	**F**ailure **R**ate
FTSP	**F**looding **T**ime **S**ynchronization **P**rotocol
GPS	**G**lobal **P**ositioning **S**ystem
GSM	**G**lobal **S**ystem of **M**obile communication
HNB	**H**ome **N**ode**B**
ICI	**I**nter-**C**arrier **I**nterference
IEEE	**I**nstitute of **E**lectrical and **E**lectronics **E**ngineers
ISI	**I**nter-**S**ymbol **I**nterference
LAN	**L**ocal **A**rea **N**etwork
LR	**L**inear **R**egression

LTE	**L**ong **T**erm **E**volution
MLE	**M**aximum **L**ikelihood **E**stimator
MLR	**M**ultiple **L**inear **R**egression
MS	**M**obile **S**tation
MSE	**M**ean **S**quared **E**rror
NLR	**N**ormal **L**inear **R**egression
NTP	**N**etwork **T**ime **P**rotocol
OCXO	**O**ven-**C**ontrolled **C**rystal **O**scillator
OFDM	**O**rthogonal **F**requency-**D**ivision **M**ultiplexing
PBS	**P**airwise **B**roadcast **S**ynchronization
PBX	**P**rivate **B**ranch e**X**change
PLR	**P**acket **L**oss **R**ate
PTP	**P**recision **T**ime **P**rotocol
RBS	**R**eference **B**roadcast **S**ynchronization
RMSE	**R**oot **M**ean **S**quared **E**rror
RRS	**R**eceiver-**R**eceiver **S**ynchronization
RSS	**R**eceived **S**ignal **S**trength
RTT	**R**ound **T**rip **T**ime
SOHO	**S**mall **O**ffice/**H**ome **O**ffice
SON	**S**elf-**O**rganizing **N**etwork
TCXO	**T**emperature-**C**ompensated **C**rystal **O**scillator
TDD	**T**ime-**D**ivision **D**uplexing
TDOA	**T**ime **D**ifference of **A**rrival
TD-SCDMA	**T**ime **D**ivision **S**ynchronous **C**ode **D**ivision **M**ultiple **A**ccess
TOA	**T**ime of **A**rrival
TPSN	**T**iming-sync **P**rotocol for **S**ensor **N**etworks
Tx/Rx	**T**ransmit/**R**eceive

UMTS **U**niversal **M**obile **T**elecommunications **S**ystem

VDSL **V**ery-high-bit-rate **D**igital **S**ubscriber **L**ine

WAN **W**ide **A**rea **N**etwork

WCDMA **W**ideband **C**ode **D**ivision **M**ultiple **A**ccess

WiMAX **W**orldwide **I**nteroperability for **M**icrowave **A**ccess

WMLR **W**eighted **M**ultiple **L**inear **R**egression

WSN **W**ireless **S**ensor **N**etwork

1 Introduction

1.1 Introduction to Femtocells

1.1.1 Why Femtocells?

The demand for higher data rates in cellular networks is unrelenting. A recent study shows that the amount of global mobile data traffic nearly tripled for the third year in a row in 2010, and exceeded the traffic on the entire global Internet in 2000 [1]. Nearly one billion people are expected to access the Internet exclusively through a mobile wireless device by the year 2015 [1]. The network traffic increase for North America from 2007 to 2020 is shown in Fig. 1.1. Obviously, the traffic is predicted to grow exponentially over many years with wireless data increasing the most rapidly.

It is estimated that two thirds of calls and over 90% of data services occur indoors [2]. So it is extremely important for cellular operators to provide good indoor coverage for both voice and high speed data services. Traditional voice networks are designed to tolerate low signal quality, since the required data rate for voice signals is only on the order of 10 kbps or even less [3]. Data networks, on the other hand, require much higher signal quality in order to provide multimegabit per second data rates. However for indoor cellular services, especially at higher carrier frequencies that is often deployed in many wireless broadband systems, attenuation losses will make it difficult to achieve high data rates. This is evidenced by some surveys, which show that 45% of households and 30%

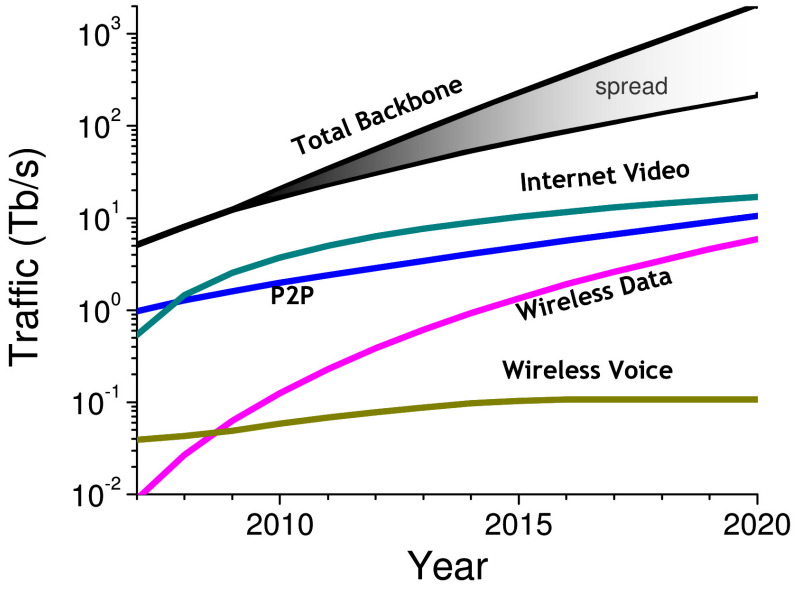

Figure 1.1: Traffic demand in North America [10].

of businesses [4] experience poor indoor coverage problem.

To meet this data services demand, in particular indoor coverage, the traditional approach of deploying more outdoor macrocells is not desirable, especially since the deployment of macrocells is becoming increasingly expensive and challenging, particularly in densely populated areas. In addition, as many of 3G and beyond networks work at 2 GHz or above, the building penetration is also a big challenge for the network performance.

Wi-Fi is now the most popular technology for the indoor wireless network. It provides the indoor data service to consumers at a low price. However, femtocells offer a number of potential advantages when compared with Wi-Fi. Femtocells are a natural extension of the main cellular network, thus allowing them to support most of the current services provided by the mobile operator. The wireless interface and control functions in femtocells are identical to that of the cellular network, thus allowing seamless roaming without any change to the phone. Femtocells also enhance voice coverage while Wi-Fi generally does not.

In addition, out of all the cellular network optimizations techniques, including higher order modulation, improved multiple access (in both time and frequency), more powerful error correction codes, cell size reduction and more, it is believed that reducing the inter-cell site distance is the most efficient solution. By breaking down the millionfold wireless capacity increase since 1957, studies show a 25× improvement from a wider spectrum, a 5× improvement by dividing the spectrum into smaller slices, a 5× improvement by designing better modulation schemes, and an enormous 1600× gain through reduced cell sizes and transmit distances, which arises from efficient spatial reuse of spectrum or higher area spectral efficiency [5]. It is thus predicted that the short-range femtocells can effectively improve the wireless capacity.

Therefore the short-range low-cost low-power base stations – femtocells, which deliver high-quality services to users both at home and at work, including reliable coverage and high data rates, while reducing the cost of deployment, arise as the solution to the aforementioned increasing capacity demand and the poor indoor coverage problem.

1.1.2 What is a Femtocell?

A femtocell is a low-power access point, based on mobile technology, providing wireless voice and broadband services to customers in a relatively small area. A femtocell usually connects to the mobile operator's network via a standard consumer broadband connection, such as a digital subscriber line (DSL), cable or wireless last-mile technologies. Fig. 1.2 shows a typical femtocell deployment scenario.

As can be seen in Fig. 1.2, a single femtocell can deliver voice and data services to several users simultaneously. Data from multiple femtocells are gathered together in a gateway, managed by the mobile operator, and then transmitted to the operator core network. The operator core network also provides services to the femtocell, ensuring that the services experienced by the user are secure and of high quality.

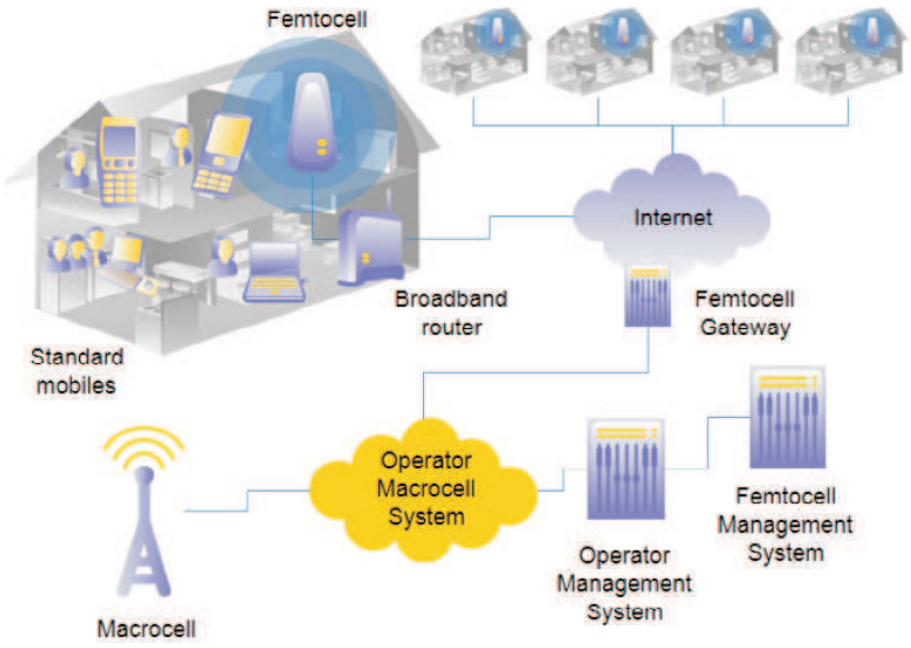

Figure 1.2: Typical femtocell deployment scenario [7].

The first interest in femtocells started around 2002 when a group of engineers at Motorola were investigating possible new applications and later Motorola announced the first 3G-based home base station product. Later in 2004, the idea began to gain some momentum and a variety of companies were looking into the idea. In particular two new companies, Ubiquisys and 3WayNetworks were formed in the UK focusing on the technology of femtocells. With this idea gaining momentum, many more companies started their business developing femtocell technology. The Femto Forum (www.femtoforum.org) was set up in July 2007 and its aim was to promote femtocell standardization and deployment worldwide. In 2008, Home NodeB (HNB) and Home eNodeB (HeNB) were first introduced in the 3rd Generation Partnership Project (3GPP) Release 8, indicating that it had become a mainstream wireless access technology. Recently, with the spread of a broader name called 'Small Cell' which includes femtocell as a subset, Femto Forum changed its name to Small Cell Forum [6].

In practice, the femtocell may be either a stand-alone device (Fig. 1.3), which connects

into the customer's existing broadband router, or it may form a key component of a home gateway device which incorporates the router and other technologies, such as a broadband modem, Internet router and Wi-Fi access point into a single integrated device.

Figure 1.3: Examples of four stand-alone femtocells, manufactured by Samsung, Ubiqusys and Nokia Siemens Networks.

1.1.3 Femtocell Attributes

The Small Cell Forum indicates the following seven key attributes of femtocells [7]. In other words, a femtocell should incorporate all of the following attributes, which differentiate a femtocell from other similar wireless access technologies, such as Wi-Fi access points, repeaters, or cordless telephones:

- **Using mobile technology:** Femtocells use fully standard wireless protocols over the air to communicate with standard mobile devices, such as mobile phones, mobile-enabled tablets and laptops. They use existing telecommunication standard protocols, such as GSM, WCDMA, CDMA, LTE, WiMAX and other current and future

protocols standardized by 3GPP, 3GPP2 and IEEE. This distinguishes femtocells from Wi-Fi access points, which implement Wi-Fi standards such as IEEE 802.11b, 802.11g, and 802.11n.

- **Operating in licensed spectrum:** A femtocell is operated only in the spectrum that is licensed by the service provider. This is also different from Wi-Fi access points, which operate in the unlicensed spectrum.

- **Generating coverage and capacity:** Femtocells are designed to provide improved coverage for a relatively small area, like home or office, and improve network capacity by serving users with high data-rate services. This is one of the main differences between femtocells and 'repeaters' which usually only improve the coverage.

- **Over internet-grade backhaul:** Femtocells transmit data to the service provider over internet-grade broadband backhaul, including DSL, cable or wireless last-mile technologies.

- **Cost effective:** Compared with the huge construction price of macrocells, femtocells can provide coverage, especially to indoor end users, in a cost effective way. In addition, femtocells can provide significant power saving to end users, and hence longer battery life due to the short transmission distance between the user and the basestation.

- **Self-organizing and self-managing:** Femtocells are designed to be plug-and-play. They set themselves up to operate with high performance according to the local and network-wide conditions on radio, regulatory and operator policies, with no need for intervention by the customer or operator.

- **Control maintained by licensed operators:** Femtocells only operate with the parameters set by the licensed operator. While they have a high degree of intelligence

to automatically ensure that they operate at power levels and frequencies which are unlikely to create interference, the limits on these parameters are always set by operators, and not by the end user. The operator has the right to create or deny the service to an individual femtocell. This control is maintained no matter whether the femtocell is owned by the operator or the end user.

1.1.4 Femtocell Applications

Femtocell applications can be divided into the following categories: residential use, enterprise use and operator use, as demonstrated by Fig. 1.4.

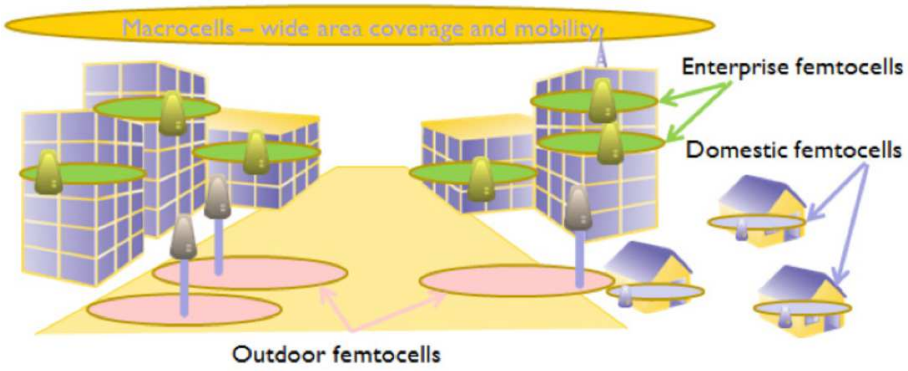

Figure 1.4: Femtocell market status [7].

Initially, femtocells were designed to improve the poor indoor coverage for residential environments. This remains a core application for femtocells and requires femtocell technology to be produced in large volumes and low costs. These femtocells are installed in home by the end user as stand-alone devices or integrated with other technology such as residential gateways. Access to the residential femtocells is mostly closed – restricted to a specified group of users.

Enterprise femtocells are usually deployed in a branch of offices or in large enterprise buildings. This type of femtocells typically support additional functionality compared to the residential devices such as handover between femtocells, integration with PBX

(Private Branch eXchange) and local call routing. They are primarily used indoor, but can also be used to serve a corporate campus. Installation is typically managed by the operator, but can be achieved by the enterprise itself or its IT subcontractors. Access may be closed or open.

Unlike residential or enterprise femtocells, operator-use femtocells are mostly installed outdoor to offload Macrocell traffic or provide additional coverage or capacity. Access to the operator femtocells will usually be open access. They will be installed by the operator or third parties under the operator's instruction.

Apart from these three major applications, new femtocell applications are also emerging, such as femtocells on aircraft, trains or buses. Driven by the growing applications, the concept of 'femtocell' is rapidly expanding.

1.1.5 Benefits from Femtocell

Femtocells can bring a number of benefits to users as well as operators.

- **Coverage:** The essential benefit from femtocells is the coverage improvement. With the use of femtocells, broadband mobile services can be delivered to an indoor environment, rural and remote areas, without the need to deploy large numbers of high cost macro basestations.

- **Capacity:** Femtocells enable mobile phones to work at the peak of their capability, including the highest possible data rates available over the air and the highest possible call quality. For example, Qualcomm claims that their femtocells can help increase the user's data rate by up to 80 times compared to macrocell only [8].

- **Traffic offload:** Femtocells can offload traffic from the macrocell layer and improve macrocell capacity, both in radio access and in backhaul across the operator's broadband internet link. According to the same research from Qualcomm [8], when

femtocells are deployed in a macrocell area, the macrocell user's data rate can be increased by up to 50%, benefiting from the traffic offloaded by the femtocells. As illustrated by Fig. 1.5, the peak transmission rates of the users can be improved up to 80 times (from 180kbps to 14.5Mbps) if they are served by both macro and femto basestations; and the data rate of macro users is increased by 50% when the macrocell traffic is offloaded by femtocells. Femtocells, along with Wi-Fi offloading, are expected to carry over 60% of all global data traffic by 2015 [9].

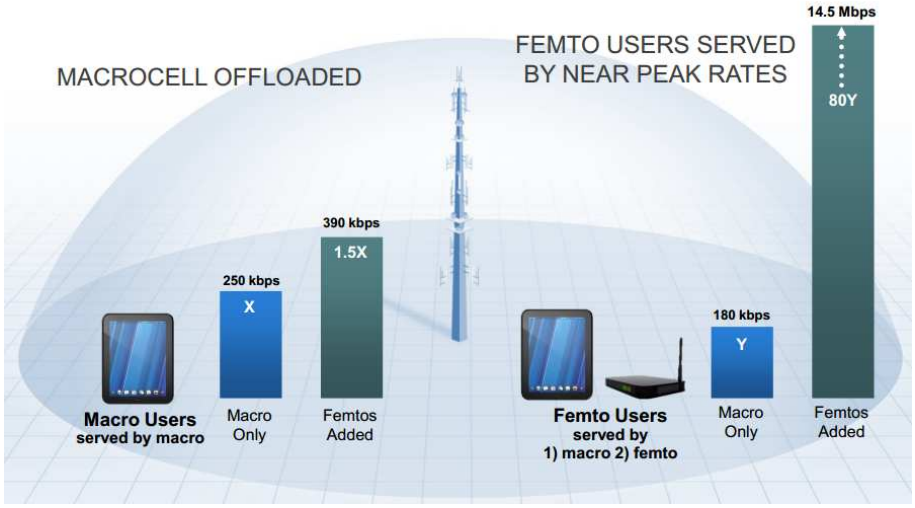

Figure 1.5: Femtocells help increase capacity and offload traffic from macrocells [8].

- **Spectrum efficiency:** Femtocells operate on existing mobile operator spectrum, including both currently unused frequencies and those already used by outdoor sites. They also open up the use of higher frequencies whose range might be excessively limited for wide-area operation, thus increasing the overall available spectrum. Fig. 1.6 shows a macrocell/femtocell scenario that the macro user and the two femto users can operate in the same spectrum, and they do not interfere with each other when they are sufficiently far apart.

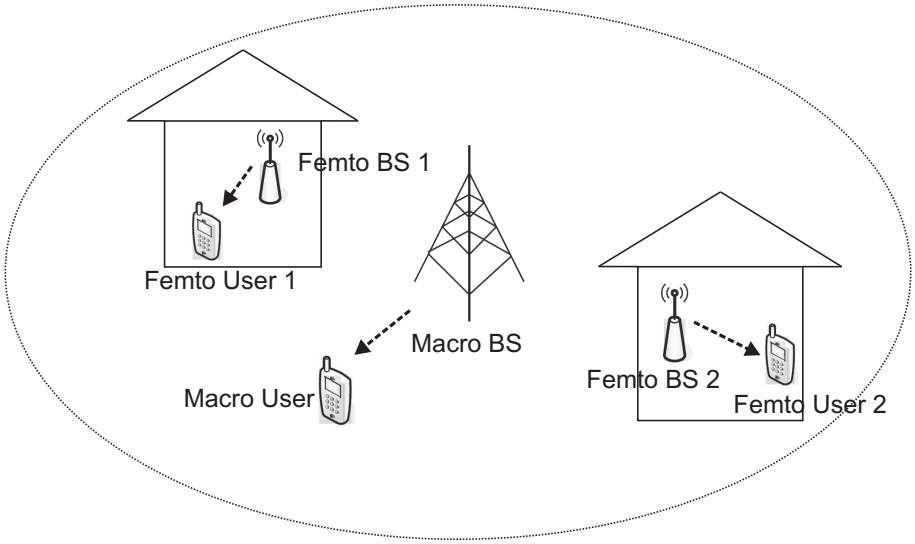

Figure 1.6: A femtocell spectrum reuse scenario.

- **Green benefits:** Femtocells reduce total network energy consumption. Femtocells are low power access points providing coverage for a small area. Macrocell base stations have power outputs of typically tens of watts. Compared with that, femtocells save a lot of energy with the power outputs at a much lower level between 10 to 100 milliwatts. So potentially, power can be supplied in an environmentally sustainable manner. The short transmission distance reduces the power consumption of the end user and consequently prolongs handset battery life. In addition, a femtocell basestation can enter sleep mode if no mobile user is connected to it, and further improve energy efficiency.

- **Better in-building user experience:** Femtocell users are supplied with better in-building experience, including excellent coverage, higher mobile data rate, better signal quality, longer battery life, etc.

- **Innovation and opportunity:** From all the benefits mentioned above, femtocells can fundamentally increase the range of service models available to operators, encouraging competition and efficiency. They also enable newer technologies to be delivered to customers more quickly. They also provide a new platform for deliver-

ing new applications and services to existing devices with attractive tariffs.

1.1.6 Technical Challenges

As an emerging technology, there are a number of business and technical issues that need to be addressed. Both the pricing and the ongoing cost of femtocells are still relatively high for consumers, which requires the cellular operators to reduce the pricing or change the current business model. In addition, although many researches have been dedicated to some of the technical challenges for femtocells, there are still many problems to be solved.

Interference One key issue associated with femtocells is interference. Femtocells can use the same spectrum band which has already been allocated to macrocells. The femtocells are deployed in an ad-hoc fashion by end users without appropriate network planning. Thus, interference would arise between macrocells and femtocells, and within femtocells, as shown in Fig. 1.7. This occurs mainly when femtocells are deployed in the same spectrum, but can also occur even when femtocells are in adjacent spectrum because of out-of-band radiation [10]. This could cause problems to the main network resulting in performance degradation of the overall network.

Standards bodies have devoted considerable attention to the femtocell interference management including those by the Small Cell Forum [11] and 3GPP [12, 13]. In [14, 15], the interference conditions in cross-tier macro/femto networks have been investigated. For 3G CDMA femtocells, power control based strategies [16, 17] are seen as the primary method for interference coordination. The interference management of 4G LTE femtocells, on the other hand, is more diverse which includes spectrum scheduling, backhaul-based coordination, adaptive fractional frequency reuse and more [18, 19, 20, 21, 22, 23]. Interference cancelation based solution has been researched in [24].

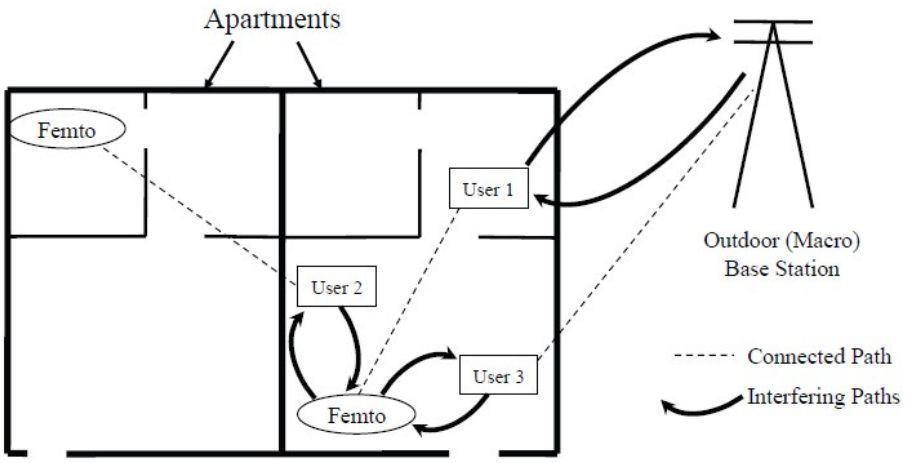

Figure 1.7: Cross-tier interference in a Macro/Femto scenario [10].

Mobility and Handover Femtocell handover or femtocell handoff techniques are needed to ensure that seamless coverage is perceived by the user when moving onto or off a femtocell. It is essential that users do not see any problems with the handover process; otherwise this would provide a basic distrust of the system and lead to signal loss or other failure conditions. Since the coverage area of an individual femtocell is small, the femtocell handover, either femto-to-macro or femto-to-femto, will be more often than macro-to-macro scenario. The problem of femtocell handover is that there may be many femtocells located within the same footprint of a macrocell – too many to be included in the neighbour list broadcast message, and too many for the handset to scan. Femtocell handover is also more challenging than normal macrocell cellular handover because the backhaul network is different and there is also little possibility of direct communication between the femtocell and the macrocell.

Recognizing these challenges, standards bodies such as 3GPP have initiated several study efforts on these mobility issues, for example the specifications [13, 25]. Meanwhile, the improved methods for cell identification and discovery signaling have been considered in [26, 27].

Configuration and installation One of the key elements of the femtocell is that its installation, organization and configuration should be completely trouble free without any intervention from the home owner. As mentioned before, the femtocells are deployed in an ad-hoc fashion by end users without traditional RF planning, site selection, deployment and maintenance by the operator. It is a prime requirement that femtocells must be able to be installed by people with no technical knowledge of their operation. And once installed, they should continue to operate without any intervention, even if the surrounding environment changes. Therefore the installation of the femtocell should be totally 'plug and play', with automatic configuration and network adaptation. This requires a considerable amount of intelligence in the design of the femtocell itself.

Due to these features, femtocells are sometimes referred to as a self-organizing network (SON) [10]. The 3GPP standards body has defined the procedures for automatic registration and authentication of femtocells, management and provisioning, neighbouring cells discovery, synchronization, cell ID selection and network optimization [28, 29, 30, 31]. In addition, the adaptive and autonomous nature of interference management in SONs also bears some similarities to the cognitive radio concept. Several studies have been proposed for so-called cognitive femtocells [32, 33, 34, 35].

Security Privacy and security are among the top concerns of potential femtocell users. As the data is transmitted via the Internet in femtocell networks, it is necessary to provide security for these IP communications and prevent monitoring of the data, potential Denial of Service (DoS) attacks or any other behavior that can degrade the service. For instance, it should prevent unauthorized users connected to a femtocell and making illegal use of it - for example, transferring the cost of their calls to the authorized femtocell user.

The 3GPP standards body has placed considerable attention on femtocell security, such as in [36, 37]. In [38], the authors analyze the security of femtocells based on 3GPP system architecture. In [39], the authors demonstrate several security flaws that allowing

attackers to gain root access and to install malicious applications on the femtocell.

Time Synchronization Synchronization is an important aspect of femtocell design. Since femtocells are deployed by users in an ad-hoc fashion, there is not a centralized management of their radio resources. Hence, network time synchronization is critical between macrocells and femtocells in order to minimize multi-access interference, and to operate a smooth handover. Without accurate time synchronization, the transmission instants vary between cells, leading to overlap between uplink periods with the downlink of others in TDD systems and resulting in inter-cell-interference. Many femtocell operations require high level synchronization and 3GPP specifies that base station frequencies need to be very accurate. Also, phase synchronization is required in many standards. However, as a low cost solution, it is not realistic for femtocells to use accurate but expensive crystal oscillators to maintain frequency stability. In these circumstances, synchronization methods are needed for femtocells to be precisely synchronized with accurate timing references. As femtocells are deployed in a variety of scenarios, they may be synchronized to different timing references. Based on the synchronization source, these methods can be categorized as: synchronization via GPS, synchronization via TV signals, synchronization via backhaul and synchronization via neighbouring cells listening. However, these methods have different problems: GPS based synchronization methods have indoor signal reception problem; IEEE 1588, the most popular backhaul synchronization method, can be seriously affected by random transmission delay and link-asymmetry, especially when ADSL cable is used as the backhaul; neighbouring cells listening methods depend on the availability of synchronized neighbour cells; TV signal based methods are very location dependent.

This thesis will focus on the investigation of accurate and reliable time synchronization for femtocell systems.

1.2 Research Objectives

This thesis is dedicated to solving the time synchronization problem for femtocells. Femtocell time synchronization faces two unique challenges:

1. The synchronization accuracy requirement is high but the femtocells are normally only equipped with low accuracy oscillators for economic reasons.

2. As the synchronization condition (available synchronization source, synchronization requirement, etc.) varies, there is no "one solution fits all".

Based on the synchronization source, the available synchronization methods can be categorized as: synchronization via GPS, synchronization via TV signals, synchronization via backhaul and synchronization via neighbouring cells listening. In this thesis, two of these methods are investigated: synchronization via backhaul and synchronization via neighbouring cells listening.

Firstly, IEEE 1588 is used increasingly widely and is very effective in providing both frequency control and time synchronization. However, the performance of the conventional IEEE 1588 synchronization algorithm is affected by the asymmetric link and random delay. Several works have been carried out to solve the problem but they either need additional hardware or introduce significant overheads. This motivates us to develop new IEEE 1588 based synchronization schemes to alleviate the asymmetric link and random delays problems, with low overheads and without the need for extra hardware.

Secondly, synchronization by listening to other synchronized femtocells is a potential approach for wireless femtocell networks, especially when wireless backhaul is used. The receiver-receiver synchronization (RRS) method has proved to be efficient and accurate for packet-based wireless network synchronization, i.e., wireless sensor networks (WSNs). However, time synchronization for WSNs and femtocells are different, and thus the most widely used RRS scheme – reference broadcast synchronization (RBS) can not

be simply utilized in femtocell networks. This motivates us to explore a new RRS based synchronization strategy to apply this mechanism into femtocell networks.

Thirdly, for a wireless femtocell network that is formed by a cluster of femtocells, where often only few of them have synchronization references, i.e., equipped with GPS receivers, these synchronized femtocells are used to synchronize other femtocells. Wireless IEEE 1588 is suggested to be the synchronization solution for this scenario. However, wireless IEEE 1588 needs the exchange of a large number of timing packets and is vulnerable to packet loss. This motivates us to propose a new synchronization scheme for wireless femtocell networks.

Lastly, a very unique situation for the femtocell is that it may connect to more than one synchronization sources, i.e., GPS and IEEE 1588, or IEEE 1588 and a neighbouring cell. Instead of selecting the best one, combining them has been proved to be more effective. However, this area has not been investigated in existing works. This motivates us to explore a combination method for the femtocells that are connected with two synchronization sources in order to make the best use of both of them.

1.3 Major Contribution

The major contributions of this thesis can be summarized as follows:

1. Firstly, an improved IEEE 1588 based synchronization scheme is proposed. This scheme utilizes additional packets with different sizes to overcome the aforementioned asymmetric link and random delay problems of IEEE 1588, without adding hardware or overheads. Based on the 'improved IEEE 1588' scheme, the maximum likelihood estimators (MLEs) of the clock offset are derived and the corresponding Cramer-Rao lower bounds (CRLBs) (for both Gaussian and exponential random delay models) are analyzed. The performance of the estimator is evaluated in two scenarios with different random delay distribution. The impact of the size of the

transmitted packets is studied by simulation. The results show that the 'improved IEEE 1588' scheme and estimators can successfully overcome the detrimental effect of the asymmetric link and random delay problems. The synchronization accuracy of the 'improved IEEE 1588' scheme significantly outperforms both the conventional IEEE 1588 scheme and an existing method in terms of clock offset bias error, but without the need of extra hardware.

2. Secondly, based on the 'improved IEEE 1588' scheme, another so called 'variable-length IEEE 1588' scheme is proposed to further reduce the overhead of the 'improved IEEE 1588' scheme. It also solves the IEEE 1588 asymmetric link and random delay problems. The scheme uses variable-length packets to mitigate both these problems. The MLE for the clock offset is derived based on the proposed scheme for two scenarios – Gaussian and exponentially distributed random delays. The MLE, which depends on two new parameters, is then optimized (in an MSE sense) with respect to these parameters. Simulation results show that the 'variable-length IEEE 1588' scheme can provide similar synchronization accuracy as the 'improved IEEE 1588' scheme but with lower overheads.

3. Thirdly, two RRS based synchronization schemes are proposed for femtocells. Synchronization via neighbouring cells listening is cost-effective because no extra provisions are required to ensure synchronization even on a regular basis. In wireless networks, RRS has proved to be efficient and accurate for wireless network synchronization. Two schemes are proposed for different scenarios to ensure a more comprehensive availability. Analysis and simulation results demonstrate that the schemes provide sufficient synchronization accuracy for practical scenarios with reduced exchanged packets compared with RBS.

4. Fourthly, a hybrid synchronization scheme based on wireless IEEE 1588 and RRS

is proposed for wireless femtocell networks. The scheme slightly changes how messages are exchanged in conventional IEEE 1588 and then makes the best use of the advantages of these two synchronization methods. This scheme can provide better synchronization accuracy with less exchanged messages than IEEE 1588. It is also proven that this scheme is more robust against the packet loss in the network than conventional IEEE 1588 and RBS.

5. Lastly, a two-step weighted multiple linear regression (WMLR) based synchronization scheme is proposed for femtocells that connect to two synchronization sources. Simulation results show that the proposed scheme provides better synchronization accuracy and better stability than any of the individual sources. It is also suggested in the simulation results that the proposed scheme performs better when the observations from the two synchronization sources are more comparable.

1.4 Thesis Organization

The rest of the thesis is organized as follows:

In Chapter 2, the femtocell synchronization problem is discussed in details. The reasons for femtocells synchronization are firstly presented. In particular, the dilemma between the higher accuracy requirement and lower oscillator accuracy for femtocell synchronization is introduced. Based on the synchronization source, the aforementioned four major single-source femtocell synchronization methods are also depicted detailedly, including the advantages and disadvantages of these methods and some related researches in the literature.

Chapter 3 and Chapter 4 focus on IEEE 1588 synchronization for femtocells. In Chapter 3, the basic mechanism and the asymmetric link and random delay problems of IEEE 1588 are firstly analyzed. Then an 'improved IEEE 1588' scheme is devised to solve these

problems and simulation results are given to demonstrate the performance improvement.

Although the 'improved IEEE 1588' scheme successfully alleviates the aforementioned two problems of IEEE 1588, it brings an additional undesirable overhead. Therefore, Chapter 4 continues the study of the IEEE 1588 synchronization for femtocells and presents a 'variable-length IEEE 1588' scheme. Simulation results show that the synchronization accuracy of the 'variable-length IEEE 1588' scheme is similar to the 'improved IEEE 1588' scheme but with a significantly reduced number of transmitted messages.

Femtocell synchronization via neighbouring cells listening, in particular the wireless femtocell network synchronization, will be investigated in Chapter 5 and Chapter 6. Chapter 5 concentrates on the RRS applying in the femtocell networks. Two new RRS based synchronization schemes are proposed for different scenarios to ensure better availability. Analysis and simulation results demonstrate that both of the schemes provide satisfactory performance for femtocells in terms of synchronization accuracy. In addition, the second scheme significantly reduces the number of overall timing messages compared with RBS, which is the most widely used RRS scheme.

Chapter 6 presents a hybrid synchronization scheme based on wireless IEEE 1588 and RRS for wireless femtocell networks. The hybrid scheme proposes a way to combine both wireless IEEE 1588 and RRS, and make the best use of the advantages of these two synchronization methods. Analysis shows that this hybrid scheme can provide better synchronization accuracy with less exchanged messages than conventional wireless IEEE 1588, especially when there are a large number of 'slave' femtocells in the network. It is also shown that the proposed hybrid scheme is more robust than conventional wireless IEEE 1588 and RBS against the packet loss in the network.

Different femtocell synchronization methods are compatible with each other. On some occasions, there may be more than one synchronization sources to provide timing references for the femtocell. Chapter 7 studies this scenario and proposes a two-step weighted

multiple linear regression (WMLR) based synchronization scheme. Simulation results show that the proposed scheme provides better synchronization accuracy and better stability than any of the individual sources.

Finally, Chapter 8 draws conclusions and suggests possible future work.

1.5 List of Publications

Published papers:

- Jinlin Peng, Li Zhang, Des McLernon and Jibo Wei, "A Novel Receiver-Receiver Time Synchronization Scheme for Femtocells", in *Wireless Communication Systems (ISWCS), 2010 7th International Symposium on*, vol., no., pp.937,940, 19-22 Sept. 2010.

- Jinlin Peng, Li Zhang and Des McLernon, "MS-Assisted Receiver-Receiver Time Synchronization Strategy for Femtocells", in *Vehicular Technology Conference (VTC Spring), 2011 IEEE 73rd*, vol., no., pp.1,5, 15-18 May 2011.

- Jinlin Peng, Li Zhang and Des McLernon, "On the Clock Offset Estimation in an Improved IEEE 1588 Synchronization Scheme", in *Wireless Conference (EW), Proceedings of the 2013 19th European*, vol., no., pp.1,6, 16-18 April 2013.

- Jinlin Peng, Li Zhang and Des McLernon, "Enhanced IEEE 1588 Time Synchronization Scheme with Variable-Length Packets", in *Wireless Communication Systems (ISWCS), 2013 10th International Symposium on*, Aug. 2013.

- Jinlin Peng, Pengfei Sun, Li Zhang, Keshave Kuber, and Des McLernon, "Timing Synchronization for OFDMA Femtocells in the Presence of Co-Channel Interference", in *Wireless Communications and Mobile Computing Conference (IWCMC), 2012 8th International*, vol., no., pp.1215,1220, 27-31 Aug. 2012. However the

content of this paper is only discussed in the future work (Section 8.2) because it is less relevant to the rest of this thesis.

Unpublished papers:

- Jinlin Peng, Li Zhang and Des McLernon, "Variable-Length IEEE 1588 Clock Synchronization for Femtocell Network", *submitted to IEEE Trans. Commun.*. This paper is based on the finished work included in Chapter 4.

- Jinlin Peng, Li Zhang and Des McLernon, "A Hybrid Synchronization Scheme Based on Wireless IEEE 1588 and Receiver-Receiver Synchronization for Wireless Femtocell Networks", *in preparation*. This paper will be based on the finished work included in Chapter 6.

- Jinlin Peng, Li Zhang and Des McLernon, "A Two-Step Weighted Multiple Linear Regression Based Synchronization Scheme for Femtocells", *in preparation*. This paper will be based on the finished work included in Chapter 7.

2 Time Synchronization for Femtocells

2.1 Reasons for Femtocell Synchronization

Synchronization is critical for the successful operation of femtocells. The two aspects of time synchronization, namely phase synchronization (getting clocks synchronized in phase) and frequency synchronization (getting clocks running at the same rate) are both required for the femtocell. Phase synchronization makes the femtocell aware of the current global time. Frequency synchronization ensures the femtocell clock running at the right speed.

Fig. 2.1 illustrates phase synchronization and frequency synchronization for the femtocell. In Fig. 2.1, the femtocell clock is plotted as the local clock time being a function of the real time. With the ideal clock, which is represented by the dashed line, the local clock time always equals to the real time. The slope of the ideal clock, which represents the clock frequency, equals to 1. The intercept of the ideal clock, which represents the initial clock offset (phase), equals to 0. Fig. 2.1(a) shows the perfect synchronization where the solid line, which represents the femtocell clock, overlaps with the dashed line. In Fig. 2.1(b), the phase is synchronized at the original point, but the clock offset still occurs later since the frequency is not synchronized. The femtocell clock is not well synchronized in

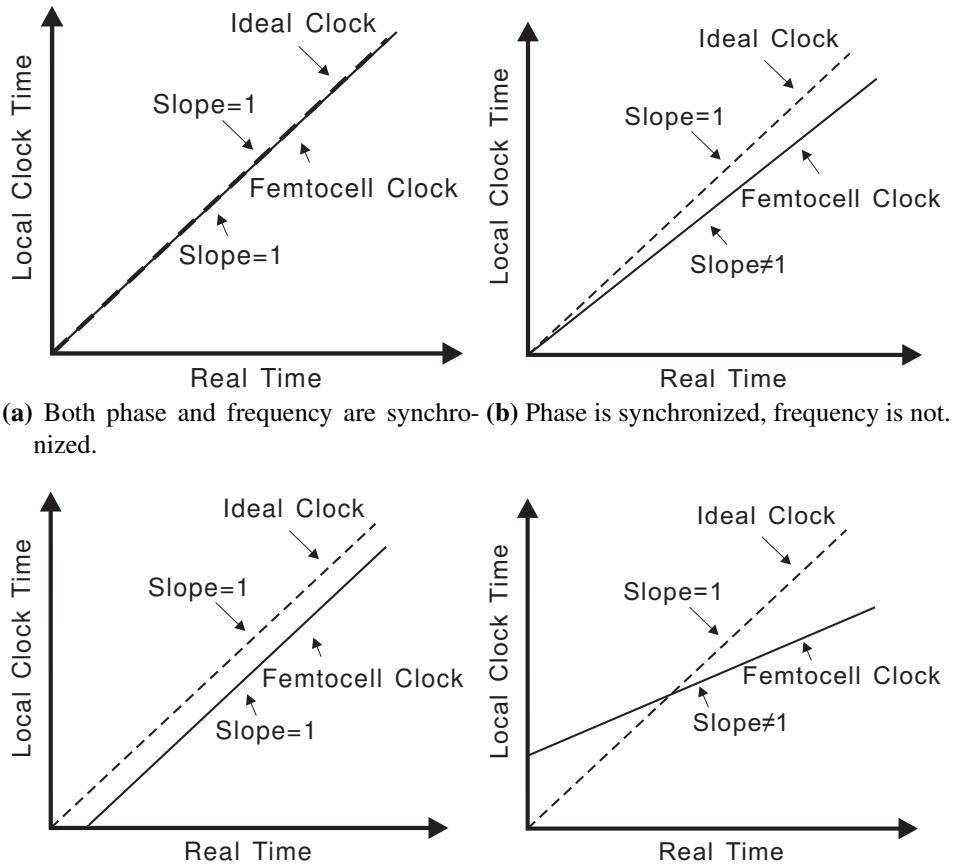

(a) Both phase and frequency are synchronized. **(b)** Phase is synchronized, frequency is not. **(c)** Frequency is synchronized, phase is not. **(d)** Both phase and frequency are not synchronized.

Figure 2.1: Phase synchronization and frequency synchronization for the femtocell.

Fig. 2.1(c), where frequency is synchronized but phase is not, and in Fig. 2.1(d), where neither frequency nor phase is synchronized.

Cellular air interface standards impose strict phase and frequency requirements on femtocell synchronization. The requirements of the standards for frequency synchronization accuracy vary from 200 parts-per-billion (ppb) for a WCDMA femtocell to 100 ppb for CDMA2000 and TD-SCDMA. The requirements for phase synchronization accuracy vary from no requirement for FDD WCDMA and FDD LTE to 1 μs for CDMA. There are a number of areas of femtocell operation that require time synchronization for them to be able to perform satisfactorily and these will now be listed:

- **Supply phase and frequency information to handsets:** Base stations supply phase and frequency information to mobile stations. The mobile stations are usually not equipped with high quality oscillators to maintain frequency stability, and so can only achieve this by synchronizing to base stations. Femtocell users also need phase synchronization to achieve alignment with the femtocell base stations for successful communication.

- **Ensure reliable handover:** The femtocell must be synchronized to the network at a sufficient level to make sure of successful handover for mobile users. If the femtocell is not synchronized to adjacent base stations, then offsets may exist and mobile users may fail in handover and transmission could be disrupted. In the worst case, the handset would not be able to immediately lock onto and acquire the new signal, and the call would drop.

- **Interference reduction:** If the femtocell is not synchronized to the network, interference may be produced and the call quality and the network capacity will be reduced. This is especially important for OFDM based techniques, where synchronization errors will introduce inter-carrier-interference (ICI) and inter-symbol-interference (ISI).

- **Avoid Tx/Rx clashes in TDD systems:** TDD systems are more sensitive to phase synchronization errors. Successful phase synchronization is required for femtocells to achieve alignment with neighbouring cells operating on the same channel to avoid Tx/Rx clashes in TDD systems.

- **Ensure the femtocell is aware of adjacent cell sites:** If the femtocell is accurately synchronized to the rest of the network it can detect other cells more quickly and thereby improve the operation of the femtocell and some potential cooperation with other base stations.

2.2 Strict Accuracy Requirements Meet Stringent Cost Limits

Crystal oscillators are generally at the heart of the femtocell clock system and are used to provide a timing and frequency reference. A crystal oscillator is an electronic oscillator circuit that uses the mechanical resonance of a vibrating crystal of piezoelectric material to create an electrical signal with a very precise frequency. The accuracy of an oscillator is usually measured in ppb or parts-per-million (ppm), representing the maximum variation obtained over a high number of oscillations. For example, a normal oscillator has a typical error of 10 ppm, meaning that the timing error can be as much as 10μs in a second and this gives a maximum error per day equal to $24 \times 60 \times 60$ seconds$\times 10 \times 10^{-6} = 8.6$ seconds. Because of the variation, the crystal oscillator clock will drift apart from the accurate clock after some time, even when it was initially set accurately. That is why a femtocell needs to synchronize to an accurate external timing reference periodically.

The clock accuracy (both frequency accuracy and time/phase accuracy) requirements of different standards are listed in Table 2.1.

Table 2.1: Clock Accuracy Requirements [2].

Standard	Frequency accuracy	Time/phase accuracy
GSM	100ppb	N/A
CDMA	100ppb	$1\mu s$
CDMA2000	100ppb	$3\mu s$
WCDMA/FDD	200ppb	N/A
WCDMA/TDD	200ppb	$2.5\mu s$
TD-SCDMA	100ppb	$2.5\mu s$
WiMAX FDD	8ppm	$5\mu s$
WiMAX TDD	8ppm	N/A

As we can see in Table 2.1, the accuracy requirements for femtocells are strict, although it differs from one standard to another.

Different types of crystal oscillator may be used in the femtocell with different cost

implications. Generally, accurate oscillators are very expensive. The price and accuracy comparison of different types of crystal oscillators are shown in Table 2.2 [40].

Table 2.2: Types of Crystal Oscillators [40].

	TCXO	OCXO	Hybrid
Price	Lower	Higher	Medium
Accuracy	Lower	Higher	Medium

It can be seen that the accuracy is broadly reflected in the cost. It may be reasonable for macrocell base stations to afford expensive and accurate oscillators, this is not the case for femtocells, which need to be manufactured at low prices. As the cost of both the OCXO and hybrid solutions are normally too high for the maximum manufacturing costs that are viable for femtocell production, therefore femtocells are normally equipped with TCXO. Obviously, with higher accuracy requirement and lower oscillator accuracy, the femtocell relies more on the external timing references. That is why other solutions with high synchronization accuracy have to be used, in order to ensure the time synchronization requirements are satisfied with the equipment of low accuracy oscillators.

2.3 Overview of Synchronization Methods for Femtocells

Femtocells are deployed in a variety of scenarios, with different synchronization requirements and conditions. For instance, several femtocell scenarios and their respective synchronization problems are:

- A femtocell installed deep indoor which can hardly receive the GPS signal can be only synchronized to the ‘master clock’ over the internet via backhaul, and then needs to overcome the potential link-asymmetry problem.

- A cluster of outdoor femtocells need to minimize the GPS use for geographic or economic reason. Thus, only few of them are equipped with GPS receivers and other femtocells need to synchronize with them via exchanging wireless packets.
- A femtocell is able to connect to more than one synchronization sources and then the problem converts to how to make the optimum combination.

Thus, the synchronization solution must be specific for the femtocell scenario and the respective problem. When it comes to the femtocell synchronization solution, there is certainly no 'one size fits all'.

Some synchronization methods have been investigated for different femtocell scenarios. Based on the available synchronization sources, these methods can be categorized as: synchronization via GPS, synchronization via TV signals, synchronization via backhaul and synchronization via neighbouring cells listening. These major time synchronization sources are shown in Fig. 2.2 [41].

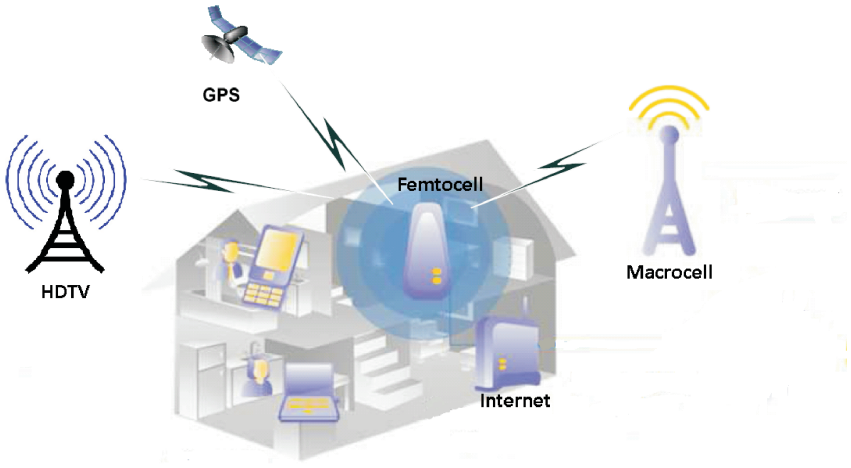

Figure 2.2: Major Synchronization Sources for Femtocells [41].

2.3.1 GPS

When available, GPS is a prominent way of acquiring time references for cellular base stations. GPS provides not only timing references with high accuracy that can meet almost all the requirements, but also location information of the GPS receiver which is also important for many telecommunication operations and functions. For this reason, GPS signals are used as a synchronization source for most of the macro base stations. After its widespread use and mass production, GPS receivers are now also at a reasonable price.

However, one big obstacle for femtocells to use GPS as the synchronization reference is that GPS is often not viable indoor because of the high GPS signal loss. The attenuation of the GPS signal when it passes through walls, roofs, floors, windows or any other obstacles can make the GPS signal undetectable by the receiver. Also, GPS signals reflected by the walls of neighboring buildings may introduce large timing errors. In urban area, femtocells installed on lampposts may not have an open view of the sky and cannot receive a strong GPS signal. For these reasons, reliable GPS signals may not always be available. This disadvantage is vital for femtocells, which are mostly used for home and office. Although femtocells could be located by a window or installed an external antenna to receive GPS signals, this makes the implementation more complicated and expensive.

A possible solution to solve the GPS indoor reception problem is known as assisted GPS (AGPS) [42]. AGPS enhances the capability of GPS by using a network-based approach to improve the acquisition performance of GPS receivers. In an AGPS enabled femtocell, a small amount of data carried by the satellite signal is instead supplied as assistance data via a backhaul connection [43]. AGPS removes the requirement to demodulate the unknown data when processing the signal, allowing the GPS receiver to operate at a lower signal level. For example, a strategy known as Tightly-Coupled Opportunistic Navigation (TCON) is proposed in [44] for extending the penetration of AGPS femtocells in weak-signal indoor environments. The paper claims that a TCON solution fusing GPS

with CDMA cellular signals offers significant sensitivity gains over state-of-the-art AGPS receivers. However, AGPS still cannot guarantee the required timing and frequency synchronization with 100% availability. Additionally, the extra cost and operation of both the receivers and the core network need to be taken into account.

2.3.2 Synchronization via TV signals

There are a number of terrestrial radio broadcast sources that can provide timing references for femtocells, such as most commonly used TV signals. Nowadays TV transmissions can be received at good strength in most areas, because they are broadcast at frequencies below 1GHz. This is good for indoor femtocells to use as synchronization sources without an external antenna. Besides, television receivers suitable for providing femtocell synchronization can be built into femtocells at a lower price than GPS receivers. The main drawback of this method is that the usage of TV receivers is area dependent as the TV signals are different in different regions. For this reason, the femtocells manufacture will need to install a specific TV receiver for its area. This also brings uncertainty to the synchronization accuracy. Although most digital TV signals like DVB-H can provide synchronization references with high accuracy, there are areas that only have traditional TV reception which is not able to support femtocell synchronization at the required level. Moreover, it is impossible to use this method where there is no TV coverage.

Now some enterprises focus on the manufacture of more advanced GPS, which uses the TV signals to help synchronize the femtocell. For example, Rosum Corporation has proposed a hybrid TV+GPS solution, ALLOY, trying to provide timing and frequency synchronization for femtocells that are always deployed in-building [45], as shown in Fig. 2.3.

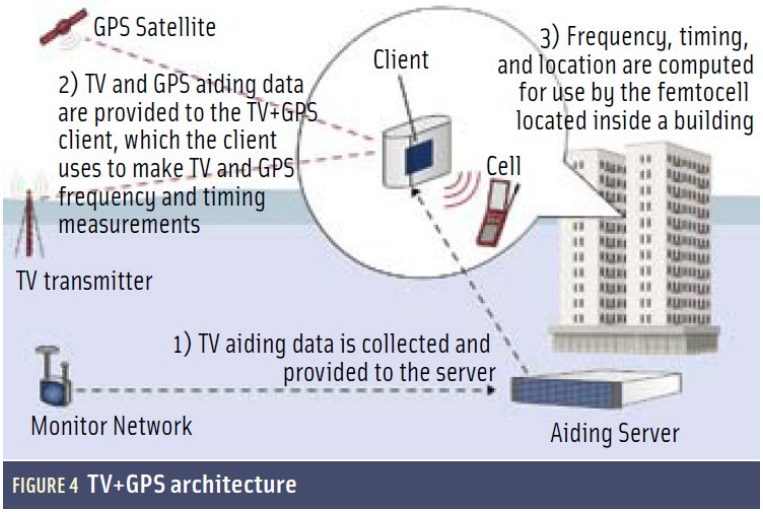

Figure 2.3: Femtocell synchronization using TV+GPS signals [45].

2.3.3 Packet Timing via Backhaul

In this approach, a femtocell use the backhaul connection to synchronize to a clock on the network of the operator. Protocols such as IEEE 1588, which specifies the use of Precision Time Protocol (PTP) and Network Time Protocol (NTP) are widely used in synchronization on the Internet. In principle, both of these protocols can be used to provide frequency and time synchronization throughout packet networks. IEEE 1588 and NTP operate in a fundamentally identical way, relying on a short exchange of time-stamped packets to estimate the time at the client. Frequency is derived from a 'rate-of-change-of-time' [43] observation at the client using time measurements spread over some duration. However, they differ in some detail in their application to femtocells. Generally, IEEE 1588 can provide better synchronization accuracy than NTP and is seen as a common service in future networks. Essentially it operates in two stages:

1. Establishes a 'Master-Slave' hierarchy of suitable clocks.

2. Synchronizes the slave clock with the relevant master clock.

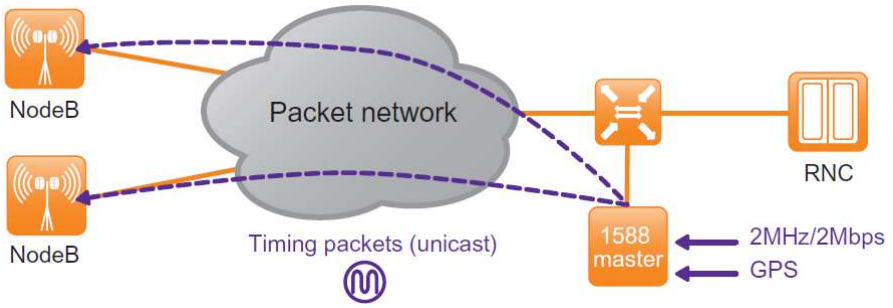

Figure 2.4: IEEE 1588 Master-Slave hierarchy [46].

Fig. 2.4 shows a typical IEEE 1588 hierarchy. As shown, the IEEE 1588 master clock is an accurate clock equipped with a GPS receiver [46]. The two NodeBs are 'slave clocks' in the hierarchy. The 'slave clock' calculates the clock offset with the 'master clock' by exchanging timing packets with the 'master clock'. And the frequency skew of the 'slave clock' can then be estimated via a statistical method of the individual measurements of clock offset. The most fundamental method could be nothing more than a simple average. The accuracy of the measured frequency is affected by both the performance of the network and the stability of the oscillator. IEEE 1588 is used increasingly widely and very effectively to provide both frequency control and time synchronization in Local Area Networks (LAN) and in telecommunications 'core networks'. However, there are two primary problems that must be overcome:

1. Random delay problem: Variability in the transfer latency (jitter) of the timing messages due to the network latency created by hubs, switches, cables, and other hardware that resides between the clocks.

2. Link-asymmetry problem: Time uncertainty introduced by the asymmetry between the uplink (from 'slave clock' to 'master clock') and the downlink (from 'master clock' to 'slave clock'). IEEE 1588 calculates the clock offset between 'master clock' and 'slave clock' based on the assumption that the uplink and downlink delays are symmetric. However, it will introduce asymmetric errors when the fem-

tocell connects to an asymmetric backhaul such as asymmetric digital subscriber line (ADSL) or very-high-bit-rate digital subscriber line (VDSL).

These two problems can seriously degrade the synchronization performance of IEEE 1588 - especially the link-asymmetry problem, which may introduce large fixed errors when the uplink and downlink communication rates are very different. Several works have been focused on the link-asymmetry problem [47, 48, 49]. However, they either need additional hardware, introduce significant overheads, or produce low accuracy. Thus, new methods are required to solve these two problems more effectively.

2.3.4 Neighbouring Cells Listening

Another approach is to listen to neighbouring cells, including macrocells and synchronized femtocells.

Synchronization to Macrocells

Macrocells are always equipped with accurate oscillators and GPS receivers. This provides a convenient and reliable source of synchronization for a femtocell equipped with a suitable receiver. Clearly this approach is not applicable where femtocells are deployed purely to provide coverage for an area without macrocell coverage. Note that it is not necessary that the femtocell use the same standard as the macrocell. For example, a UMTS femtocell can use the GSM network to get synchronized, though it needs to install a GSM chip.

Frequency synchronization is relatively easy with this approach. Any macrocells have a frequency synchronization accuracy better than 50ppb which is more than enough for any femtocell requirement [43]. Thus a femtocell can use any macrocell transmission to get synchronized, only needs instant frequency control. In the femtocell, a separate set of front-end filters may be required to monitor out-of-band macrocells. In many cases this

is not additional overhead, for the existing receiver sub-system is often flexible enough to perform frequency measurements on an occasional basis, say daily or every few hours.

On the other hand, phase synchronization of a femtocell with macrocell listening is more complicated. Since radio waves travel at the speed of about 300m per microsecond, ranging information is required for the phase synchronization of microsecond level. However, some femtocells are not able to provide the information since the lack of an up-link makes it impossible to measure round-trip delay. Thus, it requires an independent method to acquire the location information of both the macrocell and the femtocell, and then the propagation error in the synchronization can be removed. Time difference of arrival (TDOA) based method can measure the femtocell location with the accuracy of 100-300m level, which still allows the phase synchronization within 1-3μs and is sufficient for femtocell applications. However, in this case, at least three synchronized macro base stations must be received.

In summary, the macrocell listening synchronization method can provide sufficient synchronization accuracy, in both frequency and phase, with low additional overhead, but cannot be relied upon for universal coverage. Single macrocell coverage is required for frequency control and at least three macrocells coverage is required for phase synchronization. The coverage requirement is stringent for femtocells. Because femtocells have initially been designed to improve indoor coverage when the macrocell reception is poor, or even no macrocell reception at all. Note that even when the femtocell and macrocell do not overlap, accurate synchronization is still necessary for femtocells. Because it is still possible that a mobile user might be traveling between the macrocell and the femtocell, then a handover problem would happen if the femtocell is not synchronized. Frequency synchronization of the femtocell is also needed for that large frequency shift may render a mobile user unable to decode the femtocell's signal.

Synchronization to Other Femtocells

When synchronization via macrocell listening is not available, listening to other synchronized femtocells is another potential approach. In many femtocell deployments, it is very possible that many femtocells will overlap each other and then form a wireless femtocell network. In these circumstances, femtocell synchronization can be achieved using network synchronization schemes that have been well investigated in distributed networks such as wireless sensor networks (WSNs).

A number of time synchronization methods have been investigated in wireless networks. Many of these are based on packet synchronization techniques which can be categorized as sender-receiver synchronization like TPSN [50], receiver-receiver synchronization like RBS [51] or a hybrid of both schemes like FTSP [52] and PBS [53]. The receiver-receiver synchronization (RRS) completely eliminates the uncertainty at the sender, and thus performs better than the classical sender-receiver synchronization [54]. However, it has not been implemented in femtocell networks, and always needs a large number of exchanged timing messages. So, further research on the implementation of RRS in wireless femtocell networks is required.

2.4 Summary

Time synchronization is an important aspect of femtocell design. There are a number of femtocell operations that require accurate time synchronization. Based on the synchronization source, these methods can be categorized as: synchronization via GPS, synchronization via TV signals, synchronization via backhaul and synchronization via neighbouring cells listening. The advantages and disadvantages of the four major single-source femtocell synchronization methods are listed in Table 2.3.

This thesis mainly investigates two of these methods: synchronization via backhaul and

Table 2.3: Four Major Single-source Femtocell Synchronization Methods.

Options	Advantages	Disadvantages
GPS	High accuracy; location service	Poor indoor reception; additional cost
Backhaul	Stable; easy to implement	Accuracy can not be promised; potential link-asymmetry problem
Neighbour Cell Listening	Low cost	Requires coverage of synchronized neighbour cells
TV	Low cost	Location Dependent

synchronization via neighbouring cells listening. Chapter 3 and Chapter 4 focus on IEEE 1588 synchronization for femtocells. Femtocell synchronization via neighbouring cells listening will be studied in Chapter 5 and Chapter 6.

These synchronization sources are compatible with each other. In many situations, a femtocell may connect to more than one synchronization sources. And then the hybrid solution is to utilize all available synchronization sources. Only a few works have examined the hybrid solution. The fundamental way is to simply select the best possible synchronization source when available. For example, a hybrid GPS-IEEE 1588 method is introduced in [43]. This method is well suited for indoor femtocell deployment. As a preference, GPS-IEEE 1588 recovers timing and frequency from GPS. However, when GPS is not available due to poor GPS signal strength, GPS-IEEE 1588 switches to the reference of IEEE 1588 packets that are transmitted from the IEEE 1588 master so as to ensure phase and frequency are synchronized. However in some other scenarios, a femtocell may be able to use two comparable synchronization sources, such as neighbour cell listening and IEEE 1588, which have similar synchronization accuracy. In this situation, a more complicated combining method will lead to better synchronization performance. This area has not been investigated in existing works and will be examined in Chapter 7.

3 An Improved IEEE 1588 Time Synchronization Scheme

3.1 Introduction

IEEE 1588 [55] is a packet-based standard to synchronize independent clocks running on separate nodes of a distributed measurement and control system. IEEE 1588 provides a variety of mechanisms to allow a slave clock to synchronize to a master clock via the exchange of time stamp information. However, the synchronization performance of the conventional IEEE 1588 algorithm is affected by two main problems. Firstly, the conventional IEEE 1588 assumes symmetrical uplink and downlink delay, which is unrealistic in many cases and causes errors for the calculation of the time difference between the master clock and the slave clock when the links are asymmetric. Secondly, the conventional IEEE 1588 does not consider the impact of random delays, which are made up by jitter, queuing delay and other unexpected delays. In some situations, the random delay can seriously affect the synchronization quality.

In the literature, some works have been carried out to mitigate the above mentioned problems. In [56], the authors proposed the block burst transmission method, which calculates the asymmetric ratio before calculating the clock offset. However, it assumes that the transmission delays are asymmetric and fixed, neglecting the random delay in trans-

mission. In [49] and [48], the authors propose to use either dual clocks or a controllable buffer to improve the synchronization accuracy of IEEE 1588, at the expense of additional hardware, which is of course undesirable. The two-way clock offset estimation problem has been investigated in [57], [58] and [59]. These works studied several general estimation problems in two-way transmission based synchronization mechanism, but did not take the asymmetric communication link problem into account.

In this chapter, the clock offset estimation issue in an asymmetric communication link environment is studied. The contributions of this chapter are as follows. First, an improved IEEE 1588 based synchronization scheme is proposed by transmitting additional packets with different size. Second, based on the timing information transmitted between the master clock and the slave clock, the maximum likelihood estimators (MLEs) of the clock offset are derived and the corresponding Cramer-Rao lower bounds (CRLBs) are analyzed, where the random delays are assumed to follow Gaussian and exponential distributions, respectively. Third, the performance of the 'improved IEEE 1588' scheme is evaluated in different random delay environments and the impact of the transmitted packet size on the synchronization accuracy is analyzed.

The rest of the chapter is organized as follows. In Section 3.2, the system model is presented, including the femtocell IEEE 1588 synchronization scenario and the clock model. In Section 3.3, the basic mechanism of IEEE 1588 is introduced. In Section 3.4, three related works existing in the literature are briefly introduced. In Section 3.5, the improved IEEE 1588 based synchronization scheme is proposed. The MLEs of clock offset are derived and the corresponding CRLBs are analyzed for Gaussian and exponential random delay models. The mean squared errors (MSEs) of the estimators are also analyzed. In Section 3.6, the synchronization performance of the 'improved IEEE 1588' scheme and the estimators is evaluated by comparing with the conventional IEEE 1588 scheme and the block burst transmission method [56] in terms of clock offset bias error. Finally,

Section 3.7 concludes this chapter.

3.2 System Model

3.2.1 Femtocell IEEE 1588 Synchronization Scenario

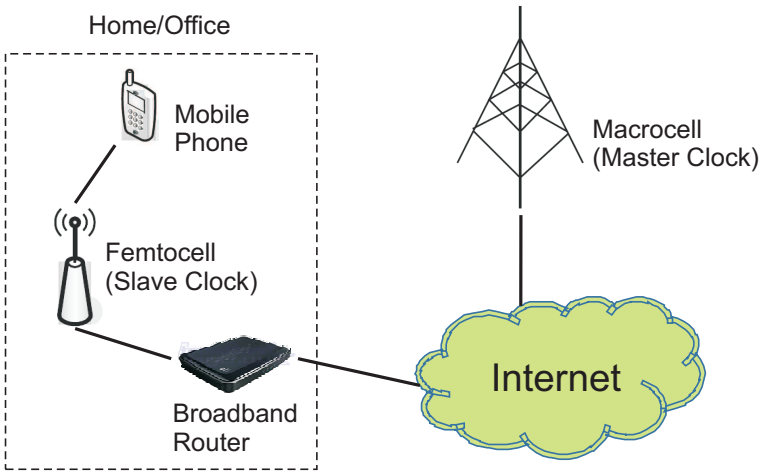

Figure 3.1: Femtocell IEEE 1588 synchronization scenario.

Fig. 3.1 shows the femtocell IEEE 1588 synchronization scenario. The femtocell is installed in a home or in an office, connected to the wireless operator's core network using one of the Wide Area Network (WAN) technologies such as Asymmetric Digital Subscriber Line (ADSL) or Very-high-bit-rate Digital Subscriber Line (VDSL) [47]. The femtocell acts as a slave clock in the IEEE 1588 mechanism to get it synchronized to the macrocell (master clock) in the wireless operator's core network.

3.2.2 Clock Model

Ideally, the clock of a femtocell should be configured as $T_s(t) = t$, where t is the ideal universal time and $T_s(t)$ is the femtocell clock at time t. However, due to the imperfection of the clock oscillator, clock offset (phase difference) and clock skew (frequency difference)

may exist, which will change the clock model to:

$$T_s(t) = \phi_0 + (1+\rho)t \tag{3.1}$$

where ϕ_0 is the initial clock offset (the clock offset when $t = 0$) and ρ is the clock skew. Note that ρ is assumed as a constant, because the clock skew normally changes very slowly [60, 61]. Some time synchronization works have considered the clock model where the clock skew is time-varying, such as in [62, 63, 64], however it is not that case in this thesis. Define $\phi(t)$ as the clock offset at time t and now:

$$\phi(t) = T_s(t) - t = \phi_0 + \rho t. \tag{3.2}$$

For the clock synchronization via message exchanging within a very short time, such as in IEEE 1588, the clock skew impact can be neglected and then the clock offset can be considered as a fixed value during the short period, i.e. $\rho = 0$. Then the femtocell clock can be reduced to:

$$T_s(t) = \phi + t \tag{3.3}$$

where ϕ is the constant clock offset.

3.3 Basic Mechanism of IEEE 1588

The IEEE 1588 messaging between the master clock and the slave clock in a synchronization process is illustrated in Fig. 3.2. Assuming no clock skew between the master clock T_m and the slave clock T_s, using clock model (3.3), the slave clock can be written as:

$$T_s = T_m + \phi \tag{3.4}$$

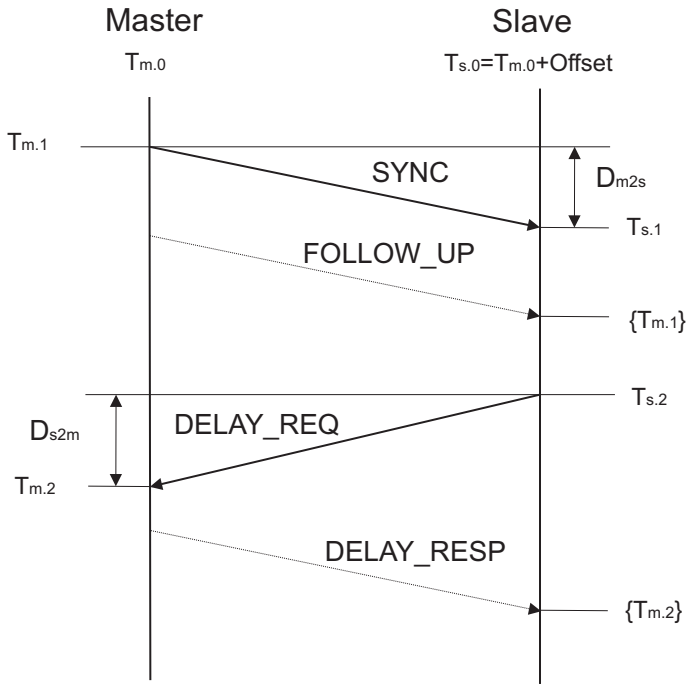

Figure 3.2: IEEE 1588 PTP messaging timing diagram.

where ϕ is the constant clock offset. The master clock triggers the synchronization process by sending a *SYNC* message, and measures the time $T_{m.1}$ at which the message is sent. The slave clock receives the *SYNC* message and stores the message arrival time $T_{s.1}$, based on its own clock. Then, the master clock sends a *FOLLOW_UP* message containing the value of the timestamp $T_{m.1}$. The slave clock sends a *DELAY_REQ* message and stores the transmission time with a timestamp $T_{s.2}$. When the master clock receives the *DELAY_REQ* message, it sends a *DELAY_RESP* message, which contains the arrival time of *DELAY_REQ* denoted as $T_{m.2}$. As analyzed in [57], the overall communication delay can be modeled as the sum of a fixed delay and a random delay. Then the downlink delay observation (U) and the uplink delay observation (V) can be recorded as:

$$U = T_{s.1} - T_{m.1} = d + \phi + X \tag{3.5}$$

$$V = T_{m.2} - T_{s.2} = l - \phi + Y \tag{3.6}$$

where d and l are the fixed delays, and X and Y are the random delays in the downlink and uplink respectively. Thus the clock offset can be calculated as:

$$\begin{aligned} \phi &= \frac{(T_{s.1} - T_{m.1}) - (T_{m.2} - T_{s.2})}{2} + \frac{l-d}{2} + \frac{Y-X}{2} \\ &= \hat{\phi} + \frac{l-d}{2} + \frac{Y-X}{2}. \end{aligned} \tag{3.7}$$

By assuming that the uplink and downlink delays are fixed and equal, the slave clock calculates the clock offset (ϕ) as:

$$\hat{\phi} = \frac{(T_{s.1} - T_{m.1}) - (T_{m.2} - T_{s.2})}{2}. \tag{3.8}$$

Then the slave clock adjusts its clock by subtracting $\hat{\phi}$, and thereby synchronizes with the master clock. However, as previously stated, the link delays are neither fixed nor equal in most cases. And so the asymmetry of the fixed delays and the random delays can seriously deteriorate the IEEE 1588 performance.

The fixed delay is dominated by the transmission delay, which is dependent on the data rate of the communication link. In asymmetric links, the uplink and downlink fixed delays are not equal. For instance, some femtocells use ADSL or VDSL to connect to the operator's core network. ADSL provides 1.5 to 1.8Mbps for downlink transmission and 16 to 640kbps for uplink transmission. VDSL provides 13 to 52Mbps for downlink and 1.5 to 2.3Mbps for uplink. This asymmetric characteristic introduces bias error if (3.8) is used to calculate the clock offset. And the bias error increases with the increase of the asymmetric ratio (defined as the ratio of the downlink fixed delay to the uplink fixed delay). On the other hand, the random part of the communication delay is also not negligible. In [65], it is shown that the random delay occurs in almost every step of a packet based communication. Moreover, the random delay is affected by the network configuration (including such aspects as the number of hops and the type of network

equipment) which makes it hard to predict, and can seriously deteriorate the IEEE 1588 performance. So, an improved IEEE 1588 synchronization method should be developed to mitigate the effect of the asymmetric links and random delays.

3.4 Related Works

In the literature, a number of studies have been proposed to solve the asymmetric link and random delay problems of IEEE 1588.

3.4.1 An Enhanced IEEE 1588 with Buffering Time Control

An Enhanced IEEE 1588 scheme with buffering time control was proposed in [48]. The goal of this scheme was to calculate the correct clock offset value in a slave clock for asymmetric links. This scheme modified the conventional IEEE 1588 in two aspects:

1. All the packet transit nodes (router or switch) along the synchronization packet propagation route must be deployed as shown in Fig. 3.3(a).

2. After conventional IEEE 1588 procedures, an additional procedure called Offset Correction is proposed as depicted in Fig. 3.3(b).

In the Offset Correction procedure, four messages (i.e. *M2S EXPLORER 1, M2S EXPLORER 2*, *S2M EXPLORER 1* and *S2M EXPLORER 2*) are transmitted between the 'master' and 'slave'. The packet length of *M2S EXPLORER 2* and *S2M EXPLORER 2* is set twice as long as that of *M2S EXPLORER 1* and *S2M EXPLORER 1*, and so are the respective buffering times of these messages. By doing this, the transmission delays and the buffering times of both uplink and downlink change at the same rate. This is based on the assumption that the transmission delay is proportional to the length of the packets, and that the buffering time can be precisely controlled. Then, by recording the sending

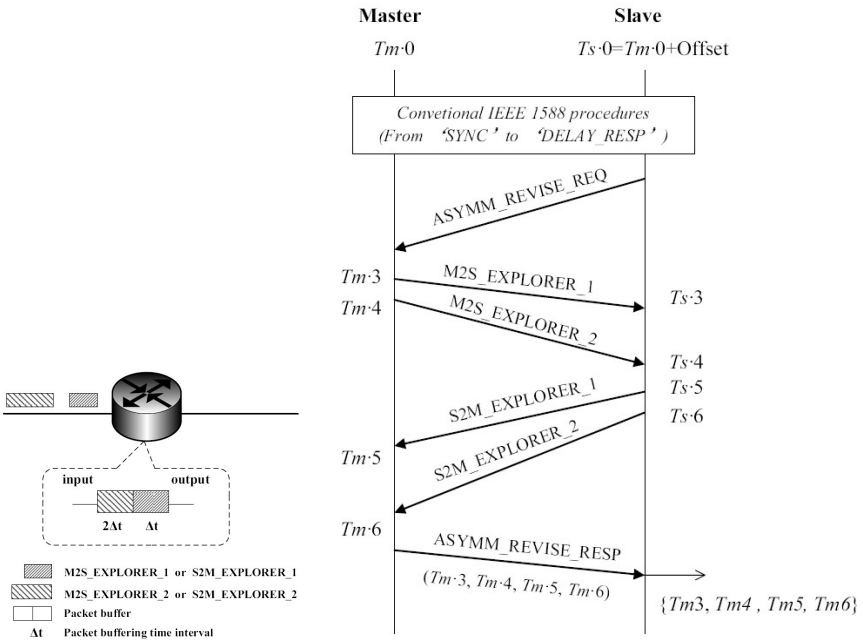

(a) Buffering time control in the packet transit nodes.

(b) The Offset Correction procedure.

Figure 3.3: Enhanced IEEE 1588 with buffering time control [48].

and receiving times of these four messages, four more equations can be written, which along with the conventional IEEE 1588 equations can help calculate the correct value of ϕ.

To summarize, this scheme proposes to eliminate the asymmetric error by controlling the buffering time and adding an Offset Correction procedure. However, it requires to change the deployment of all the packet transit nodes, which is not realistic in the femto-cell scenario.

3.4.2 IEEE 1588 Clock Synchronization Using Dual Slave Clocks in a Slave

An IEEE 1588 based synchronization scheme using dual 'slave clocks' in a 'slave' was proposed in [49]. In this scheme, every 'slave' is equipped with two 'slave clocks'. Fig. 3.4 depicts the schematic that generates the two slave clocks. A D-type Flip-Flop is

employed to divide the frequency by two; therefore, slave clock 2 runs at a frequency which is half of that of slave clock 1. Meanwhile, since both slave clocks are triggered by a single signal, they have the same clock offset. With the help of two 'slave clocks', the approach creates more equations than that in the conventional IEEE 1588. In this way, the approach requires only one-way time transfer to calculate the clock offset, and then the link-asymmetry will not impact on the clock offset calculation. This scheme also takes the random delay into account by proposing an estimator of the clock offset based on the statistical property of the random delay (i.e. assuming the random delay is normally distributed). However, as with the 'enhanced IEEE 1588 with buffering time control' scheme, this scheme also requires additional hardware modification, which makes it hard to implement into cost-constrained systems such as a femtocell.

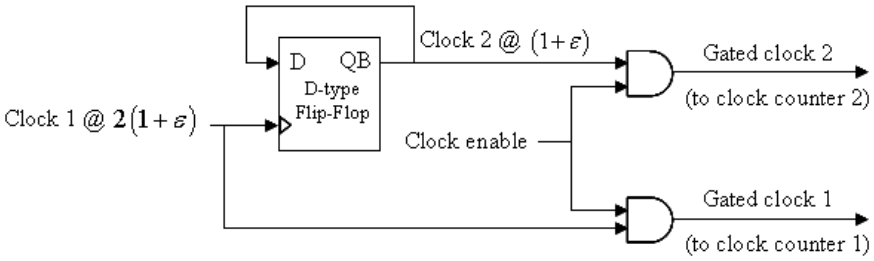

Figure 3.4: Schematic for the dual clocks generation [49].

3.4.3 An Enhanced IEEE 1588 using Block Burst Transmission

An Enhanced IEEE 1588 scheme using block burst transmission is proposed in [56]. After conventional IEEE 1588 procedure, an additional procedure called Block Burst Transmission was proposed in this scheme to calculate the asymmetric ratio of the communication link, as illustrated in Fig. 3.5. A slave clock sends an *Asymm_Check_Req* message to a master clock to trigger the block burst (several dummy packets) transmission. Each block transmission is a form of *Loop_Req* message which includes a flag to indicate whether a packet is start, middle or end of the burst. Also, this message has a dummy traffic which

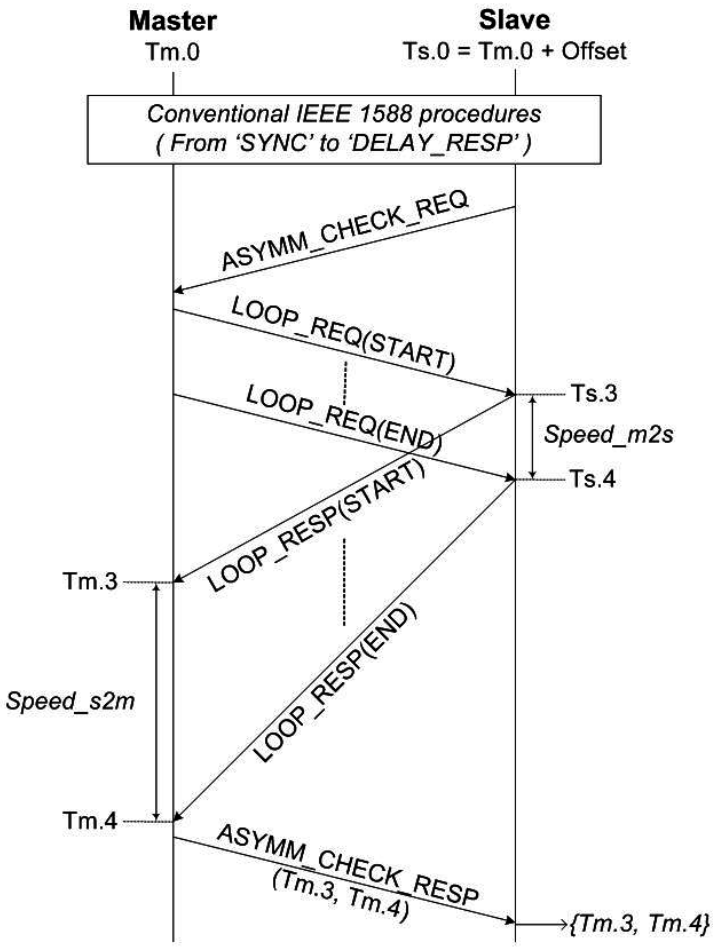

Figure 3.5: Block burst transmission for the asymmetric ratio calculation [56].

will be loop-backed to the master clock via the slave clock. When the first *Loop_Req* message is received at a slave clock, it re-transmits the received packet to the master clock, and stores the reception time as $T_{s.3}$. When the last *Loop_Req* message is received at the slave clock, it re-transmits the received packet to the master clock, and stores the reception time as $T_{s.4}$. When the first *Loop_Req* message is received at the master clock, it stores the reception time as $T_{m.3}$. When the last *Loop_Req* message is received at the master clock, it stores the reception time as $T_{m.4}$, and sends an *Asymm_Check_Resp* message to the slave clock with time records $T_{m.3}$ and $T_{m.4}$. After the Block Burst Transmission, the

asymmetric ratio (R) of the communication link can be calculated as:

$$R = \frac{T_{m.4} - T_{m.3}}{T_{s.4} - T_{s.3}}. \tag{3.9}$$

Neglecting the random delay impact, the clock offset (ϕ) can then be calculated from (3.7) and (3.9) as:

$$\hat{\phi} = \frac{R}{1+R}(T_{s.1} - T_{m.1}) + \frac{1}{1+R}(T_{m.2} - T_{s.2}). \tag{3.10}$$

Different from the previous two schemes, this scheme calculates the clock offset without additional hardware. However, it assumes that the transmission delays are asymmetric and fixed, neglecting the random delay in transmission.

From the above analysis, it is seen that neither of these schemes can mitigate both the IEEE 1588 asymmetric link and random delay problems at a low cost. Thus, further study is required to overcome the above problems.

3.5 An Improved IEEE 1588 Scheme and Clock Offset Estimation

An improved IEEE 1588-based synchronization scheme is proposed in this section, which is different from the conventional scheme in that the master clock and slave clock exchange packets with different lengths.

As mentioned before, in the IEEE 1588 messages exchanging, the overall delay of either uplink or downlink can be written as the sum of the fixed delay and the random delay. In many cases, the fixed delay is dominated by the transmission delay, which is dependent on the data rate of the communication link. In these circumstances, the fixed delay can be assumed to be proportional to the length of the packet, as in [56] and [48]. The random delay is usually modeled as either a Gaussian or an exponential random

variable [57]. If the random delay is mainly caused by a single queuing delay, then a single server M/M/1 queue can appropriately represent the delay, and the queuing time can be modeled as an exponential random variable as explained in [57]. On the other hand, if the random delay is the addition of a large number of independent random variables, then based on the central limit theorem, it can be approximately modeled as a Gaussian random variable. In this chapter, the fixed delays of the uplink and downlink are both assumed to be proportional to the length of the packet but with different constants of proportionality. Random delays are modeled as either Gaussian or exponential random variables according to the specific scenario. Random delays are assumed to be independent as the interval time between two adjacent synchronization processes is much larger than the delays.

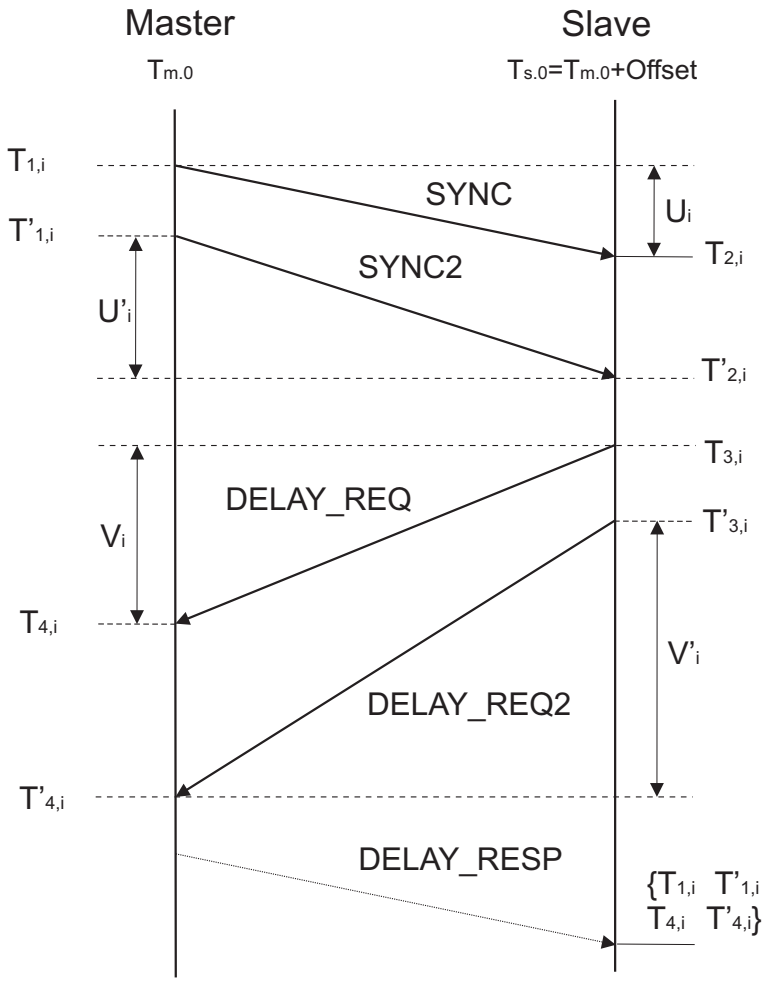

Figure 3.6: The improved IEEE 1588 synchronization scheme.

The improved IEEE 1588 synchronization scheme is illustrated in Fig. 3.6. The master clock starts the ith synchronization process by sending a *SYNC* message and a *SYNC2* message to the slave clock, and records the times $T_{1,i}$, $T_{1,i}^{'}$ at which the two messages are sent. These two messages are transmitted on packets with different lengths. The slave clock records the arrival time of these two messages as $T_{2,i}$ and $T_{2,i}^{'}$ respectively. Then a similar exchange is performed from the slave clock to the master clock. The messages are labeled as *DELAY_REQ* and *DELAY_REQ2*. The sending times recorded by the slave clock are $T_{3,i}$ and $T_{3,i}^{'}$. The arrival times recorded by the master clock are $T_{4,i}$ and $T_{4,i}^{'}$. Finally, the master clock sends a *DELAY_RESP* message back to the slave clock, which contains the timestamps $T_{1,i}$, $T_{1,i}^{'}$, $T_{4,i}$ and $T_{4,i}^{'}$. Thus, in the ith synchronization process, two downlink delay observations U_i, $U_i^{'}$ and two uplink delay observations V_i, $V_i^{'}$ can be recorded:

$$U_i \triangleq T_{2,i} - T_{1,i} = d + \phi + X_i \tag{3.11}$$

$$U_i^{'} \triangleq T_{2,i}^{'} - T_{1,i}^{'} = \alpha \cdot d + \phi + X_i^{'} \tag{3.12}$$

$$V_i \triangleq T_{4,i} - T_{3,i} = l - \phi + Y_i \tag{3.13}$$

$$V_i^{'} \triangleq T_{4,i}^{'} - T_{3,i}^{'} = \alpha \cdot l - \phi + Y_i^{'} \tag{3.14}$$

where d is the downlink fixed delay, l is the uplink fixed delay, α is the ratio of the second packet length to the first packet length ($\alpha > 1$), ϕ is the clock offset between the slave clock and the master clock, and X_i, $X_i^{'}$, Y_i, $Y_i^{'}$, are the random delays experienced in these four transmissions, respectively. Here, we assume that these variables are independent and identically distributed. With these four sets of observations, we propose to firstly estimate the fixed delays d and l, and then substitute them back to estimate the clock offset, ϕ. We will derive the MLEs and analyze the corresponding CRLBs for the clock offset based on two random delay models, i.e., Gaussian and exponential.

3.5.1 Clock Offset (ϕ) Estimation with a Gaussian Delay Model

With a Gaussian delay model, both the uplink and downlink random delays are assumed to follow the same Gaussian distribution with mean μ and variance σ^2.

Maximum Likelihood Estimation

Maximum likelihood estimation is a method of estimating the parameters of a statistical model. Let P_1, P_2, ..., P_n denote n independent, identically distributed random variables with density $f(p \mid \theta_1, \theta_2, ..., \theta_m)$ where $f(\cdot)$ is of known form and $\theta = (\theta_1, \theta_2, ..., \theta_m)$ belongs to a subset Θ of m dimensional space. Then the joint density of P_1, P_2, ..., P_n is given by $\prod_{i=1}^{n} f(p_i \mid \theta)$. Now consider this expression as a function of θ for fixed observations p_1, p_2, ..., p_n and denote this function by

$$L(\theta \mid p_1, p_2, ..., p_n) = L(\theta \mid \mathbf{p}). \tag{3.15}$$

Then $L(\theta \mid \mathbf{p})$ is called the likelihood function. The idea of the maximum likelihood principle is to search for the value $\hat{\theta}(\mathbf{p})$ which is most likely to have produced the observations p_1, p_2, ..., p_n:

$$\hat{\theta}(\mathbf{p}) = \arg\max_{\theta}[L(\theta \mid \mathbf{p})],\ \theta \in \Theta. \tag{3.16}$$

$\hat{\theta}(\mathbf{p})$ is then called the maximum likelihood estimator of θ. Since $\ln L(\theta \mid \mathbf{p})$ attains its maximum for the same value of θ as does $L(\theta \mid \mathbf{p})$, $\hat{\theta}(\mathbf{p})$ may also be found from

$$\hat{\theta}(\mathbf{p}) = \arg\max_{\theta}[\ln L(\theta \mid \mathbf{p})],\ \theta \in \Theta. \tag{3.17}$$

In practice it is usually more convenient from a mathematical point of view to work with $\ln L(\theta \mid \mathbf{p})$ than with $L(\theta \mid \mathbf{p})$.

Fixed Delay Estimation

After N synchronization processes, by subtracting (3.11) from (3.12), a simple estimator of d can be written as

$$\hat{d} = \frac{1}{N(\alpha-1)} \sum_{i=1}^{N} (U_i^{'} - U_i). \tag{3.18}$$

Similarly, l can be estimated as

$$\hat{l} = \frac{1}{N(\alpha-1)} \sum_{i=1}^{N} (V_i^{'} - V_i). \tag{3.19}$$

MLE of the Clock Offset

The likelihood function (from the multivariate p.d.f.) for $(\phi, \mu, \sigma^2, d, l)$ based on the independent observations $\{U_i\}_{i=1}^{N}$, $\{U_i^{'}\}_{i=1}^{N}$, $\{V_i\}_{i=1}^{N}$ and $\{V_i^{'}\}_{i=1}^{N}$ can be shown as

$$\begin{aligned} L(\phi) &= (2\pi\sigma^2)^{-2N} \exp\{-\frac{1}{2\sigma^2}[\sum_{i=1}^{N}(U_i - d - \phi - \mu)^2 \\ &+ \sum_{i=1}^{N}(U_i^{'} - \alpha \cdot d - \phi - \mu)^2 + \sum_{i=1}^{N}(V_i - l + \phi - \mu)^2 \\ &+ \sum_{i=1}^{N}(V_i^{'} - \alpha \cdot l + \phi - \mu)^2]\}. \end{aligned} \tag{3.20}$$

Differentiating the log-likelihood function gives

$$\begin{aligned} \frac{\partial \ln L(\phi)}{\partial \phi} &= -\frac{1}{\sigma^2} \sum_{i=1}^{N} [4\phi - (U_i + U_i^{'} - V_i - V_i^{'}) \\ &\quad + (1+\alpha)d - (1+\alpha)l]. \end{aligned} \tag{3.21}$$

Thus, we can derive the MLE of ϕ as

$$\begin{aligned} \hat{\phi} &= \arg\max_{\phi} [\ln L(\phi)] \\ &= \frac{1}{4N} \sum_{i=1}^{N} [(U_i + U_i^{'} - V_i - V_i^{'}) - (1+\alpha)d + (1+\alpha)l]. \end{aligned} \tag{3.22}$$

Substituting (3.18) and (3.19) into (3.22) gives:

$$\hat{\phi} = \frac{1}{2}(\frac{\alpha}{\alpha-1}\bar{U}_i - \frac{1}{\alpha-1}\bar{U_i^{'}} - \frac{\alpha}{\alpha-1}\bar{V}_i + \frac{1}{\alpha-1}\bar{V_i^{'}}) \tag{3.23}$$

where $\bar{U}_i$, $\bar{U_i^{'}}$, $\bar{V}_i$ and $\bar{V_i^{'}}$ are the mean values of the observations $\{U_i\}_{i=1}^{N}$, $\{U_i^{'}\}_{i=1}^{N}$, $\{V_i\}_{i=1}^{N}$ and $\{V_i^{'}\}_{i=1}^{N}$, respectively.

CRLB

The regularity condition holds for the given estimate since the expected value of (3.21) is zero [66]. Differentiating (3.21) with respect to ϕ gives:

$$\frac{\partial^2 \ln L(\phi)}{\partial \phi^2} = -\frac{4N}{\sigma^2}. \tag{3.24}$$

Hence, the CRLB for the MLE is given by

$$var(\phi) \geq -E[\frac{\partial^2 \ln L(\phi)}{\partial \phi^2}]^{-1} = \frac{\sigma^2}{4N}. \tag{3.25}$$

3.5.2 Clock Offset (ϕ) Estimation with Exponential Delay Model

Fixed Delay Estimation

With the exponential delay model, the uplink and downlink random delays are assumed to be exponentially distributed random variables both with a mean λ. Subtracting (3.11) from (3.12) yields:

$$U_i^{'} - U_i = (\alpha - 1)d + (X_i^{'} - X_i). \tag{3.26}$$

Since $X_i^{'}$ and X_i follow an exponential distribution, the likelihood function for (d,λ) can be derived as

$$\begin{aligned} L(d,\lambda) &= (\frac{\lambda}{2})^N \exp\{-\lambda|\sum_{i=1}^{N}[U_i^{'}-U_i-(\alpha-1)d]|\} \\ &\quad \times \mathbf{1}[U_{(1)} \geq d+\phi, U_{(1)}^{'} \geq \alpha \cdot d+\phi] \end{aligned} \tag{3.27}$$

where $\mathbf{1}[\cdot]$ is an indicator function and $U_{(1)}$ and $U_{(1)}^{'}$ are the minimum values of the observations $\{U_i\}_{i=1}^N$ and $\{U_i^{'}\}_{i=1}^N$, respectively. Then the MLE of d can be derived by maximizing (3.27) over the set $\Theta = \{(d,\phi) : d > 0, -\infty < \phi < \infty, \phi \leq U_{(1)} - d, \phi \leq U_{(1)}^{'} - \alpha \cdot d\}$. Similar to the experimental result of the MnLD (Minimum Link Delay) algorithm in [57] and from the theoretical analysis in [58], the MLE of d can be derived as:

$$\hat{d} = \frac{U_{(1)}^{'} - U_{(1)}}{\alpha - 1}. \tag{3.28}$$

Similarly, the MLE of l is

$$\hat{l} = \frac{V_{(1)}^{'} - V_{(1)}}{\alpha - 1} \tag{3.29}$$

where $V_{(1)}$ and $V_{(1)}^{'}$ denote the minimum values of the observations $\{V_i\}_{i=1}^N$ and $\{V_i^{'}\}_{i=1}^N$, respectively. Note that the MLEs of d and l are both calculated based on the minimum values of the observations. Since the random delays are exponentially distributed, they are much more likely to be close to zero than be close to, for example, the mean value λ. Thus here calculating the MLEs of d and l based on the minimum values of the observations can effectively alleviate the random delay impact. This is also verified in the experimental result of the MnLD (Minimum Link Delay) algorithm in [57].

MLE of the Clock Offset

The likelihood function for (ϕ,λ,d,l) based on the independent observations $\{U_i\}_{i=1}^N$, $\{U_i^{'}\}_{i=1}^N$, $\{V_i\}_{i=1}^N$ and $\{V_i^{'}\}_{i=1}^N$ is

$$\begin{aligned} L(\phi) &= \lambda^{-4N}\exp\{-\frac{1}{\lambda}[\sum_{i=1}^{N}(U_i-d-\phi) \\ &\quad +\sum_{i=1}^{N}(U_i^{'}-\alpha\cdot d-\phi)+\sum_{i=1}^{N}(V_i-l+\phi)+\sum_{i=1}^{N}(V_i^{'}-\alpha\cdot l+\phi)]\} \\ &\quad \times\mathbf{1}[U_{(1)}\geq d+\phi,U_{(1)}^{'}\geq\alpha\cdot d+\phi,V_{(1)}\geq l-\phi,V_{(1)}^{'}\geq\alpha\cdot l-\phi]. \end{aligned} \tag{3.30}$$

Clearly, ϕ is canceled out in the joint likelihood function. However, similar to (3.28) and (3.29), a MLE of the clock offset ϕ can be derived based on the observations $\{U_i\}_{i=1}^N$ and $\{V_i\}_{i=1}^N$ as

$$\hat{\phi}=\frac{1}{2}(U_{(1)}-V_{(1)}+l-d). \tag{3.31}$$

Substituting (3.28) and (3.29) into (3.31) produces:

$$\hat{\phi}=\frac{1}{2}(\frac{\alpha}{\alpha-1}U_{(1)}-\frac{1}{\alpha-1}U_{(1)}^{'}-\frac{\alpha}{\alpha-1}V_{(1)}+\frac{1}{\alpha-1}V_{(1)}^{'}). \tag{3.32}$$

The same estimator can be derived based on the observations $\{U_i^{'}\}_{i=1}^N$ and $\{V_i^{'}\}_{i=1}^N$.

CRLB

Substituting (3.11), (3.12), (3.13) and (3.14) into (3.32) gives:

$$\hat{\phi}=\phi+\frac{1}{2}(\frac{\alpha}{\alpha-1}X_{(1)}-\frac{1}{\alpha-1}X_{(1)}^{'}-\frac{\alpha}{\alpha-1}Y_{(1)}+\frac{1}{\alpha-1}Y_{(1)}^{'}) \tag{3.33}$$

where $X_{(1)}$, $X_{(1)}^{'}$, $Y_{(1)}$ and $Y_{(1)}^{'}$ denote the minimum values of $\{X_i\}_{i=1}^N$, $\{X_i^{'}\}_{i=1}^N$, $\{Y_i\}_{i=1}^N$ and $\{Y_i^{'}\}_{i=1}^N$, respectively. $X_{(1)}$, $X_{(1)}^{'}$, $Y_{(1)}$ and $Y_{(1)}^{'}$ all follow the exponential distribution with mean $\frac{\lambda}{N}$. Let $Z=X_{(1)}-Y_{(1)}$, $Z^{'}=X_{(1)}^{'}-Y_{(1)}^{'}$, and so Z and $Z^{'}$ follow Laplace distributions

with the location parameter $\upsilon = 0$ and the scale parameter $b = \frac{N}{\lambda}$. Thus, (3.33) can be written as

$$\hat{\phi} = \phi + \frac{1}{2}(\frac{\alpha}{\alpha-1}Z - \frac{1}{\alpha-1}Z^{'}). \tag{3.34}$$

The linear combination of Laplace random variables has been studied in [67]. Using the Corollary 2 in [67], the CDF of the estimation error $W = \frac{1}{2}(\frac{\alpha}{\alpha-1}Z - \frac{1}{\alpha-1}Z^{'})$ can be written as

$$F(w) = \begin{cases} \frac{\exp(\frac{w}{\alpha c})}{4(1+\frac{1}{\alpha})} + \frac{\exp(\frac{w}{\alpha c}) - \exp(\frac{w}{c})}{4(1-\frac{1}{\alpha})} + \frac{\exp(\frac{w}{c})}{2} - \frac{\exp(\frac{w}{c})}{4(1+\frac{1}{\alpha})}, & w < 0 \\ \\ 1 + \frac{\exp(-\frac{w}{c})}{4(1+\frac{1}{\alpha})} - \frac{\exp(-\frac{w}{c})}{2} - \frac{\exp(-\frac{w}{\alpha c}) - \exp(-\frac{w}{c})}{4(1-\frac{1}{\alpha})} - \frac{\exp(-\frac{w}{\alpha c})}{4(1+\frac{1}{\alpha})}, & w > 0 \end{cases} \tag{3.35}$$

where $c = \frac{N}{2(\alpha-1)\lambda}$. Differentiating (3.35) with respect to w and substituting $w = \hat{\phi} - \phi$ into it, the PDF of $\hat{\phi}$ as a function of ϕ is given by

$$f_q(\hat{\phi};\phi) = \frac{\alpha \exp(-\frac{|\hat{\phi}-\phi|}{\alpha c})}{2c(\alpha^2-1)} - \frac{\exp(-\frac{|\hat{\phi}-\phi|}{c})}{2c(\alpha^2-1)}. \tag{3.36}$$

Since $E[\frac{\partial \ln f_q(\hat{\phi};\phi)}{\partial \phi}] \neq 0$, the regularity condition of the CRLB is not satisfied and thus the CRLB does not exist.

3.5.3 Mean Squared Error Analysis

Similar to (3.33), (3.23) can be written as

$$\hat{\phi} = \phi + \frac{1}{2}(\frac{\alpha}{\alpha-1}\bar{X}_i - \frac{1}{\alpha-1}\bar{X_i^{'}} - \frac{\alpha}{\alpha-1}\bar{Y}_i + \frac{1}{\alpha-1}\bar{Y_i^{'}}) \tag{3.37}$$

where $\bar{X}_i$, $\bar{X_i^{'}}$, $\bar{Y}_i$ and $\bar{Y_i^{'}}$ denote the mean of $\{X_i\}_{i=1}^N$, $\{X_i^{'}\}_{i=1}^N$, $\{Y_i\}_{i=1}^N$ and $\{Y_i^{'}\}_{i=1}^N$, respectively. Since X_i, $X_i^{'}$, Y_i and $Y_i^{'}$ are independent random delays, the overall variance for

Gaussian delay model is:

$$\begin{aligned} var_{Gau}(\hat{\phi}) &= \frac{\sigma^2}{4N}[(\frac{\alpha}{\alpha-1})^2+(\frac{1}{\alpha-1})^2+(\frac{\alpha}{\alpha-1})^2+(\frac{1}{\alpha-1})^2] \\ &= \frac{(\alpha^2+1)\sigma^2}{2N(\alpha-1)^2}. \end{aligned} \tag{3.38}$$

Similarly, in the exponential random delay model, the variance is

$$\begin{aligned} var_{Exp}(\hat{\phi}) &= \frac{\lambda^2}{4N^2}[(\frac{\alpha}{\alpha-1})^2+(\frac{1}{\alpha-1})^2+(\frac{\alpha}{\alpha-1})^2+(\frac{1}{\alpha-1})^2] \\ &= \frac{(\alpha^2+1)\lambda^2}{2N^2(\alpha-1)^2}. \end{aligned} \tag{3.39}$$

In Fig. 3.7 and Fig. 3.8, the MSEs of the MLEs (3.23) and (3.32) are simulated for Gaussian and exponential random delay environments. It can be seen that the performance of the clock offset estimator is strongly dependent on the type of random delay environments, and so correctly modeling the random delay is critically important.

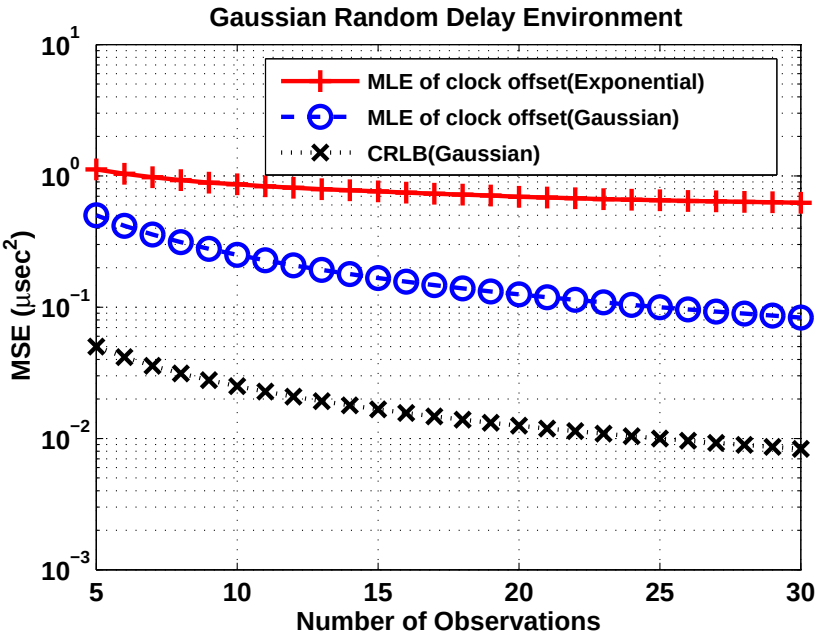

Figure 3.7: MSEs of both MLEs in a Gaussian random delay environment ($\sigma = 1\mu s, \alpha = 2$).

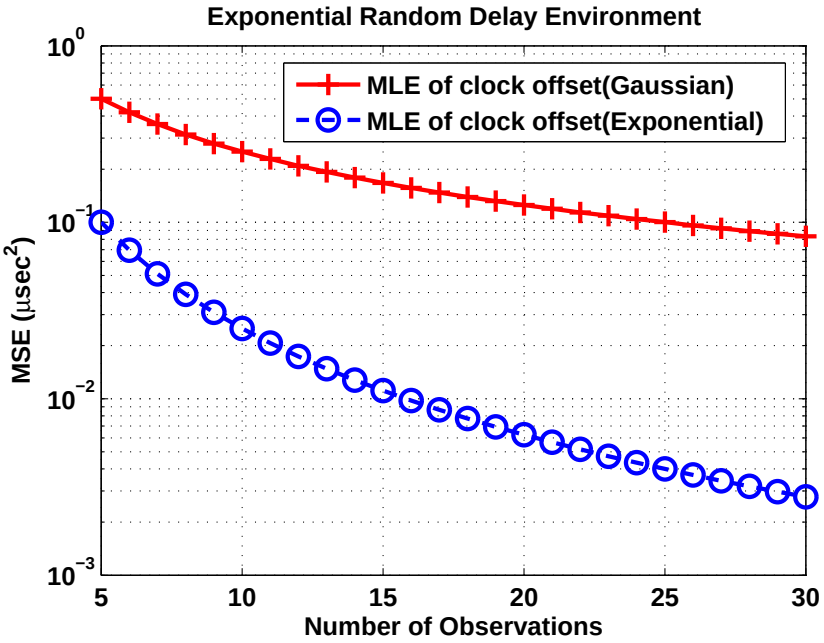

Figure 3.8: MSEs of both MLEs in an exponential random delay environment ($\lambda = 1\mu s, \alpha = 2$).

From (3.38) and (3.39), it can also be seen that the performance of both MLEs relate to the value of α instead of the absolute length of the packets. According to 3GPP, the minimum packet length is 64bytes and the maximum length is 1518 bytes [68]. Assuming IEEE 1588 transmits the original packets with minimum packet length, then $\alpha > 1$ and $\alpha_{\max} = 1518/64 \approx 23.7$.

In Fig. 3.9, the MSEs of the estimators (3.23) and (3.32) are plotted with respect to α from $\alpha = 2$ to $\alpha = 23.7$ when $N = 10$, for Gaussian distributed random delay and exponential distributed random delay environments, respectively. It can be seen that the larger the packet length ratio is, the better synchronization performance the MLEs can achieve. Clearly, choosing two packets with the biggest difference in length will lead to the best performance.

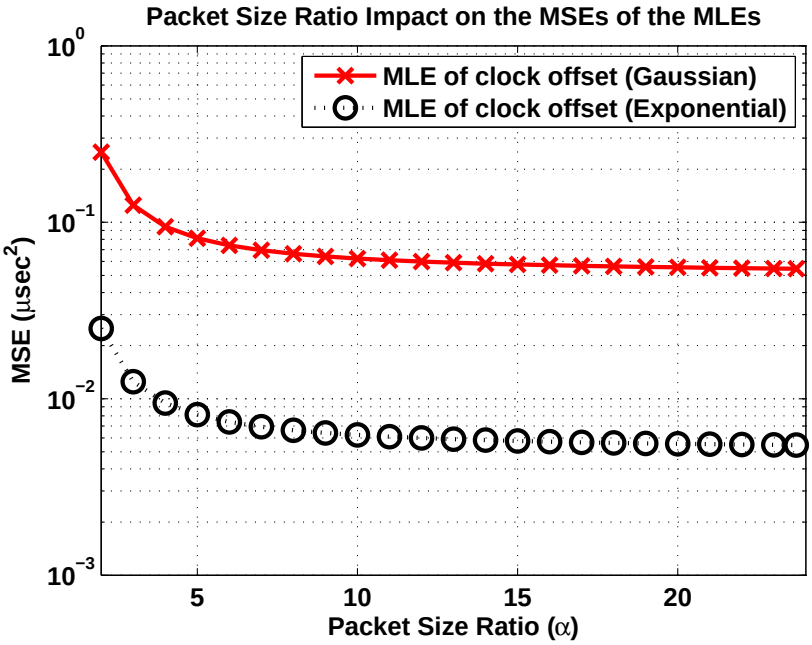

Figure 3.9: MSEs of both MLEs of clock offset as a function of the packet length ratio α ($\sigma = 1\mu s$, $\lambda = 1\mu s$, $N = 10$).

3.6 Performance Evaluation

In this section, the synchronization accuracy performance of the 'improved IEEE 1588' scheme is compared with the conventional IEEE 1588 scheme and the block burst transmission method [56] using Monte Carlo simulation. The IEEE 1588 synchronization process has been repeated 10000 times. In every process the packet delays are randomly generated based on the previously introduced delay model. Then the synchronization accuracies of these three methods are evaluated in terms of the bias error of the clock offset estimation against the asymmetric ratio after these synchronization processes, in Gaussian or exponential random delay environments in Fig. 3.10 and Fig. 3.11, respectively. The bias error is defined as the expected value of the absolute difference between the true clock offset value and the estimated value.

As the performance of the estimator relies on the number of observations, the 'improved IEEE 1588' scheme is simulated for both a short term case ($N = 10$) and a long term case

($N = 100$). In the Gaussian random delay scenario, $\mu = 100\mu s$ and $\sigma = 20\mu s$. In the exponential random delay scenario, $\lambda = 100\mu s$. The packet length ratio $\alpha = 23.7$. The downlink fixed delay $d = 1ms$. The asymmetric ratios (defined as the ratio of the uplink fixed delay to the downlink fixed delay, l/d) range from 2 to 16.

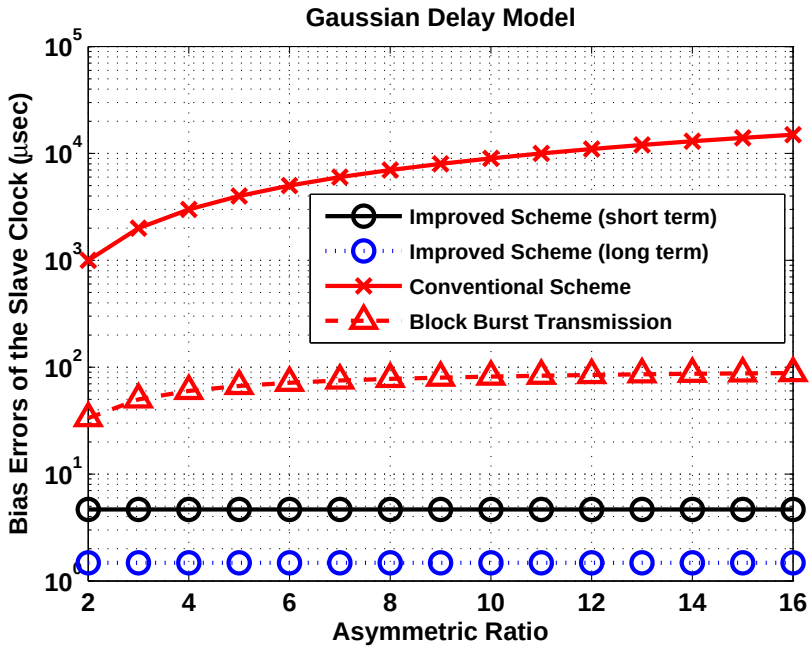

Figure 3.10: Bias errors of the slave clock for different synchronization schemes as a function of the asymmetric ratio in a Gaussian random delay model ($\mu = 100\mu s$, $\sigma = 20\mu s$, $\alpha = 23.7$).

Both figures show that the synchronization performances of the 'improved IEEE 1588' scheme and estimators are irrelevant to the asymmetric ratio. However, the bias error of the conventional IEEE 1588 scheme increases with the asymmetric ratio because of the unrealistic assumption of symmetric links. Although the block burst transmission scheme alleviates the impact of the asymmetric ratio, the bias error still increases with the asymmetric ratio because the scheme does not take the random delay into account. It is also shown that the bias errors of the 'improved IEEE 1588' scheme can reach an accuracy of $4.7\mu s$ in the short term case and $1.5\mu s$ in the long term case for all asymmetric ratios in a Gaussian random delay scenario. In the exponential random delay scenario, the

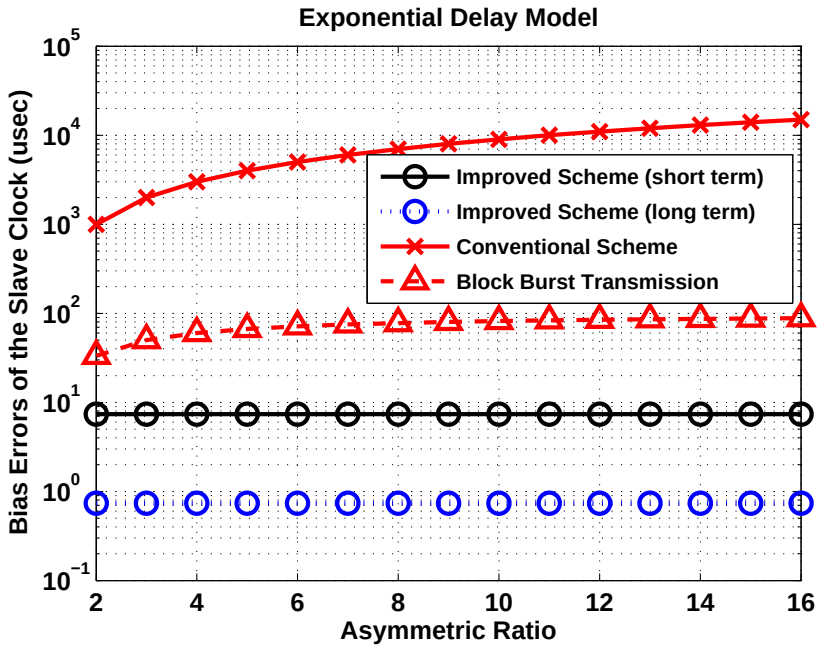

Figure 3.11: Bias errors of the slave clock for different synchronization schemes as a function of the asymmetric ratio in an exponential random delay model ($\lambda = 100\mu s$, $\alpha = 23.7$).

synchronization accuracies for the short term case and the long term case are $7.4\mu s$ and $0.74\mu s$, respectively. Compared with them, the bias error of the conventional IEEE 1588 scheme is always greater than $1ms$, and that of the block burst transmission method varies between $30\mu s$ and $90\mu s$. Both of them increase with the increase of the asymmetric ratio.

3.7 Summary

This chapter analyzed the basic mechanism of IEEE 1588 and proposed an 'improved IEEE 1588' synchronization scheme by utilizing additional packets with different lengths to overcome the asymmetric link and random delay problems of conventional IEEE 1588. Two different random delay models are considered, following Gaussian and exponential distributions respectively. Maximum likelihood estimators of clock offset are derived based on the proposed scheme for both random delay models and the corresponding

Cramer-Rao lower bounds are analyzed. It is shown that the performance of the clock offset estimators is dependent on the model of the random delay and the ratio of the length of the transmitted packets. Simulation results show that the 'improved IEEE 1588' synchronization scheme successfully addresses the problems of the asymmetric link and random delays, providing significantly better performance compared to the conventional IEEE 1588 approach and an existing method in terms of clock offset bias error. However, in the 'improved IEEE 1588' scheme, two more messages are transmitted in every IEEE 1588 synchronization process. This brings an additional undesirable overhead, which will be further reduced by another enhanced scheme that will be discussed in Chapter 4.

4 Variable-Length IEEE 1588 Time Synchronization Scheme

4.1 Introduction

In the last chapter, an 'improved IEEE 1588' scheme was proposed which can successfully overcome the asymmetric problem. However it needs two more packets in every IEEE 1588 synchronization process and this increases the traffic load. In this chapter, based on the 'improved IEEE 1588' scheme, a 'variable-length IEEE 1588' scheme is proposed to use variable-length packets in the IEEE 1588 messaging process, instead of inserting two additional packets in every process. Compared to the method proposed in Chapter 3, the number of overall transmitted packets is significantly reduced, and the synchronization error caused by the asymmetric link and random delays can still be mitigated effectively. Simulation results show that the synchronization performance of the 'variable-length IEEE 1588' scheme matches the 'improved IEEE 1588' scheme, and outperforms the conventional IEEE 1588 and the block burst transmission method [56].

In this chapter, the clock model without clock skew (i.e. clock skew is assumed to be zero) is first considered and the clock offset is assumed to be constant throughout the observation time, which is the same as in the last chapter. Consequently, the clock offset estimation method is similar to that of the 'improved IEEE 1588' scheme proposed in

Chapter 3. The maximum likelihood estimate ($\hat{\phi}$) for the clock offset (ϕ) is derived based on the 'variable-length IEEE 1588' scheme for two random delay models, i.e. Gaussian and exponential. The estimate $\hat{\phi}$, which depends on two new parameters α and β, is then optimized (in an MSE sense) with respect to these parameters.

Then the clock skew is taken into account, and the goal of the relative estimation method is to estimate the asymmetric fixed error, clock offset and clock skew at the same time. A Multiple Linear Regression (MLR) method is applied to solve the femtocell synchronization problem. Then the optimal values of the two new parameters, α and β, are analyzed. Simulation results show that the estimation accuracy of MLR outperforms that of the normal linear regression method.

The rest of the chapter is organized as follows. In Section 4.2, the main idea of the 'variable-length IEEE 1588' scheme is proposed. In Section 4.3, the clock offset estimation in the scenario without clock skew is proposed, and the maximum likelihood estimators (MLEs) of the clock offset for both the Gaussian and exponential random delay models are derived. The values of the two parameters (α, β) that are involved in the 'variable-length IEEE 1588' scheme are optimized in an MSE sense. The synchronization performance of the scheme is evaluated by comparing it with the conventional IEEE 1588, block burst transmission method [56] and the 'improved IEEE 1588' scheme using Monte Carlo simulations. In Section 4.4, a MLR based estimation method is proposed to estimate the asymmetric fixed error, clock offset and clock skew at the same time, when the clock skew is being taken into account. Both matrix and algebraic solutions are derived for the MLR. The optimal values of the parameters α and β are analyzed. And then the synchronization performance of the 'variable-length IEEE 1588' scheme with MLR is evaluated using Monte Carlo simulations. Finally, Section 4.5 concludes this chapter.

4.2 Main Idea

The clock offset - clock skew based clock model which has been introduced in Section 3.2.2 is also used in this chapter. As an IEEE 1588 synchronization process usually takes a very short time, the clock offset during the kth synchronization process can be expressed as:

$$\phi(t_k) = \phi_0 + \rho t_k, \tag{4.1}$$

where ϕ_0 is the initial clock offset, ρ is the constant clock skew and t_k is the ending time of the kth synchronization process. It is assumed that the master has an accurate clock. Then the slave clock at the ending time of the kth synchronization cycle, $T_s(t_k)$, can be written as:

$$T_s(t_k) = t_k + \phi(t_k). \tag{4.2}$$

The message exchanging process in the 'variable-length IEEE 1588' scheme is the same as in the conventional scheme, which is shown in Fig 3.2. However, the 'variable-length IEEE 1588' synchronization scheme is different from the conventional scheme in that the lengths of the *SYNC* and *DELAY_REQ* messages vary periodically.

Assuming that the packet lengths of the *SYNC* and *DELAY_REQ* messages in the conventional IEEE 1588 are each one unit, and then we propose to lengthen the length of the *SYNC* and *DELAY_REQ* messages by α times ($\alpha > 1$) for every β synchronization processes ($\beta \geq 2$), as shown in Fig. 4.1. Note that it is different from that in the 'improved IEEE 1588' scheme, where two more packets (i.e. *SYNC2* and *DELAY_REQ2*) are transmitted in every process, and the 'variable-length IEEE 1588' scheme transmits the same number of packets as the conventional IEEE 1588 does. Therefore, the overall number of transmitted packets is much less than that in the 'improved IEEE 1588' scheme.

After N synchronization processes, N_I downlink delay observations (U_i) and uplink delay observations (V_i) from the original length packets, and N_J downlink delay observa-

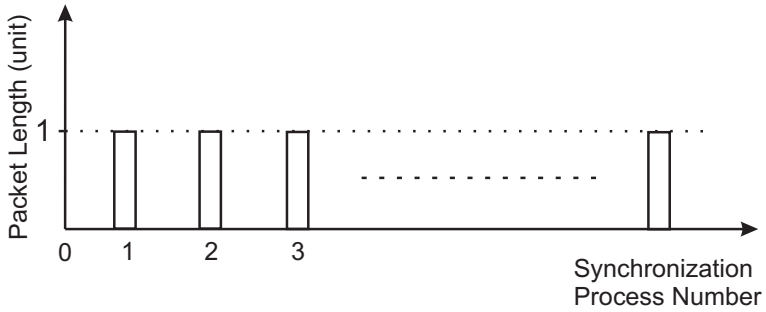

(a) The packet length of *SYNC* and *DELAY_REQ* messages is fixed in the conventional IEEE 1588

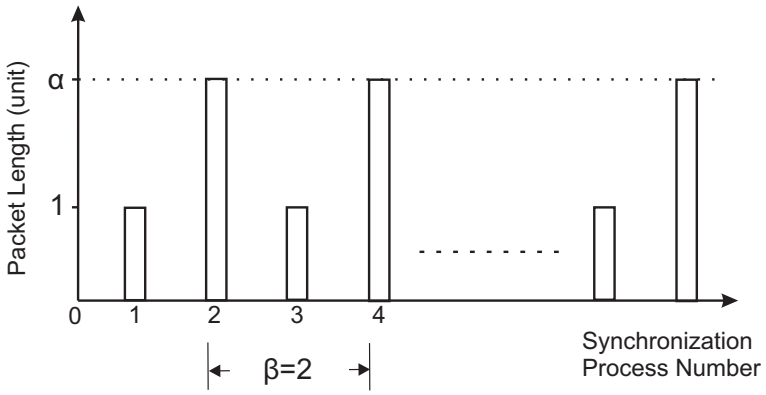

(b) The packet length of *SYNC* and *DELAY_REQ* messages varies in the 'variable-length IEEE 1588' scheme

Figure 4.1: Comparison between conventional IEEE 1588 and the 'variable-length IEEE 1588' scheme.

tions ($U_j^{'}$) and uplink delay observations ($V_j^{'}$) from the lengthened packets can be recorded, where $N = N_I + N_J = \beta \times N_J$. Similar to (3.11)-(3.14), these four groups of observations can be written as:

$$U_i = d + \phi(t_i) + X_i,\ i = 1,2,...,N_I \tag{4.3}$$

$$V_i = l - \phi(t_i) + Y_i,\ i = 1,2,...,N_I \tag{4.4}$$

$$U_j^{'} = \alpha d + \phi(t_j^{'}) + X_j^{'},\ j = 1,2,...,N_J \tag{4.5}$$

$$V_j^{'} = \alpha l - \phi(t_j^{'}) + Y_j^{'},\ j = 1,2,...,N_J \tag{4.6}$$

where t_i is the ending time of the ith synchronization process with original length packets, $t_j^{'}$ is the ending time of the jth synchronization process with lengthened packets, d is the

downlink fixed delay from the original length packets, l is the uplink fixed delay from the original length packets, and X_i, Y_i, $X_i^{'}$, $Y_i^{'}$, are the random delays in these four transmissions, respectively. As the fixed delays are proportional to the length of the packets as explained in Chapter 3, the products αd and αl are the downlink and uplink fixed delays for the N_J synchronization processes with lengthened packets, respectively.

In the next two sections, a simplified clock model without clock skew is firstly considered, and then clock skew is taken into account. This leads to different estimation methods.

4.3 Clock Offset Estimation with No Clock Skew

With the first scenario of the clock model, the clock skew is neglected ($\rho = 0$) and the clock offset is a constant ($\phi(t_k) = \phi$). The delay observations (4.3)-(4.6) can then be written as:

$$U_i = d + \phi + X_i, i = 1,2,...,N_I \tag{4.7}$$

$$V_i = l - \phi + Y_i, i = 1,2,...,N_I \tag{4.8}$$

$$U_j^{'} = \alpha d + \phi + X_j^{'}, j = 1,2,...,N_J \tag{4.9}$$

$$V_j^{'} = \alpha l - \phi + Y_j^{'}, j = 1,2,...,N_J \tag{4.10}$$

Similar to the last chapter, the estimate of the clock offset ϕ for both Gaussian and exponential random delay models will be derived based on these four sets of observations.

4.3.1 Clock Offset Estimation ($\hat{\phi}$) for Gaussian Delay Model

With a Gaussian delay model, both the uplink and downlink random delays (X_i, Y_i, $X_i^{'}$, $Y_i^{'}$) are assumed to follow the same Gaussian distribution with mean μ and variance σ^2.

After N synchronization processes, (4.7) and (4.9) can be rewritten as:

$$\sum_{i=1}^{N_I} U_i = N_I \cdot d + N_I \phi + \sum_{i=1}^{N_I} X_i \tag{4.11}$$

$$\sum_{j=1}^{N_J} U_j^{'} = N_J \cdot \alpha d + N_J \phi + \sum_{j=1}^{N_J} X_j^{'}. \tag{4.12}$$

Since $N_I = (\beta - 1) \times N_J$, then from (4.11) and (4.12):

$$(\beta - 1) \sum_{j=1}^{N_J} U_j^{'} - \sum_{i=1}^{N_I} U_i = N_I(\alpha - 1)d + (\beta - 1) \sum_{j=1}^{N_J} X_j^{'} - \sum_{i=1}^{N_I} X_i \tag{4.13}$$

and a simple MLE of d can easily be derived as:

$$\hat{d} = \frac{\bar{U_j^{'}} - \bar{U_i}}{\alpha - 1} \tag{4.14}$$

where $\bar{U_i}$ and $\bar{U_j^{'}}$ denote the means of $\{U_i\}_{i=1}^{N_I}$ and $\{U_j^{'}\}_{j=1}^{N_J}$, respectively. Similarly, the MLE for l is

$$\hat{l} = \frac{\bar{V_j^{'}} - \bar{V_i}}{\alpha - 1} \tag{4.15}$$

where $\bar{V_i}$ and $\bar{V_j^{'}}$ denote the mean of $\{V_i\}_{i=1}^{N_I}$ and $\{V_j^{'}\}_{j=1}^{N_J}$, respectively. The likelihood function (from the multivariate p.d.f.) based on the independent observations $\{U_i\}_{i=1}^{N_I}$, $\{U_j^{'}\}_{j=1}^{N_J}$, $\{V_i\}_{i=1}^{N_I}$ and $\{V_j^{'}\}_{j=1}^{N_J}$ can be written as:

$$\begin{aligned} L(\phi) &= (2\pi\sigma^2)^{-N} \exp\{-\frac{1}{2\sigma^2}[\sum_{i=1}^{N_I}(U_i - d - \phi - \mu)^2 \\ &+ \sum_{j=1}^{N_J}(U_j^{'} - \alpha d - \phi - \mu)^2 + \sum_{i=1}^{N_I}(V_i - l + \phi - \mu)^2 \\ &+ \sum_{j=1}^{N_J}(V_j^{'} - \alpha l + \phi - \mu)^2]\}. \end{aligned} \tag{4.16}$$

Therefore,

$$\begin{aligned}\frac{\partial \ln L(\phi)}{\partial \phi} &= -\frac{1}{2\sigma^2}[4N\phi - 2\sum_{i=1}^{N_I} U_i - 2\sum_{j=1}^{N_J} U_j^{'} + 2\sum_{i=1}^{N_I} V_i \\ &\quad +2\sum_{j=1}^{N_J} V_j^{'}) + 2(N_I + \alpha N_J)(d-l)] = 0 \end{aligned} \tag{4.17}$$

$$\begin{aligned}\Longrightarrow \hat{\phi} &= \arg\max_{\phi}[\ln L(\phi)] \\ &= \frac{1}{2N}[N_I\bar{U}_i + N_J\bar{U}_j^{'} - N_I\bar{V}_i - N_J\bar{V}_j^{'} \\ &\quad -(N_I + \alpha N_J)(d-l)]. \end{aligned} \tag{4.18}$$

Substituting (4.14) and (4.15) into (4.18) gives:

$$\hat{\phi} = \frac{1}{2}(\frac{\alpha}{\alpha-1}\bar{U}_i - \frac{1}{\alpha-1}\bar{U}_j^{'} - \frac{\alpha}{\alpha-1}\bar{V}_i + \frac{1}{\alpha-1}\bar{V}_j^{'}). \tag{4.19}$$

4.3.2 Clock Offset Estimation ($\hat{\phi}$) for Exponential Delay Model

With the exponential delay model, the uplink and downlink random delays (X_i, Y_i, $X_i^{'}$, $Y_i^{'}$) are assumed to be both exponentially distributed random variables with mean λ. The likelihood function based on the independent observations $\{U_i\}_{i=1}^{N_I}$, $\{U_j^{'}\}_{j=1}^{N_J}$, $\{V_i\}_{i=1}^{N_I}$ and $\{V_j^{'}\}_{j=1}^{N_J}$ in (4.3) to (4.6) can be written as:

$$\begin{aligned}L(\phi) &= \lambda^{-2N}\exp\{-\frac{1}{\lambda}[\sum_{i=1}^{N_I}(U_i - d - \phi) + \sum_{j=1}^{N_J}(U_j^{'} - \alpha\cdot d - \phi) + \sum_{i=1}^{N_I}(V_i - l + \phi) \\ &\quad + \sum_{j=1}^{N_J}(V_j^{'} - \alpha\cdot l + \phi)]\} \times \mathbf{1}[U_{(1)} \geq d+\phi, U_{(1)}^{'} \geq \alpha d + \phi, \\ &\quad V_{(1)} \geq l - \phi, V_{(1)}^{'} \geq \alpha l - \phi] \end{aligned} \tag{4.20}$$

where $\mathbf{1}[\cdot]$ is an Indicator Function and $U_{(1)}$, $U^{'}_{(1)}$, $V_{(1)}$ and $V^{'}_{(1)}$ are the minimum values of the observations $\{U_i\}_{i=1}^{N_I}$, $\{U^{'}_j\}_{j=1}^{N_J}$, $\{V_i\}_{i=1}^{N_I}$ and $\{V^{'}_j\}_{j=1}^{N_J}$, respectively. But ϕ vanishes on the R.H.S. of (4.20). However, if we rewrite the likelihood function based only on the observations $\{U_i\}_{i=1}^{N_I}$ and $\{U^{'}_j\}_{j=1}^{N_J}$ then:

$$\begin{aligned} L(\phi) &= \lambda^{-N}\exp\{-\frac{1}{\lambda}[\sum_{i=1}^{N_I}(U_i-d-\phi)+\sum_{j=1}^{N_J}(U^{'}_j-\alpha d-\phi)]\} \\ &\quad \times\mathbf{1}[U_{(1)}\geq d+\phi, U^{'}_{(1)}\geq \alpha d+\phi] \\ &= \lambda^{-N}\exp\{-\frac{1}{\lambda}[\sum_{i=1}^{N_I}U_i+\sum_{j=1}^{N_J}U^{'}_j-(N_I+\alpha N_J)d-N\phi]\} \\ &\quad \times\mathbf{1}[U_{(1)}\geq d+\phi, U^{'}_{(1)}\geq \alpha d+\phi]. \end{aligned} \tag{4.21}$$

Then the MLE for the clock offset ϕ based on the observations $\{U_i\}_{i=1}^{N_I}$ and $\{U^{'}_j\}_{j=1}^{N_J}$ can be derived by maximizing (4.21), which is the same as maximizing $(N_I+\alpha N_J)d+N\phi$, over the set $\Theta=\{(d,\phi): d>0, -\infty<\phi<\infty, \phi\leq U_{(1)}-d, \phi\leq U^{'}_{(1)}-\alpha\cdot d\}$. Define:

$$\begin{aligned} P(d,\phi) &= (N_I+\alpha N_J)d+N\phi \\ &= N\times(p\times d+\phi) \end{aligned} \tag{4.22}$$

where $p=\frac{N_I+\alpha N_J}{N}$ and $\alpha>1 \Longrightarrow 1<p<\alpha$. Similar to the analysis in [58], Fig. 4.2 shows that within the shaded region, the value of (d,ϕ) that maximizes $P(d,\phi)$ corresponds to the intersection of the two lines $\phi=U_{(1)}-d$ and $\phi=U^{'}_{(1)}-\alpha d$. By maximizing $P(d,\phi)$, the MLE of d when $U_{(1)}-d=U^{'}_{(1)}-\alpha d$ can be derived. That is

$$\hat{d}=\frac{U^{'}_{(1)}-U_{(1)}}{\alpha-1}. \tag{4.23}$$

And then the MLE of ϕ can be calculated as:

$$\begin{aligned}\hat{\phi} &= U_{(1)} - \hat{d} \\ &= \frac{\alpha}{\alpha-1}U_{(1)} - \frac{1}{\alpha-1}U'_{(1)}. \end{aligned} \tag{4.24}$$

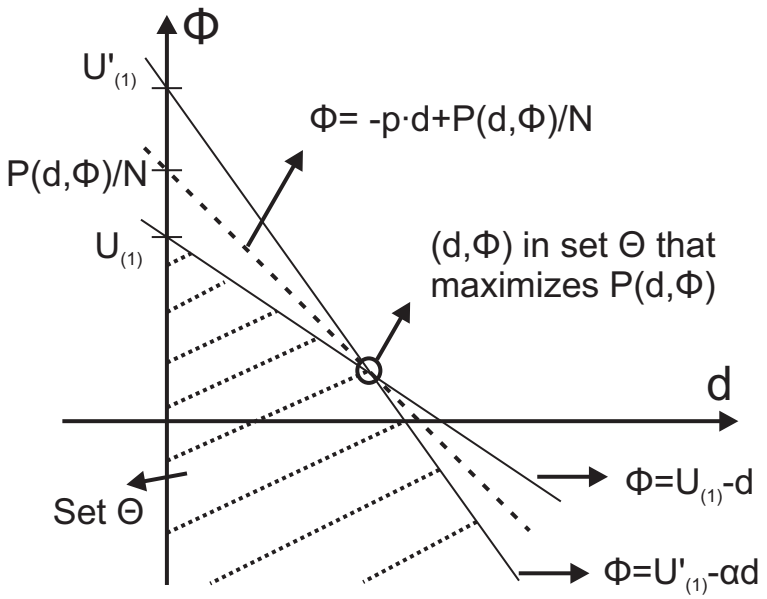

Figure 4.2: Set Θ and the point (d,ϕ) that maximizes (4.21) and (4.22).

A similar MLE of the clock offset ϕ can be derived based on the observations $\{V_i\}_{i=1}^{N_I}$ and $\{V'_j\}_{j=1}^{N_J}$ as:

$$\hat{\phi} = \frac{1}{\alpha-1}V'_{(1)} - \frac{\alpha}{\alpha-1}V_{(1)}. \tag{4.25}$$

Using a simple linear combination of (4.24) and (4.25) gives us the estimate of clock offset:

$$\hat{\phi} = \frac{1}{2}\left(\frac{\alpha}{\alpha-1}U_{(1)} - \frac{1}{\alpha-1}U'_{(1)} - \frac{\alpha}{\alpha-1}V_{(1)} + \frac{1}{\alpha-1}V'_{(1)}\right). \tag{4.26}$$

4.3.3 Parameter Optimization

Now $\hat{\phi}$ in (4.19) and (4.26) is parameterized on (α, β) – where $\bar{U}_i$, $U_{(1)}$, etc. are dependent on β. Parameters (α, β) can be optimized to minimize the mean squared estimation error

$E[|\hat{\phi}-\phi|^2] = var_{Gau}(\hat{\phi})$ or $var_{Exp}(\hat{\phi})$ (as $\hat{\phi}$ is unbiased), where $var_{Gau}(\hat{\phi})$ and $var_{Exp}(\hat{\phi})$ are the variances of (4.19) and (4.26), respectively. Substituting (4.7), (4.8), (4.9) and (4.10) into (4.19) yields:

$$\hat{\phi} = \phi + \frac{1}{2}(\frac{\alpha}{\alpha-1}\bar{X}_i - \frac{1}{\alpha-1}\bar{X}_j^{'} - \frac{\alpha}{\alpha-1}\bar{Y}_i + \frac{1}{\alpha-1}\bar{Y}_j^{'}) \tag{4.27}$$

where $\bar{X}_i$, $\bar{X}_j^{'}$, $\bar{Y}_i$ and $\bar{Y}_j^{'}$denote the means of the random delays $\{X_i\}_{i=1}^{N_I}$, $\{X_j^{'}\}_{j=1}^{N_J}$, $\{Y_i\}_{i=1}^{N_I}$ and $\{Y_j^{'}\}_{j=1}^{N_J}$, respectively. Since X_i, $X_j^{'}$, Y_i and $Y_j^{'}$ are independent random delays, then

$$\begin{aligned} var_{Gau}(\hat{\phi}) &= \frac{\sigma^2}{4N_I}\Big(\frac{\alpha}{\alpha-1}\Big)^2 \times 2 + \frac{\sigma^2}{4N_J}\Big(\frac{1}{\alpha-1}\Big)^2 \times 2 \\ &= \frac{\sigma^2}{2N}\Big[\frac{\alpha^2}{(\alpha-1)^2} \times \Big(\frac{\beta}{\beta-1}\Big) + \frac{\beta}{(\alpha-1)^2}\Big]. \end{aligned} \tag{4.28}$$

Similarly, by substituting (4.7), (4.8), (4.9) and (4.10) into (4.26) produces:

$$\hat{\phi} = \phi + \frac{1}{2}\Big(\frac{\alpha}{\alpha-1}X_{(1)} - \frac{1}{\alpha-1}X_{(1)}^{'} - \frac{\alpha}{\alpha-1}Y_{(1)} + \frac{1}{\alpha-1}Y_{(1)}^{'}\Big) \tag{4.29}$$

where $X_{(1)}$, $X_{(1)}^{'}$, $Y_{(1)}$ and $Y_{(1)}^{'}$ denote the minimum values of $\{X_i\}_{i=1}^{N_I}$, $\{X_j^{'}\}_{j=1}^{N_J}$, $\{Y_i\}_{i=1}^{N_I}$ and $\{Y_j^{'}\}_{j=1}^{N_J}$, respectively. Now, it is well-known that $X_{(1)}$, $X_{(1)}^{'}$, $Y_{(1)}$ and $Y_{(1)}^{'}$ will all follow exponential distributions with means of $\frac{\lambda}{N}$. The variance of (4.29) is

$$\begin{aligned} var_{Exp}(\hat{\phi}) &= \frac{\lambda^2}{4N_I^2}(\frac{\alpha}{\alpha-1})^2 \times 2 + \frac{\lambda^2}{4N_J^2}(\frac{1}{\alpha-1})^2 \times 2 \\ &= \frac{\lambda^2}{2N^2}[\frac{\alpha^2\beta^2}{(\alpha-1)^2(\beta-1)^2} + \frac{\beta^2}{(\alpha-1)^2}]. \end{aligned} \tag{4.30}$$

Optimization of β

Differentiating (4.28) with respect to β gives:

$$\frac{\partial var_{Gau}(\hat{\phi})}{\partial \beta} = \frac{\sigma^2}{2N}[\frac{1}{(\alpha-1)^2} - \frac{\alpha^2}{(\alpha-1)^2(\beta-1)^2}] \tag{4.31}$$

and then the optimum β for the Gaussian random delay model, $\beta_{opt,Gau}$, can be calculated by setting $\frac{\partial var_{Gau}(\hat{\phi})}{\partial \beta} = 0$:

$$\Longrightarrow \beta_{opt,Gau} = \arg\min_{\beta}[var_{Gau}(\hat{\phi})] = \alpha + 1. \tag{4.32}$$

(4.32) indicates that the the optimum β depends on the value of α. Likewise, the optimum β for the exponential random delay model, $\beta_{opt,Exp}$, can be obtained as:

$$\beta_{opt,Exp} = \arg\min_{\beta}[var_{Exp}(\hat{\phi})] = \alpha^{\frac{2}{3}} + 1. \tag{4.33}$$

Optimization of α

Similarly, differentiating (4.28) and (4.30) with respect to α gives:

$$\frac{\partial var_{Gau}(\hat{\phi})}{\partial \alpha} = -\frac{\sigma^2}{2N}[\frac{2\alpha\beta}{(\alpha-1)^3(\beta-1)} + \frac{2\beta}{(\alpha-1)^2}] \tag{4.34}$$

$$\frac{\partial var_{Exp}(\hat{\phi})}{\partial \alpha} = -\frac{\lambda^2}{2N^2}[\frac{2\alpha\beta^2}{(\alpha-1)^3(\beta-1)^2} + \frac{2\beta^2}{(\alpha-1)^2}]. \tag{4.35}$$

Because $\alpha > 1$ and $\beta \geq 2$, both $\frac{\partial var_{Gau}(\hat{\phi})}{\partial \alpha}$ and $\frac{\partial var_{Exp}(\hat{\phi})}{\partial \alpha}$ are always negative. Thus, both (4.28) and (4.30) decrease with the increase of α, and the biggest possible value of α is the optimal value for both models. According to 3GPP, as the smallest packet size is 64bytes and the largest size is 1518 bytes [68], then $\alpha_{\max} = 1518/64 \approx 23.7$. In Fig. 4.3, the MSEs of the estimators (4.19) and (4.26) are plotted against α for $\alpha = 2$ to $\alpha = 23.7$ when $N = 10$, $\beta = \alpha + 1$ in the Gaussian random delay model and $\beta = \alpha^{\frac{2}{3}} + 1$ in the exponential random delay model. It can be seen that the larger the packet size ratio α, the smaller the MSEs will be. Thus, $\alpha_{opt} = \alpha_{\max} = 23.7$, $\beta_{opt,Gau} \approx 24.7$ and $\beta_{opt,Exp} \approx 9.25$. Note that β can be non integer from the statistical point of view.

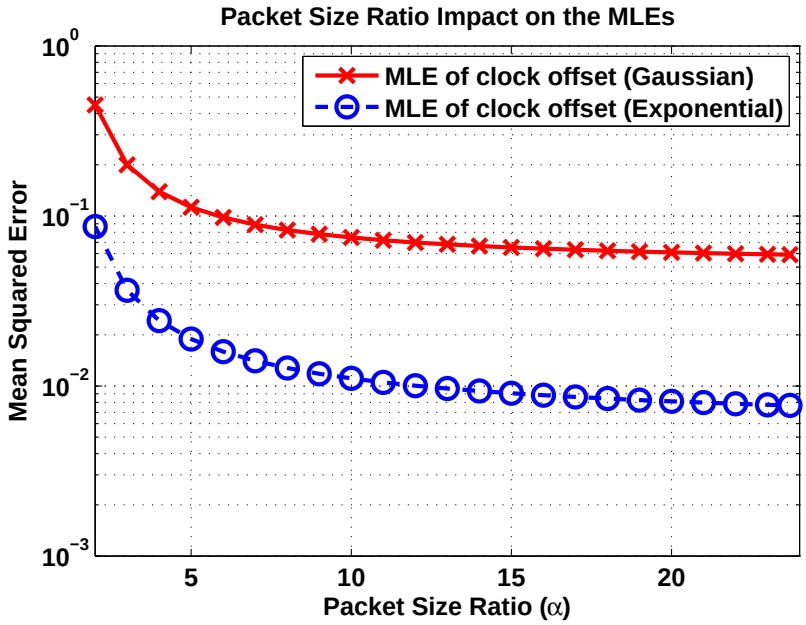

Figure 4.3: MSEs of the two estimators of clock offset ($\hat{\phi}$) as a function of the packet length ratio α ($\sigma = 1$, $\lambda = 1$, $N = 10$).

4.3.4 Synchronization Performance Evaluation

In this section, the synchronization accuracy of the 'variable-length IEEE 1588' scheme with no clock skew is evaluated using Monte Carlo simulations. The performance of the 'variable-length IEEE 1588' scheme is compared with the conventional scheme [55], the block burst transmission method [56] and the 'improved IEEE 1588' scheme. The synchronization accuracy is evaluated in terms of the root mean squared errors (RMSEs) of the clock offset estimation against the asymmetric ratio in the Gaussian or exponential random delay environments in Fig. 4.4 and Fig. 4.5, respectively. The asymmetric ratios (defined as the ratio of the uplink fixed delay to the downlink fixed delay, l/d) range from 2 to 16. The number of Monte Carlo simulation trials for each point is 10000. For the Gaussian random delay model, $\mu = 100\mu s$ and $\sigma = 20\mu s$. For the exponential random delay model, $\lambda = 100\mu s$. The number of observations is $N = 100$. Both α and β are set as the optimal values in each model. The downlink fixed delay $d = 1$ms. These simulation parameters were chosen based on empirically realistic values.

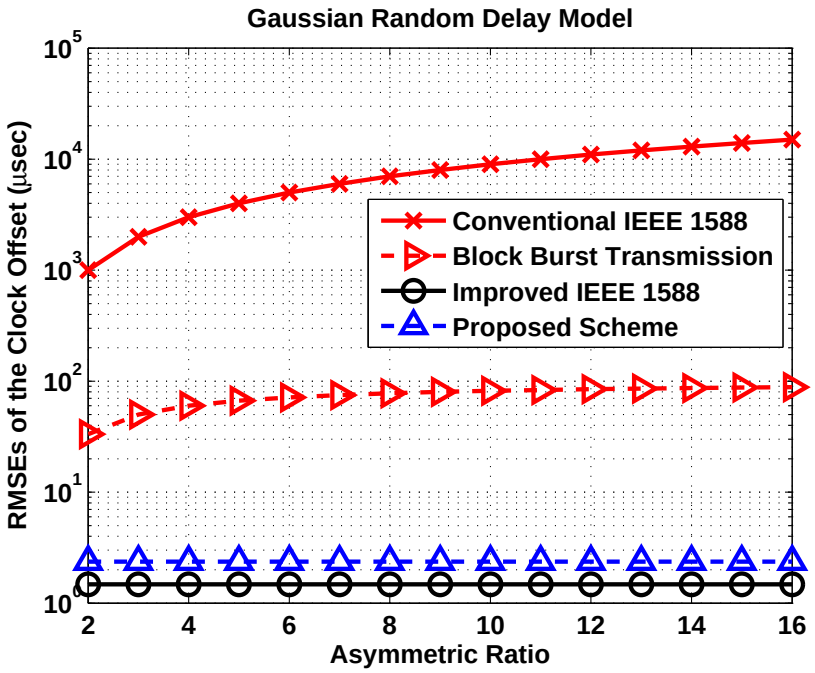

Figure 4.4: RMSEs of the slave clock offset estimate ($\hat{\phi}$) for different synchronization schemes as a function of asymmetric ratio with a Gaussian random delay model ($\mu = 100\mu s$, $\sigma = 20\mu s$, $N = 100$, $\alpha = 23.7$, $\beta = 24.7$).

Both Fig. 4.4 and Fig. 4.5 show that the synchronization performances of the 'variable-length IEEE 1588' scheme and the 'improved IEEE 1588 scheme' are not functions of the asymmetric ratio, while the RMSEs of the conventional scheme and the block burst transmission scheme increase with the asymmetric ratio. Clearly, the 'variable-length IEEE 1588' scheme can provide a similar synchronization accuracy as the 'improved IEEE 1588 scheme', but with fewer transmitted messages (i.e. two messages less in every synchronization process). Both techniques significantly outperform the conventional scheme and the block burst transmission method [56].

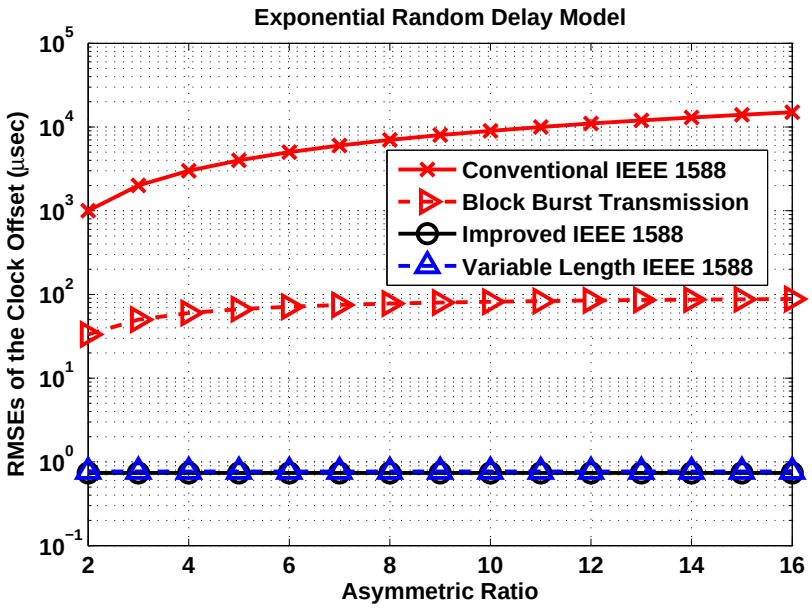

Figure 4.5: RMSEs of the slave clock offset estimate ($\hat{\phi}$) for different synchronization schemes as a function of asymmetric ratio with an exponential random delay model ($\lambda = 100\mu s, N = 100, \alpha = 23.7, \beta = 9.25$).

4.4 Multiple Linear Regression Based Clock Offset and Clock Skew Estimation

When the clock skew impact is taken into account ($\rho \neq 0$), the estimation method is completely different, since both the clock offset and the clock skew need to be estimated from (4.3)-(4.6) at the same time.

From (4.3) and (4.4), the conventional IEEE 1588 estimation of the clock offset is:

$$\begin{aligned} \hat{\phi}(t_i) &= \frac{U_i - V_i}{2} \\ &= \phi(t_i) + \frac{l-d}{2} + \frac{Y_i - X_i}{2}, i = 1,2,...,N_I. \end{aligned} \tag{4.36}$$

Define the asymmetric fixed error as $d_{asym} = \frac{l-d}{2}$ and the estimation noise as $\varepsilon_i = \frac{Y_i - X_i}{2}$. In this section, the random delays (X_i, Y_i, $X_j^{'}$ and $Y_j^{'}$) are all assumed to be Gaussian random variables with mean μ and variance σ^2 . Then ε_i also follows a Gaussian distribution with

$\varepsilon \sim (0, \frac{\sigma^2}{2})$. Similarly, the conventional IEEE 1588 estimates the clock offset from (4.5) and (4.6) as:

$$\begin{aligned}\hat{\phi}(t_j^{'}) &= \frac{U_j^{'} - V_j^{'}}{2} \\ &= \phi(t_j^{'}) + \alpha\frac{l-d}{2} + \frac{Y_j^{'} - X_j^{'}}{2} \\ &= \phi(t_j^{'}) + \alpha d_{asym} + \varepsilon_j,\ j = 1,2,...,N_J \end{aligned} \tag{4.37}$$

where $\varepsilon_j = \frac{Y_j^{'} - X_j^{'}}{2}$ is the estimation noise of the jth synchronization process with lengthened packets and also follows the Gaussian distribution $(0, \frac{\sigma^2}{2})$. Substituting (4.1) into (4.36) and (4.37) yields:

$$\hat{\phi}(t_i) = \phi_0 + \rho t_i + d_{asym} + \varepsilon_i,\ i = 1,2,...,N_I \tag{4.38}$$

$$\hat{\phi}(t_j^{'}) = \phi_0 + \rho t_j^{'} + \alpha d_{asym} + \varepsilon_j,\ j = 1,2,...,N_J. \tag{4.39}$$

Considering a slave clock can only be aware of the time on its own clock, the real time (t) can be represented using slave clock ($T_s(t)$) from (4.1) and (4.2):

$$t = \frac{T_s(t) - \phi_0}{1+\rho}. \tag{4.40}$$

Substitute (4.40) into (4.38) and (4.39) gives:

$$\begin{aligned}\hat{\phi}(t_i) &= \phi_0 + d_{asym} + \frac{T_s(t_i) - \phi_0}{1+\rho}\rho + \varepsilon_i \\ &= \frac{1}{\rho+1}\phi_0 + d_{asym} + \frac{\rho}{1+\rho}T_s(t_i) + \varepsilon_i,\ i = 1,2,...,N_I \end{aligned} \tag{4.41}$$

$$\begin{aligned}\hat{\phi}(t_j^{'}) &= \phi_0 + \alpha d_{asym} + \frac{T_s(t_j^{'}) - \phi_0}{1+\rho}\rho + \varepsilon_j \\ &= \frac{1}{\rho+1}\phi_0 + \alpha d_{asym} + \frac{\rho}{1+\rho}T_s(t_j^{'}) + \varepsilon_j,\ j = 1,2,...,N_J \end{aligned} \tag{4.42}$$

where $T_s(t_i)$ and $T_s(t_j^{'})$ are the corresponding recording times based on the slave clock at t_i and $t_j^{'}$. And then ϕ_0, ρ and d_{asym} can be estimated from the knowledge of the observations and recording times.

4.4.1 Normal Linear Regression Based Estimation

Linear regression methods have been used to solve the clock offset and clock skew estimation problem in scenarios like this [51, 69, 70]. However, if we use the conventional normal linear regression (NLR) based method to estimate ϕ_0, ρ and d_{asym} from the clock offset observations ($\hat{\phi}(t_i)$ and $\hat{\phi}(t_j^{'})$) and the slave clock observations ($T_s(t_i)$ and $T_s(t_j^{'})$) in (4.41) and (4.42) independently, the clock skew estimates ($\hat{\rho}$) from (4.41) and (4.42) may be different and computational complexity is high.

In the conventional normal linear regression (NLR) based method, the N_I clock offset observations from (4.41) can be combined into a matrix form as:

$$\hat{\phi}_I = H_I\theta_I + \varepsilon_I, \tag{4.43}$$

where $\hat{\phi}_I = [\hat{\phi}(t_1), \hat{\phi}(t_2), ..., \hat{\phi}(t_{N_I})]^T$, $\theta_I = [\theta_{0,I}, \theta_{1,I}]^T$, $\varepsilon_I = [\varepsilon_1, \varepsilon_2, ..., \varepsilon_{N_I}]^T$ and $H_I = [1, 1, ..., 1; T_s(t_1), T_s(t_2), ..., T_s(t_{N_I})]^T$, and

$$\theta_{0,I} = \frac{1}{\rho+1}\phi_0 + d_{asym}, \tag{4.44}$$

$$\theta_{1,I} = \frac{\rho}{1+\rho}. \tag{4.45}$$

In linear algebra, $H_I\theta_I \in R(H_I)$, where $R(H_I)$ is the column space of H_I. Then, the

square distance between $\hat{\phi}_I$ and $H_I\theta_I$, $S(\theta_I)$, can be defined as:

$$S(\theta_I) \equiv \left\|\hat{\phi}_I - H_I\theta_I\right\|^2. \tag{4.46}$$

Least regression method is to find the appropriate $\hat{\theta}_I$ such that the distance between $\hat{\phi}_I$ and $H_I\hat{\theta}_I$ is smaller than the one between $\hat{\phi}_I$ and any other linear combination of the column vectors of H_I. Thus, $H_I\hat{\theta}_I$ is the information which interprets $\hat{\phi}_I$ most accurately. Since

$$\begin{aligned}
S(\theta_I) &= (\hat{\phi}_I - H_I\theta_I)^T(\hat{\phi}_I - H_I\theta_I) \\
&= (\hat{\phi}_I - H_I\hat{\theta}_I + H_I\hat{\theta}_I - H_I\theta_I)^T(\hat{\phi}_I - H_I\hat{\theta}_I + H_I\hat{\theta}_I - H_I\theta_I) \\
&= (\hat{\phi}_I - H_I\hat{\theta}_I)^T(\hat{\phi}_I - H_I\hat{\theta}_I) + 2(\hat{\phi}_I - H_I\hat{\theta}_I)(H_I\hat{\theta}_I - H_I\theta_I) \\
&+ (H_I\hat{\theta}_I - H_I\theta_I)^T(H_I\hat{\theta}_I - H_I\theta_I) \\
&= \left\|\hat{\phi}_I - H_I\hat{\theta}_I\right\|^2 + \left\|H_I\hat{\theta}_I - H_I\theta_I\right\|^2 + 2(\hat{\phi}_I - H_I\hat{\theta}_I)^T H_I(\hat{\theta}_I - \theta_I).
\end{aligned} \tag{4.47}$$

If the estimate $\hat{\theta}_I$ of θ_I satisfies that $\hat{\phi}_I - H_I\hat{\theta}_I$ is orthogonal to every vector in $R(H_I)$, then $(\hat{\phi}_I - H_I\hat{\theta}_I)^T H_I = 0$. Thus

$$S(\theta_I) = \left\|\hat{\phi}_I - H_I\hat{\theta}_I\right\|^2 + \left\|H_I\hat{\theta}_I - H_I\theta_I\right\|^2. \tag{4.48}$$

Then

$$S(\hat{\theta}_I) = \left\|\hat{\phi}_I - H_I\hat{\theta}_I\right\|^2 \tag{4.49}$$

and for any other estimate $\hat{\theta}_I^{\star}$ of θ_I,

$$S(\hat{\theta}_I^{\star}) = \left\|\hat{\phi}_I - H_I\hat{\theta}_I\right\|^2 + \left\|H_I\hat{\theta}_I - H_I\hat{\theta}_I^{\star}\right\|^2 \geq S(\hat{\theta}_I). \tag{4.50}$$

Thus, $\hat{\theta}_I$ satisfying $(\hat{\phi}_I - H_I\hat{\theta}_I)^T H_I = 0$ is the least square estimate. Therefore,

$$\begin{aligned}
&(\hat{\phi}_I - H_I\hat{\theta}_I)^T H_I = 0 \\
\Leftrightarrow &{H_I}^T(\hat{\phi}_I - H_I\hat{\theta}_I) = 0 \\
\Leftrightarrow &{H_I}^T\hat{\phi}_I = {H_I}^T H_I\hat{\theta}_I \\
\Leftrightarrow &\hat{\theta}_I = ({H_I}^T H_I)^{-1}{H_I}^T\hat{\phi}_I. \qquad (4.51)
\end{aligned}$$

Then the least square estimation of θ_I is given by:

$$\hat{\theta}_I = ({H_I}^T H_I)^{-1}{H_I}^T\hat{\phi}_I. \qquad (4.52)$$

Similarly, the estimate of θ_J ($\hat{\theta}_J$) can also be calculated from (4.42) using NLR, where $\theta_J = [\theta_{0,J}, \theta_{1,J}]^T$ and

$$\theta_{0,J} = \frac{1}{\rho+1}\phi_0 + \alpha d_{asym} \qquad (4.53)$$

$$\theta_{1,J} = \frac{\rho}{1+\rho}. \qquad (4.54)$$

From the estimates of (4.44) and (4.53), d_{asym} can then be estimated as:

$$\hat{d}_{asym} = \frac{\hat{\theta}_{0,J} - \hat{\theta}_{0,I}}{\alpha - 1}. \qquad (4.55)$$

However, the estimation of ρ and ϕ_0 is not straightforward, because ρ-dependent $\theta_{1,I}$ and $\theta_{1,J}$ ought to be equal, but $\hat{\theta}_{1,I}$ and $\hat{\theta}_{1,J}$ are estimated from different observations and may be of different values. And the optimal combination of $\hat{\theta}_{1,I}$ and $\hat{\theta}_{1,J}$ would be exhausting and then significantly increase the already high computational complexity. Thus, instead of using conventional NLR, a multiple linear regression (MLR) based estimation method is proposed. It will not only avoid the aforementioned problem, but will also improve the estimation accuracy with much lower computational complexity.

4.4.2 Multiple Linear Regression Based Estimation

Rewrite the ending times of the total N synchronization processes as $t_k, k = 1,2,...,N$. The clock offset observations from (4.41) and (4.42) can now be written using a single formula with an introduced variable b_k:

$$\hat{\phi}(t_k) = \theta_0 + \theta_1 T_s(t_k) + \theta_2 b_k + \varepsilon_k \tag{4.56}$$

where

$$\theta_0 = \frac{1}{\rho+1}\phi_0 + d_{asym} \tag{4.57}$$

$$\theta_1 = \frac{\rho}{1+\rho} \tag{4.58}$$

$$\theta_2 = (\alpha-1)d_{asym} \tag{4.59}$$

and b_k is an introduced variable for the linear regression model with a value of 1 when the clock offset observation is from the N_J groups of lengthened packets or 0 for the N_I groups of original packets. So (4.56) can be written in matrix form as:

$$\hat{\phi}_M = H_M \theta_M + \varepsilon_M \tag{4.60}$$

where

$$\hat{\phi}_M = [\hat{\phi}(t_1), \hat{\phi}(t_2), ..., \hat{\phi}(t_k), ..., \hat{\phi}(t_N)]^T, \tag{4.61}$$

$$H_M = \begin{bmatrix} 1 & T_s(t_1) & b_1 \\ 1 & T_s(t_2) & b_2 \\ \vdots & \vdots & \vdots \\ 1 & T_s(t_N) & b_N \end{bmatrix}, \tag{4.62}$$

$$\theta_M = [\theta_0, \theta_1, \theta_2]^T, \tag{4.63}$$

$$\varepsilon = [\varepsilon_1, \varepsilon_2, ..., \varepsilon_N]^T. \tag{4.64}$$

Using MLR, the least square estimation of θ_M is given by:

$$\hat{\theta}_M = (H_M{}^T H_M)^{-1} H_M{}^T \hat{\phi}_M. \tag{4.65}$$

In some cases, (4.65) may not be preferred because it contains a matrix inverse computation. Write $\bar{T}_s = \frac{1}{N}\sum_{k=1}^{N} T_s(t_k)$, $\bar{b} = \frac{1}{N}\sum_{k=1}^{N} b_k$ and $\bar{\phi} = \frac{1}{N}\sum_{k=1}^{N} \hat{\phi}(t_k)$, then write $\ddot{T}_s(t_k) = T_s(t_k) - \bar{T}_s$, $\ddot{b}_k = b_k - \bar{b}$ and $\ddot{\phi}(t_k) = \hat{\phi}(t_k) - \bar{\phi}$, and so the algebraic solution for (4.56) can be derived from [71]:

$$\begin{aligned} \hat{\theta}_2 &= C^{-1} \times \Big[\sum_{k=1}^{N} \ddot{T}_s(t_k) b_k \times \sum_{k=1}^{N} \ddot{T}_s(t_k) \ddot{\phi}(t_k) \\ &\quad - \sum_{k=1}^{N} b_k \ddot{\phi}(t_k) \times \sum_{k=1}^{N} \ddot{T}_s(t_k)^2 \Big] \end{aligned} \tag{4.66}$$

$$\begin{aligned} \hat{\theta}_1 &= C^{-1} \times \Big[\sum_{k=1}^{N} \ddot{T}_s(t_k) \ddot{b}_k \times \sum_{k=1}^{N} \ddot{b}_k \ddot{\phi}(t_k) \\ &\quad - \sum_{k=1}^{N} \ddot{T}_s(t_k) \ddot{\phi}(t_k) \times \sum_{k=1}^{N} \ddot{b}_k^2 \Big] \end{aligned} \tag{4.67}$$

$$\hat{\theta}_0 = \ddot{\phi}(t_k) - \hat{\theta}_1 \bar{T}_s - \hat{\theta}_2 \bar{b} \tag{4.68}$$

where

$$C = \Big(\sum_{k=1}^{N} \ddot{T}_s(t_k) \ddot{b}_k \Big)^2 - \sum_{k=1}^{N} \ddot{b}_k^2 \times \sum_{k=1}^{N} \ddot{T}_s(t_k)^2. \tag{4.69}$$

From (4.66)-(4.68), the estimates of d_{asym}, ρ and ϕ_0 can be derived:

$$\hat{d}_{asym} = \frac{\hat{\theta}_2}{\alpha - 1} \tag{4.70}$$

$$\hat{\rho} = \frac{1}{1 - \hat{\theta}_1} - 1 \tag{4.71}$$

$$\hat{\phi}_0 = \frac{\hat{\theta}_0 - \frac{\hat{\theta}_2}{\alpha - 1}}{1 - \hat{\theta}_1}. \tag{4.72}$$

The estimated asymmetric fixed error, clock offset and clock skew can then be applied to compensate the asymmetric link and the femtocell clock.

Considering the linear regression process as trying to find a straight line that best (in a least square sense) represents plotted points of the observed data on a graph, the difference between NLR and MLR is illustrated in Fig. 4.6. As shown in Fig. 4.6(a), if the NLR approach is used to estimate the parameters in (4.41) and (4.42) separately, the two straight lines will not be parallel, which conflicts with the fact that the true values of the clock skews (ρ) are the same and thus the two lines should always have the same slope ($\frac{\rho}{1+\rho}$). By contrast, by using MLR as shown in Fig.4.6(b), the two lines are always parallel and have the same slope. In addition, the MLR based method only needs one linear regression computing process instead of two for NLR, and thus significantly reduces the computational complexity. Moreover, it will be shown later that the estimation of the asymmetric error obtained from (4.70) is more accurate than that from (4.55).

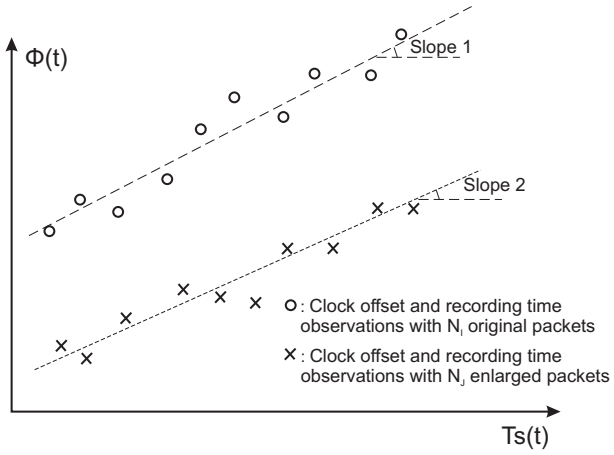

(a) With NLR, Slope 1 may not equal to Slope 2.

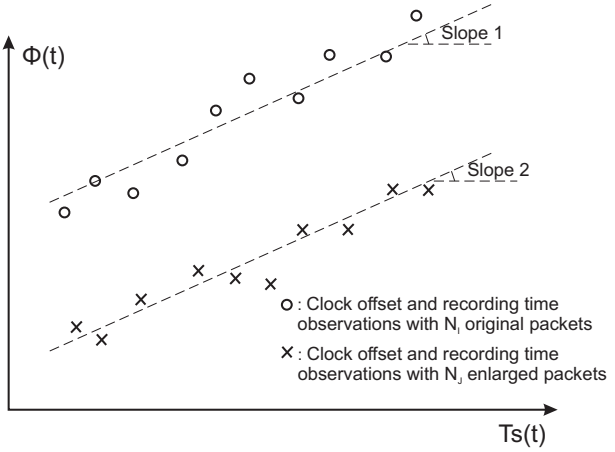

(b) With the proposed MLR, Slope 1 = Slope 2.

Figure 4.6: Normal linear regression vs. the proposed multiple linear regression.

4.4.3 Parameter Optimization

Similar as in Section 4.3.3, parameters (α, β) can be optimized to minimize the mean squared estimation error of the estimates in (4.70), (4.71) and (4.72). As analyzed in [71], these linear regression based estimators are all unbiased since the estimation noise is zero mean Gaussian distributed. Thus, the mean squared estimation error of these estimates equal to the variances of (4.70), (4.71) and (4.72), respectively.

The variances of the $\hat{\rho}$-dependent estimate $\hat{\theta}_1$ and the $\hat{d}_{asym}$-dependent estimate $\hat{\theta}_2$ are firstly analyzed. From [71], in the MLR based estimation, $var(\hat{\theta}_1)$ and $var(\hat{\theta}_2)$ are the

two elements on the diagonal of $\sigma_{sync}(\chi^T\chi)^{-1}$, where σ_{sync} is the standard deviation of the estimation noise (here $\sigma_{sync} = \frac{\sigma^2}{2}$) and

$$\chi = \begin{bmatrix} \ddot{T}_s(t_1) & \ddot{T}_s(t_2) & ... & \ddot{T}_s(t_N) \\ \ddot{b}_1 & \ddot{b}_2 & ... & \ddot{b}_N \end{bmatrix}^T. \tag{4.73}$$

Note that b_k and $\ddot{b}_k$ are only determined by β, while $T_s(t_k)$ and $\ddot{T}_s(t_k)$ are not related to either α or β, and

$$\begin{aligned} \chi^T\chi &= \begin{bmatrix} \sum_{k=1}^N \ddot{T}_s(t_k)^2 & \sum_{k=1}^N \ddot{b}_k\ddot{T}_s(t_k) \\ \sum_{k=1}^N \ddot{b}_k\ddot{T}_s(t_k) & \sum_{k=1}^N \ddot{b}_k^2 \end{bmatrix} \\ &\triangleq \begin{bmatrix} a_1 & a_2 \\ a_3 & a_4 \end{bmatrix}. \end{aligned} \tag{4.74}$$

Then

$$\begin{aligned} (\chi^T\chi)^{-1} &= \frac{1}{\det(\chi^T\chi)}\text{adj}(\chi^T\chi) \\ &= \frac{1}{a_1a_4 - a_2a_3}\begin{bmatrix} a_4 & -a_2 \\ -a_3 & a_1 \end{bmatrix} \\ &= \begin{bmatrix} \frac{a_4}{a_1a_4-a_2a_3} & \frac{-a_2}{a_1a_4-a_2a_3} \\ \frac{-a_3}{a_1a_4-a_2a_3} & \frac{a_1}{a_1a_4-a_2a_3} \end{bmatrix} \end{aligned} \tag{4.75}$$

when $a_1a_4 - a_2a_3 \neq 0$, which is true in our case, where $\text{adj}(\chi^T\chi)$ is the adjugate matrix of $\chi^T\chi$. And thus

$$var(\hat{\theta}_1) = \frac{\sigma^2}{2}(\frac{a_4}{a_1a_4 - a_2a_3})$$

$$var(\hat{\theta}_2) = \frac{\sigma^2}{2}(\frac{a_1}{a_1a_4 - a_2a_3}).$$

When $a_2a_3 = 0$, $\frac{a_4}{a_1a_4-a_2a_3}$ and $\frac{a_1}{a_1a_4-a_2a_3}$ are minimized, and then the minimum values of $var(\hat{\theta}_1)$ and $var(\hat{\theta}_2)$ are obtained. An example will be given later to show that it is possible that $a_2 = a_3 = 0$. Therefore

$$\begin{aligned} var(\hat{\theta}_1) &= \frac{\sigma^2}{2}(\frac{a_4}{a_1a_4 - a_2a_3}) \\ &= \frac{\sigma^2}{2} \times \frac{1}{a_1} \\ &= \frac{\sigma^2}{2}[\sum_{k=1}^{N} \ddot{T}_s(t_k)^2]^{-1} \end{aligned} \tag{4.76}$$

$$\begin{aligned} var(\hat{\theta}_2) &= \frac{\sigma^2}{2}(\frac{a_1}{a_1a_4 - a_2a_3}) \\ &= \frac{\sigma^2}{2} \times \frac{1}{a_4} \\ &= \frac{\sigma^2}{2}(\sum_{k=1}^{N} \ddot{b}_k^2)^{-1}. \end{aligned} \tag{4.77}$$

Since $var(\hat{\theta}_1)$ is only determined by the observing time $\ddot{T}_s(t_k)$, and so the estimation accuracy of $\hat{\theta}_1$ won't be affected by α or β. However, $var(\hat{\theta}_2)$ is a function of $\ddot{b}_k$, and can be calculated as:

$$\begin{aligned} var(\hat{\theta}_2) &= \frac{\sigma^2}{2}(\sum_{k=1}^{N} \ddot{b}_k^2)^{-1} \\ &= \frac{\sigma^2}{2}[\sum_{k=1}^{N} (b_k - \bar{b})^2]^{-1} \\ &= \frac{\sigma^2}{2}\left[N_I \times (0 - \frac{N-N_I}{N})^2 + N_J \times (1 - \frac{N-N_I}{N})^2\right]^{-1} \\ &= \frac{\sigma^2}{2}\left[N_I \times (-1 + \frac{N_I}{N})^2 + (N-N_I) \times (\frac{N_I}{N})^2\right]^{-1} \end{aligned} \tag{4.78}$$

where $N = N_I + N_J$ and $\bar{b} = \frac{1}{N}\sum_{k=1}^{N} b_k = \frac{N-N_I}{N}$. By setting $\frac{\partial var(\hat{\theta}_2)}{\partial N_I} = 0$, the value of N_I

that minimizes $var(\hat{\theta}_2)$ can be calculated:

$$N_I = \frac{N}{2} \tag{4.79}$$

so $\beta = \frac{N}{N_I} = 2$.

Now we know that $var(\hat{\theta}_2)$ is minimized when $a_2 = a_3 = 0$ and $\beta = 2$. When the original packets and the enlarged packets are transmitted by turn (i.e. $\mathbf{b} = [b_1, b_2, ..., b_k, ..., b_N] = [0, 1, 0, 1, ..., 0, 1]$) and the interval times between any two adjacent observations are the same, which makes $\ddot{T}_s(t_k)$ a zero-symmetric sequence, it can be proved that $a_2 = a_3 = \sum_{k=1}^{N} \ddot{b}_k \ddot{T}_s(t_k) = 0$ and $\beta = 2$. Therefore the optimum β is 2. The simulation result in Section 4.4.3 also proves this conclusion. Note that the optimum β here is different from (4.32) since the clock model and the mathematical tool used in these two scenarios are different.

Since $\hat{\rho}$ from (4.71) is only a function of $\hat{\theta}_1$, the values of α and β will not affect its estimation accuracy. For $\hat{d}_{asym}$ from (4.70), it is easily found that the bigger value of α leads to better estimation of d_{asym}. So the largest possible value of α is the optimal value. The simulation result in Section 4.4.3 also proves this conclusion.

The variance analysis of $\hat{\theta}_0$ and $\hat{\phi}_0$ is more complicated. However, it will be shown in Fig. 4.8 and Fig. 4.9 that the estimation accuracy of (4.72) is hardly affected by the values of α or β.

4.4.4 Performance Evaluation

The performance of the 'variable-length IEEE 1588' scheme (when $\rho \neq 0$) is evaluated in terms of the synchronization accuracy using Monte Carlo simulations. The initial clock offset $\phi_0 = 1$ sec. The clock skew $\rho = 100$ ppm (parts per million). The downlink fixed delay $d = 1m$ sec. The uplink fixed delay $l = 2m$ sec. The random delays are Gaussian random variables with mean $\mu = 100\mu$ sec and standard deviation $\sigma = 20\mu$ sec.

Figure 4.7 shows the comparison between the NLR base method and the proposed MLR based method in terms of the RMSEs of the estimations of the asymmetric fixed error d_{asym} (i.e. (4.55) and (4.70)), versus the number of overall synchronization processes N. The packet size ratio $\alpha = 4$. The period length parameter $\beta = 2$. It is noted that there is a gap of several microseconds between the RMSE lines of these two estimators. Obviously, the MLR based method provides much better accuracy on asymmetric fixed error estimation.

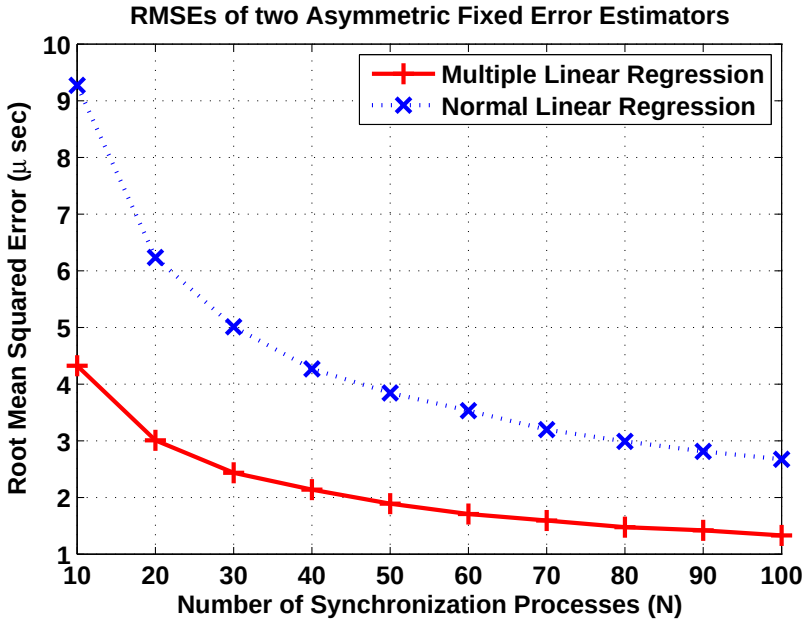

Figure 4.7: RMSEs of proposed estimator for d_{asym} versus the number of synchronization processes (N) in variable length IEEE 1588.

Figure 4.8 shows the MSEs of the proposed estimators of the asymmetric fixed error, clock skew and clock offset, versus the value of α. As stated in Section 4.3.3, $\alpha_{\max} = 23.7$. The number of overall synchronization processes $N = 20$. The period length parameter $\beta = 2$. It can be seen that the estimation accuracy of the asymmetric fixed error significantly improves when α increases. The clock offset estimation also slightly improves with an increase in α. However, the variation of α does not affect the clock skew estimation.

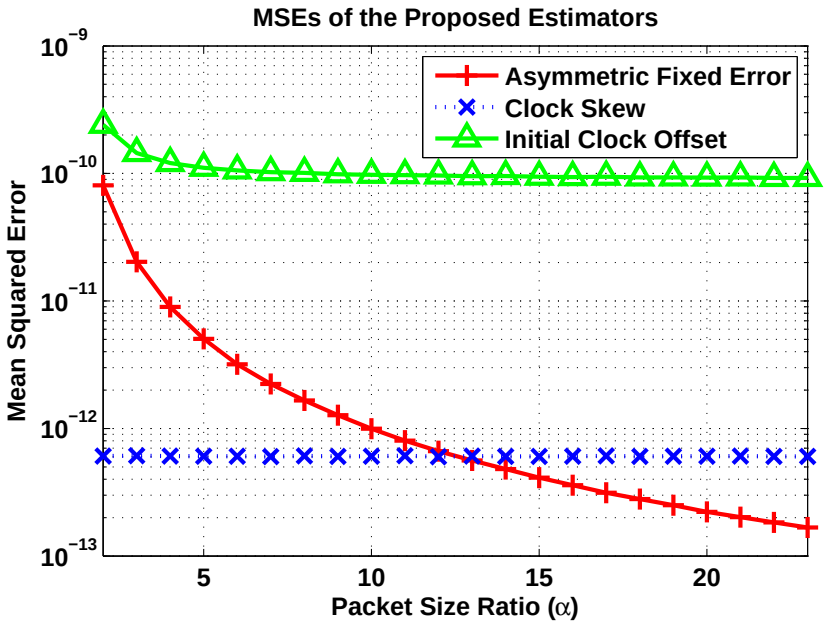

Figure 4.8: MSEs of (4.70), (4.71) and (4.72) against the value of α in variable length IEEE 1588.

In Fig. 4.9, the MSEs of the proposed estimators of asymmetric fixed error, clock skew and clock offset against the value of β ($2 \leq \beta \leq 20$) are illustrated. The packet size ratio is fixed as $\alpha = 4$. The value of N is set to be a relatively large value of 200, in order to give prominence to the impact of β. Similarly, the variation of β does not affect the clock skew estimation. The MSE of clock offset estimation varies slightly. The smallest MSE of the asymmetric fixed error estimation is achieved when $\beta = 2$.

The simulation results in both Fig. 4.8 and Fig. 4.9 prove the theoretical analysis in the Section 4.4.2. As can be seen in both these figures, the impact of β is not as significant as that of α or N. Clearly, increasing either the synchronization processes number N or the packet length ratio α can significantly improve the synchronization accuracy of the 'variable-length IEEE 1588' scheme.

Finally, the performance of the 'variable-length IEEE 1588' scheme with clock skew is compared with the conventional scheme and the block burst transmission method [56]. The synchronization accuracy is evaluated in terms of the RMSEs of the clock offset

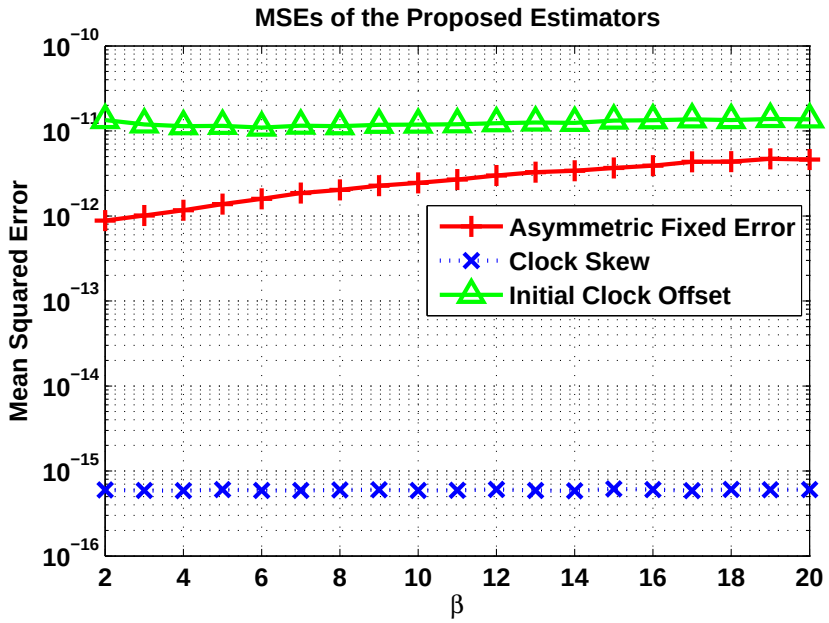

Figure 4.9: MSEs of (4.70), (4.71) and (4.72) against the value of β ($2 \leq \beta \leq 20$) in variable length IEEE 1588.

estimation against the asymmetric ratio. Now the asymmetric ratios (defined as the ratio of the uplink fixed delay to the downlink fixed delay, l/d) range from 2 to 16 in order to show the asymmetric ratio impact on these schemes, where the downlink fixed delay $d = 1m$sec. The number of overall synchronization processes $N = 20$. The period length parameter $\beta = 2$. The packet size ratio $\alpha = 23$. In order to show the impacts of random delays on these schemes, two Gaussian random delay models are considered in the simulation with mean $\mu_1 = 100\mu$ sec and standard deviation $\sigma_1 = 20\mu$ sec, or $\mu_2 = 200\mu$ sec and $\sigma_2 = 40\mu$ sec.

Fig. 4.10 shows that the synchronization performance comparison of these schemes, which is as expected very similar to that in Fig. 4.4. Thus the same conclusions can also be drawn.

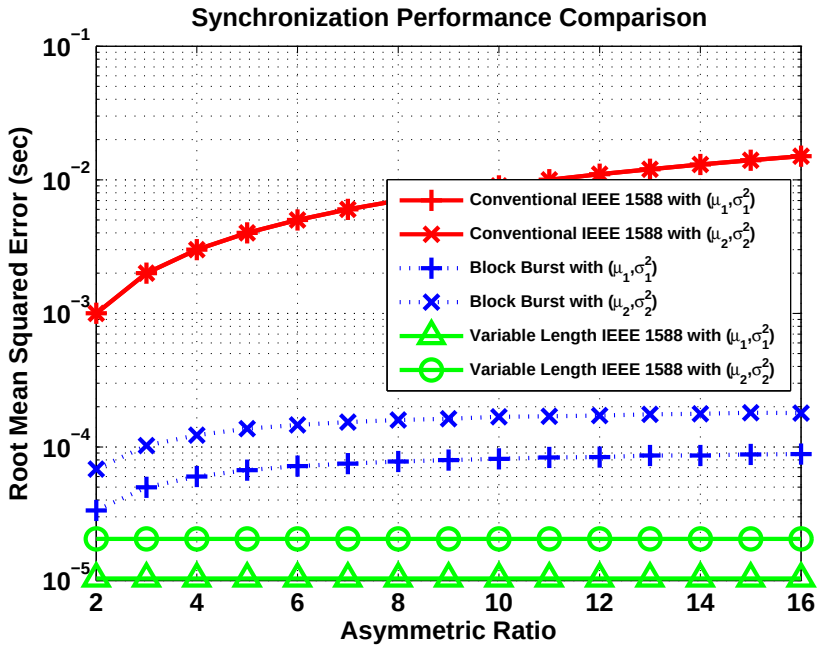

Figure 4.10: RMSEs of the slave clock for different synchronization schemes as a function of asymmetric ratio, with Gaussian random delay models (μ_1, σ_1^2) and (μ_2, σ_2^2).

4.5 Summary

This chapter has proposed a 'variable-length IEEE 1588' scheme by changing the lengths of the transmitted messages periodically to overcome the asymmetric link and random delay problems. Two scenarios of the clock model, no clock skew ($\rho = 0$) and with clock skew ($\rho \neq 0$), are both considered with the 'variable-length IEEE 1588' scheme. In the first scenario (when $\rho = 0$), the MLE of the clock offset ($\hat{\phi}$) is derived for both the Gaussian and exponential random delay models. The optimal values of the two parameters (α, β) that are involved in the 'variable-length IEEE 1588' scheme are derived based on MSE analysis. In the second scenario (when $\rho \neq 0$), a MLR based method is applied to solve the time synchronization problem and this significantly outperforms the conventional NLR based method. The optimal values of the two parameters (α, β) are derived based on the analysis and simulation results. Simulation results show that the 'variable-length IEEE 1588' scheme successfully addresses the problems of the asymmetric link

and random delays. The synchronization accuracy of the 'variable-length IEEE 1588' scheme is significantly better than that of the conventional IEEE 1588 approach and another existing method [56], and similar to the 'improved IEEE 1588' scheme of Chapter 3 but with a significantly reduced number of transmitted messages.

5 Receiver-Receiver Synchronization for Femtocells

5.1 Introduction

In this chapter, the femtocell synchronization via neighbour cell listening is investigated. Synchronization via neighbouring cells listening is cost effective because no extra provisions are required to ensure synchronization even on a regular basis. This is especially important when wireless backhaul is used.

Receiver-receiver synchronization (RRS) method is proved to be efficient and accurate in many wireless networks such as WSNs (Wireless Sensor Networks). This is because RRS completely eliminates the uncertainty at the sender, and thus performs better than the classical sender-receiver synchronization. Reference broadcast synchronization (RBS) has been proposed in [51], and is the most widely used RRS scheme. In RBS, a 'super node' is required, which is dedicated to broadcast the reference beacons to other nodes. Then other nodes can synchronize to the 'averaged time' by exchanging the receiving times of the reference beacons. However, in femtocell networks, the existence of the 'super node' is unrealistic. Also, the femtocell is required to synchronize to the universal accurate time, not the 'averaged time'. In addition, the high energy cost of message exchanging is also not desirable in femtocell networks. Therefore two new RRS based

synchronization schemes are proposed to apply this mechanism in femtocell networks.

Firstly, Scheme 1, a mobile station (MS) - assisted RRS based scheme is developed for femtocells. This simple scheme uses a mobile station to broadcast the reference beacons, and then help a femtocell synchronize to a macro base station.

Secondly, Scheme 2, a novel RRS based scheme suitable for wireless femtocell networks is considered. Different from RBS, an unsynchronized femtocell can start the synchronization process and then get synchronized to an accurate clock. In addition, the scheme significantly reduces the number of overall timing messages.

The rest of this chapter is organized as follows. In Section 5.2, wireless network synchronization and RBS are introduced. In Section 5.3, Scheme 1 is proposed. In Section 5.4, Scheme 2 is devised for wireless femtocell networks. Finally, Section 5.5 concludes this chapter.

5.2 Receiver-Receiver Synchronization for Wireless Networks

5.2.1 Introduction to Wireless Sensor Network Synchronization

Wireless time synchronization has been well investigated in wireless sensor networks (WSNs). A number of works have been done in this area, including some overview works such as [54, 72, 60]. Basically, synchronization schemes for wireless sensor networks can be categorized as sender-receiver synchronization such as timing-sync protocol for sensor networks (TPSN) [50], tiny-sync and mini-sync [73] and lightweight time synchronization [74], receiver-receiver synchronization like RBS [51] or a hybrid of both schemes like pairwise broadcast synchronization (PBS) [53]. The major problem of time synchronization is the existence of the packet delay. As shown in Figure 5.1, in all the wireless synchronization schemes, packet delay consist of four basic packet delay components:

Send time, Access time, Propagation time, and Receive time.

- **Send Time:** Time used to assemble the message and issue the send request to the MAC layer at the transmitter. Depending on the operating system and on the current processor load, the send time is non-deterministic and can be as high as hundreds of milliseconds.
- **Access Time:** Delay incurred waiting for access to the transmit channel up to the point when transmission begins. The access time is the least deterministic part of the message delivery in wireless networks varying from milliseconds up to seconds depending on the current network traffic.
- **Propagation Time:** The time it takes for the message to transmit from sender to receiver once it has left the sender. The propagation time is highly deterministic in wireless networks and it depends only on the distance between the two nodes.
- **Receive Time:** The time it takes for the receiver to receive the message. It's quite deterministic and depends on the length of the message.

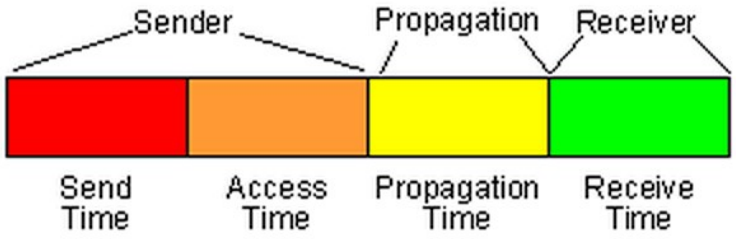

Figure 5.1: Packet delay components.

The difficulty to predict each packet delay component seriously limits the performance of the synchronization. As will be explained in Section 5.2.2, the receiver-receiver synchronization completely eliminates the uncertainty at the sender (i.e. Send Time and Access Time), and thus performs better than the classical sender-receiver synchronization.

5.2.2 Receiver-Receiver Synchronization

Receiver-receiver synchronization was first proposed in [51] as Reference Broadcast Synchronization (RBS). In RBS, one super node periodically sends beacon messages to its neighbors. Receivers use the messages' arrival times as references for comparing their clocks. The message contains no explicit timestamp, nor is it important exactly when it is sent. The accuracy of RBS is mostly determined by the amount of time each receiver takes to receive and process the reference packet. Taking a network with a super node and nodes i, j, k as an example, the RBS can be summarized as follows (where the subscript 'b' refers to the 'bth broadcast'):

1. The super node broadcasts a reference message;

2. Receivers i, j, k record the arrival times of the reference messages as T_b^i, T_b^j and T_b^k according to their own clocks;

3. Receivers i, j, k exchange their recorded times;

4. Receivers i, j, k calculate offsets between local and global times.

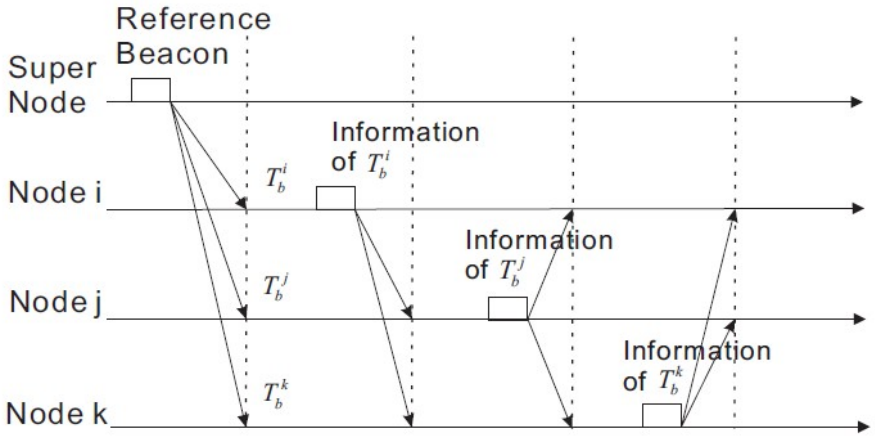

Figure 5.2: The bth message exchange process in RBS.

This is illustrated in Fig. 5.2. Thus the clock offset between node i and node j, denoted as offset$[i, j]$, can be calculated after they exchange their recorded times for m messages received from the super node. If m represents the number of reference broadcasts and T_b^i

/ T_b^j represent the times when node i / j receive the b^{th} reference broadcast respectively, then the clock offset can be calculated as:

$$\text{offset}[i,j] = \frac{1}{m}\sum_{b=1}^{m}(T_b^j - T_b^i). \tag{5.1}$$

Figure 5.3 shows that RBS eliminates error introduced by the Send Time and Access Time from 'critical path' [51] – where the delay difference accumulates. Because that Receiver 1 and Receiver 2 share the same Send Time and Access Time, the delay difference and the synchronization error between these two nodes will not be introduced from these two parts. However, in traditional sender-receiver synchronization, synchronization error from all four packet delay components will accumulate. In addition, in RBS the propagation time is considered to be effectively zero, because for a small wireless network, propagation time difference does not contribute significantly to the overall error. Thus the largest non-deterministic latency can be removed from the critical path by using the broadcast channel to synchronize receivers with one another. This results in significantly better precision synchronization than algorithms that measure the round-trip delay.

RBS is a highly influential synchronization scheme because it brings a completely new thinking to the time synchronization research. For RBS, the clock offset/skew estimation problem has been investigated in [75, 76, 77]. [78] studies the influence of jitter delay and packet loss resulting from the lower layer protocol on RBS. In [79], the author has analyzed the security of RBS and proposed optimization on security for the algorithm. In addition, a number of synchronization schemes have been developed based on RBS, such as [80, 81, 82, 53, 83], where the latter two works have combined RRS and the conventional sender-receiver synchronization.

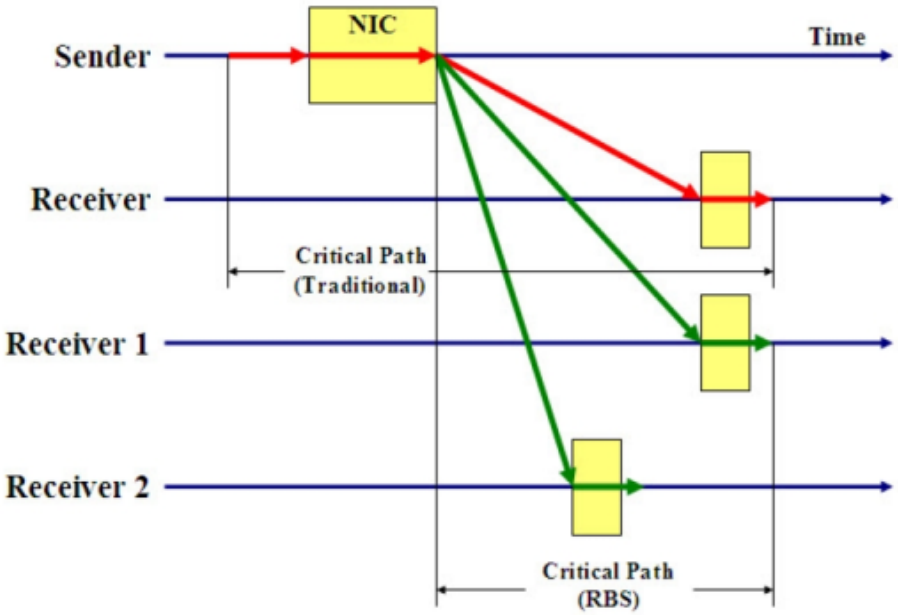

Figure 5.3: Critical path comparison. In sender-receiver synchronization, 'critical path' contains all four parts of the packet delay components. In RBS, the Send Time and Access Time are eliminated from 'critical path'.

5.2.3 Disadvantages of RBS

RBS protocol can achieve a relatively high accuracy, but the number of exchanged messages between nodes is large. For a single-hop domain network with M nodes, and where the number of reference broadcasts is N, at least $N \times M$ message will be exchanged. This will introduce a heavy load to the network.

In addition, RBS is generally used in small centralized wireless networks, in which the propagation time differences can be neglected. But in cellular networks the distance between a BS and an mMS might be as big as 3km, then the propagation delay becomes significant in the synchronization error. This will be elaborated upon later in Section 5.3. In a decentralized network which does not have a 'super node', RBS cannot be applied. Furthermore, the nodes in RBS are synchronized to an 'averaged time' instead of the universal accurate time, and this is not desirable for femtocells. To overcome these drawbacks, two RBS based schemes are proposed for different femtocell synchronization

scenarios to ensure a more comprehensive availability.

5.3 Scheme 1: MS-Assisted Receiver-Receiver Synchronization for femtocells

5.3.1 Synchronization Scenario

In a typical macrocell network, the mobile users are synchronized to the macrocell base station (mBS) by transmitting signals to the mBS with a latency related to the distance from themselves to the mBS [84]. However, femtocells normally cannot use this method because a femto base station (fBS) cannot always receive the signal from macro base station due to the poor indoor macro-signal coverage or because some fBSs do not have uplink and cannot measure the round-trip delay.

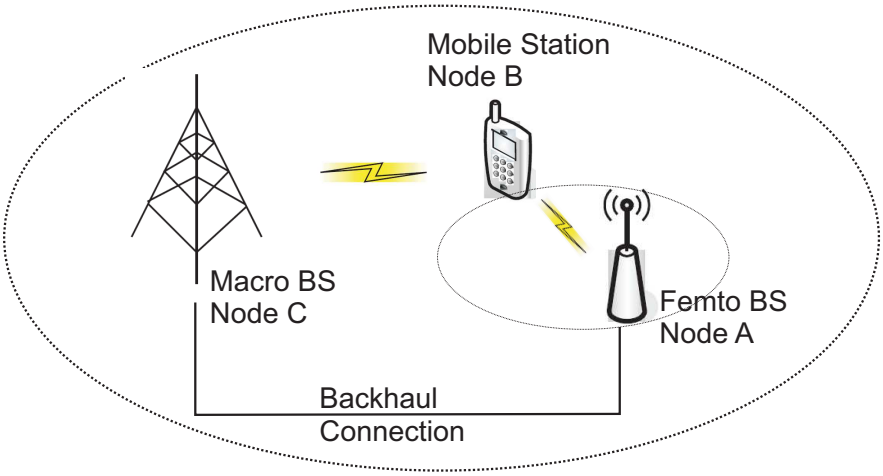

Figure 5.4: MS-assisted femtocell synchronization scenario.

Fig. 5.4 shows a typical macro/femto network. Node A is a fBS which requires synchronization; node B is a macrocell mobile station (mMS); node C is a macro base station. In this scheme, the femtocell has the access to the backhaul to get useful information.

5.3.2 Proposed Scheme

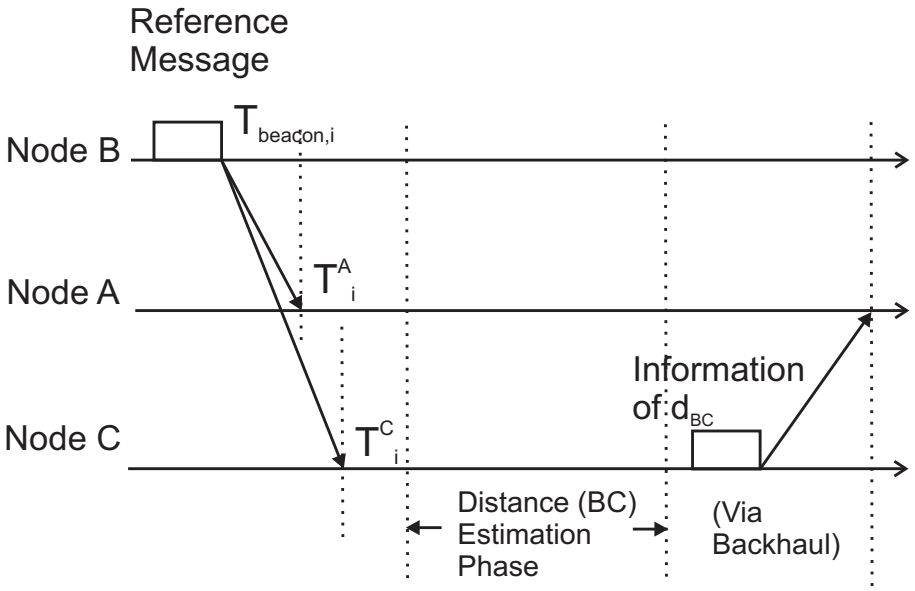

Figure 5.5: The *i*th synchronization process of Scheme 1.

The process of the scheme is illustrated in Fig. 5.5. The assistant mMS (node B) acts as a reference node, and broadcasts a reference message at $T_{beacon,i}$ to the fBS (node A) and BS (node C), in the *i*th synchronization process. The message arrival times at nodes A and C are denoted respectively as T_i^A and T_i^C. Assume that one process can be finished in a relatively short time, then the effect of clock skew can be neglected in one process. With the broadcast from the mMS, the arrival times T_i^A and T_i^C can be written:

$$T_i^A = T_{beacon,i} + \phi^{BA} + D_{prop}^{BA} + D_{rcv,i}^{BA}, \tag{5.2}$$

$$T_i^C = T_{beacon,i} + \phi^{BC} + D_{prop}^{BC} + D_{rcv,i}^{BC}, \tag{5.3}$$

where ϕ^{BA} and ϕ^{BC} are the clock offsets between node B and the receiver nodes A and C; D_{prop}^{BA} and D_{prop}^{BC} are respectively the propagation delays between node B and the receiver nodes A and C; $D_{rcv,i}^{BA}$ and $D_{rcv,i}^{BC}$ are the receive delays at these receiver nodes. From (5.2)

and (5.3), the clock offset between node A and node C (ϕ^{AC}) can be written:

$$\begin{aligned} \phi^{AC} &= \phi^{BC} - \phi^{BA} \\ &= T_i^C - T_i^A - [(D_{prop}^{BC} - D_{prop}^{BA}) + (D_{rcv,i}^{BC} - D_{rcv,i}^{BA})], \end{aligned} \tag{5.4}$$

which can be used to correct the clock of node A. In RBS, the propagation time difference is neglected because it is designed for small networks. But here $D_{prop}^{BC} - D_{prop}^{BA}$ cannot be neglected because the distance between a BS and an mMS might be measured in kilometers. The distance estimation algorithms are used in this scheme to estimate the propagation delay between the BS and the mMS, so as to minimize the error due to the propagation time difference. A variety of distance estimation algorithms have been studied in cellular networks for mobile unit location or network synchronization, such as received signal strength (RSS), time of arrival (TOA), time difference of arrival (TDOA), and round trip time (RTT) [85, 86, 87]. Most of them can achieve an accuracy of tens of meters. In this scheme, the estimation of the distance between the mMS and the BS (denoted as $\hat{d}^{BC}$) is obtained using one of the existing algorithms. And D_{prop}^{BC} can be estimated as:

$$\hat{D}_{prop}^{BC} = \frac{\hat{d}^{BC}}{c}. \tag{5.5}$$

This information as well as T_i^C can then be transmitted to node A via the backhaul. Although there might be transmission latency due to the network traffic jitter and number of hops, this information is delay-tolerant and hence it will not significantly affect the synchronization accuracy.

Following [51], $D_{rcv,i}^{BC} - D_{rcv,i}^{BA}$ can be modeled as a Gaussian distributed random variable, with zero mean and variance σ^2. Note that the femtocell radius is small, and thus D_{prop}^{BA} does not contribute significantly to the overall error. Hence ϕ^{AC} can be estimated

from the *i*th synchronization process as:

$$\hat{\phi}_i^{AC} = (T_i^C - T_i^A) - \hat{D}_{prop}^{BC}. \tag{5.6}$$

Repeating N times the synchronization processes, the estimate of ϕ^{AC} can be obtained:

$$\hat{\phi}^{AC} = \frac{1}{N}\sum_{i=1}^{N}\hat{\phi}_i^{AC} = \frac{1}{N}\sum_{i=1}^{N}(T_i^C - T_i^A) - \hat{D}_{prop}^{BC}, i = 1,2,...,N. \tag{5.7}$$

In this way, the fBS has synchronized its clocks to the BS.

In another case, Node C in Fig. 5.5 can be a synchronized fBS and Node B is a fMS. Distance estimation is not necessary here because the femtocell radius is much smaller and then the propagation time is negligible. Other than that, the whole synchronization process is similar.

The least-squares linear regression algorithm of RBS in [51] can be applied straightforwardly to estimate the clock skew between node A and node C for frequency synchronization. So the clock skew estimation will not be discussed.

5.4 Scheme 2: A Novel RRS based scheme for femtocell networks

5.4.1 Synchronization Scenario

In femtocell deployments, many femtocells may overlap with each other and then form a wireless femtocell network. Figure 5.6 shows the synchronization scenario of a wireless femtocell network. Node A is a femto BS (fBS) just installed into the network, node B is a synchronized fBS which has an accurate clock, node C, D and E are neighbour fBSs. Other fBSs like C, D or E in the network can also be synchronized at the same time if

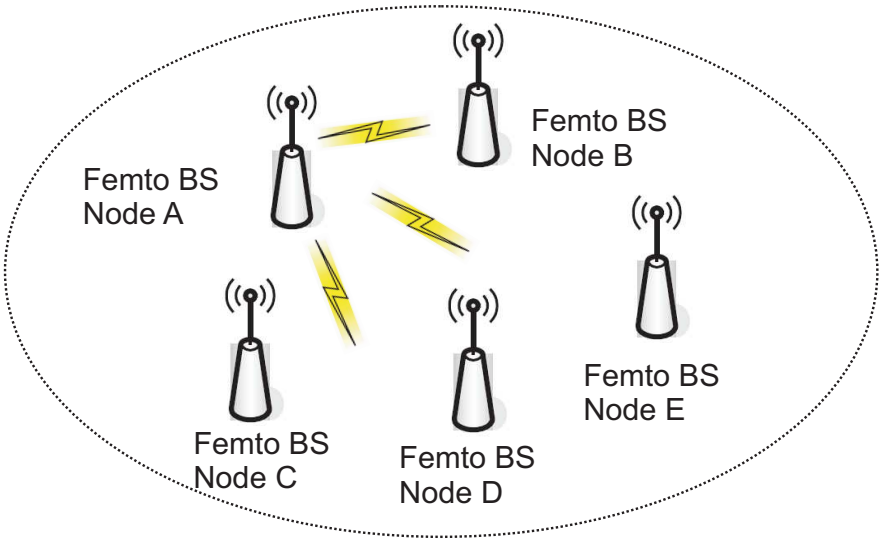

Figure 5.6: Wireless femtocell network synchronization scenario.

needed.

5.4.2 Proposed Scheme

The messaging process of this scheme is illustrated in Fig. 5.7. First, the fBS requiring synchronization, which is referred to as the node A, starts the *i*th synchronization process by broadcasting a reference beacon $T^{A}_{beacon,i}$. All other nodes record the message arrival times, which are $T^{B}_{1,i}$, $T^{C}_{1,i}$, and $T^{D}_{1,i}$. Then, a synchronized fBS, which is referred to as the node B, broadcasts a message $T^{B}_{beacon,i}$ containing the value of $T^{B}_{1,i}$. All other nodes, node A, C and D, record the arrival time of $T^{B}_{beacon,i}$, namely $T^{A}_{2,i}$, $T^{C}_{2,i}$ and $T^{D}_{2,i}$. At last, another neighbouring node, which is referred to as the node C, calculates the difference $\triangle T_i$ between $T^{C}_{1,i}$ and $T^{C}_{2,i}$ (i.e., $\triangle T_i = T^{C}_{2,i} - T^{C}_{1,i}$), and sends $\triangle T_i$ back to node A. From the first broadcast from node A, $T^{B}_{1,i}$ and $T^{C}_{1,i}$ can be represented as:

$$T^{B}_{1,i} = T^{A}_{beacon,i} + \phi^{AB} + D^{AB}_{prop} + D^{AB}_{rcv,i} \tag{5.8}$$

$$T^{C}_{1,i} = T^{A}_{beacon,i} + \phi^{AC} + D^{AC}_{prop} + D^{AC}_{rcv,i} \tag{5.9}$$

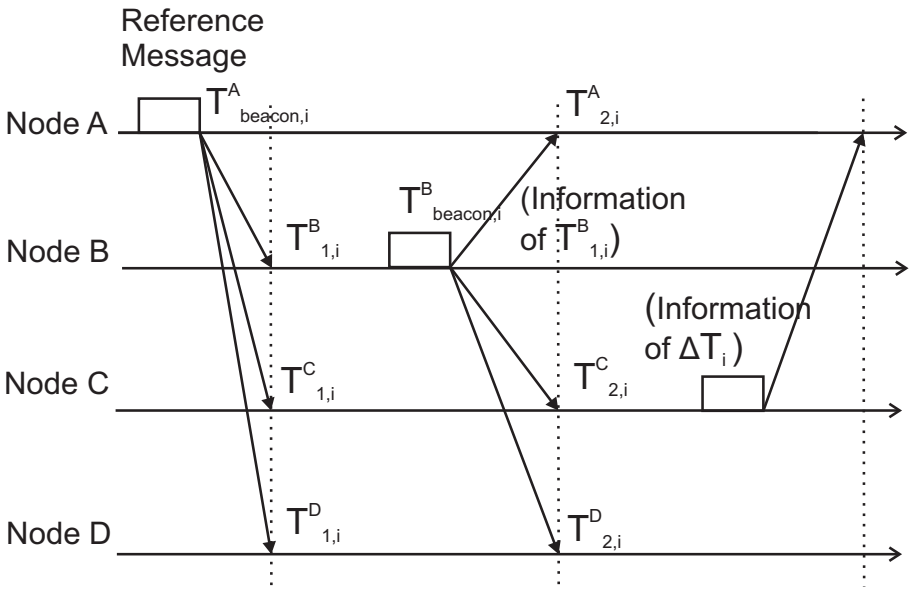

Figure 5.7: The *i*th synchronization process of Scheme 2.

where ϕ^{AB} and ϕ^{AC} are the clock offsets between node A and the receiver nodes B and C; D^{AB}_{prop} and $D^{AC}_{prop}$are the propagation delays between node A and the receiver nodes B and C; $D^{AB}_{rcv,i}$ and $D^{AC}_{rcv,i}$ are the receive delays at these receiver nodes. From (5.8) and (5.9), the clock offset between Node B and Node C can be calculated:

$$\begin{aligned} \phi^{BC} &= \phi^{AC} - \phi^{AB} \\ &= T^C_{1,i} - T^B_{1,i} - [(D^{AC}_{prop} - D^{AB}_{prop}) + (D^{AC}_{rcv,i} - D^{AB}_{rcv,i})]. \end{aligned} \tag{5.10}$$

Since in this scenario the wireless network spans only tens of meters, propagation delays like D^{AB}_{prop} and D^{AC}_{prop} do not contribute significantly to the overall error. Similar to Scheme 1, $D^{AC}_{rcv,i} - D^{AB}_{rcv,i}$ can also be modeled as a Gaussian distributed random variable with zero mean and variance σ^2. Then ϕ^{BC}_i can be approximated from this synchronization process by:

$$\hat{\phi}^{BC}_i = T^C_{1,i} - T^B_{1,i}. \tag{5.11}$$

Similar to (5.7), a simple unbiased estimator for ϕ^{BC} can be obtained:

$$\hat{\phi}^{BC} = \frac{1}{N}\sum_{i=1}^{N}\hat{\phi}_i^{BC} = \frac{1}{N}\sum_{i=1}^{N}(T_{1,i}^{C} - T_{1,i}^{B}),\ i = 1,2,...,N. \tag{5.12}$$

Node C then can be synchronized to node B. Node D and other nodes hearing the beacons can be synchronized in the same way at the same time.

From the second broadcast message from node B, $T_{2,i}^{A}$ and $T_{2,i}^{C}$ can be expressed:

$$T_{2,i}^{A} = T_{beacon,i}^{B} + \phi^{BA} + D_{prop}^{BA} + D_{rcv,i}^{BA} \tag{5.13}$$

$$T_{2,i}^{C} = T_{beacon,i}^{B} + \phi^{BC} + D_{prop}^{BC} + D_{rcv,i}^{BC} \tag{5.14}$$

where ϕ^{BA} and ϕ^{BC} are the clock offsets between node B and the receivers A and C; D_{prop}^{BA} and D_{prop}^{BC} are the propagation delays between node B and the receivers; $D_{rcv,i}^{BA}$ and $D_{rcv,i}^{BC}$ are the receive delays between node B and the receivers. Substituting (5.14) from (5.13) yields:

$$\begin{aligned}\phi^{BA} &= T_{2,i}^{A} - T_{2,i}^{C} + \phi^{BC} \\ &\quad + D_{prop}^{BC} + D_{rcv,i}^{BC} - D_{prop}^{BA} - D_{rcv,i}^{BA}.\end{aligned} \tag{5.15}$$

Putting (5.10) and $\triangle T_i = T_{2,i}^{C} - T_{1,i}^{C}$ into (5.15) gives:

$$\begin{aligned}\phi^{BA} &= T_{2,i}^{A} - (T_{1,i}^{B} + \triangle T_i) \\ &\quad - [(D_{prop}^{BA} - D_{prop}^{BC} + D_{prop}^{AC} - D_{prop}^{AB}) \\ &\quad + (D_{rcv,i}^{BA} - D_{rcv,i}^{BC} + D_{rcv,i}^{AC} - D_{rcv,i}^{AB})].\end{aligned} \tag{5.16}$$

Similar to (5.12), the estimate of ϕ^{BA} can be obtained:

$$\hat{\phi}^{BA} = \frac{1}{N}\sum_{i=1}^{N}[T_{2,i}^{A} - (T_{1,i}^{B} + \triangle T_i)], i = 1,2,...,N. \tag{5.17}$$

In this way, nodes A, C and D have synchronized their clocks to node B's clock. This process is repeated to achieve higher accuracy. Again, the least-squares linear regression algorithm of RBS can be straightforwardly applied to calculate the respective clock skew, and hence clock skew estimation will not be discussed.

5.4.3 Performance Analysis

One important improvement of Scheme 2 is a significant reduction in the number of overall timing messages. In an M - node single-hop domain using RBS for time reference broadcasts, $N \times M$ messages would need to be broadcasted to synchronize the nodes. However, Scheme 2 reduces the number of timing messages to $3 \times N$. Note that the number of messages required for Scheme 2 does not depend on the number of nodes in the network. This energy saving increases with the increase of the number of nodes in the network.

Another improvement is that the Scheme 2 does not require a fixed super node in the network. In Scheme 2, the femtocell can get synchronized by initiating the synchronization process. However, RBS requires a fixed super node which broadcasts the reference beacons to all the other nodes in the network and this is unrealistic in the setup of Fig. 5.6.

In RBS, all nodes are synchronized to an 'averaged time' by exchanging the receiving times of the reference beacons, which is not necessarily an accurate time. In contrast, all femtocells are synchronized to an accurate clock in both Scheme 1 and Scheme 2, providing higher synchronization reliability.

5.5 Simulation Results

The synchronization accuracy of the proposed schemes is evaluated using Monte Carlo simulation. For Scheme 1, the distance between the fBS (i.e. Node A) and the mMS (i.e. Node B) is randomly selected between 0 to 30m. The distance estimation error is randomly selected between 0 to 50m. For Scheme 2, the distance between the nodes (A, B, C, D) is randomly selected between 0 to 30m. In the simulation, two different receive time standard deviations ($\sigma = 10\mu s$ and $\sigma = 30\mu s$) are considered. The synchronization process is repeated $N = 30$ times for every simulation to achieve higher accuracy. All the Monte Carlo simulations are performed 10000 times.

Firstly, the synchronization accuracy performance for RBS in a 3km macro network is simulated. The average clock offset is plotted against the distance between Node A and Node C and the number of synchronization processes in Fig. 5.8. It is observed that the clock offset increases linearly as the distance between the nodes increases. Although the accuracy can be improved by repeating the synchronization process, the clock offset is still too big for femtocells when it works in a big network.

Secondly, the synchronization accuracy performance of Scheme 1 is evaluated in terms of the average clock offset of Node C ($E(|\phi^{AC}|)$) after N synchronization processes for $\sigma = 10\mu s$ and $\sigma = 30\mu s$, as shown in Fig. 5.9. It is noted that the average clock offset achieves $2.5\mu s$ after 30 processes for $\sigma = 10\mu s$. Obviously, large σ degrades the accuracy. Note that Scheme 1 removes the effect of the size of the macro cell and provides a much more stable accuracy, which is mainly attributed to the inclusion of the distance estimation between the mMS and the mBS and that eliminates a big part of the propagation error.

Finally, the synchronization accuracy performance of Scheme 2 is simulated with respect to the average clock offset of Node A and Node C ($E(|\phi^{BA}|)$ and $E(|\phi^{BC}|)$) after N synchronization processes for $\sigma = 10\mu s$ and $\sigma = 30\mu s$. Fig. 5.10 shows that the synchro-

nization performance of Scheme 2 also improves with the increase of N and the decrease of σ. However, Node A's synchronization accuracy will be slightly worse than that of Node C, because of the present of $\triangle T_i$.

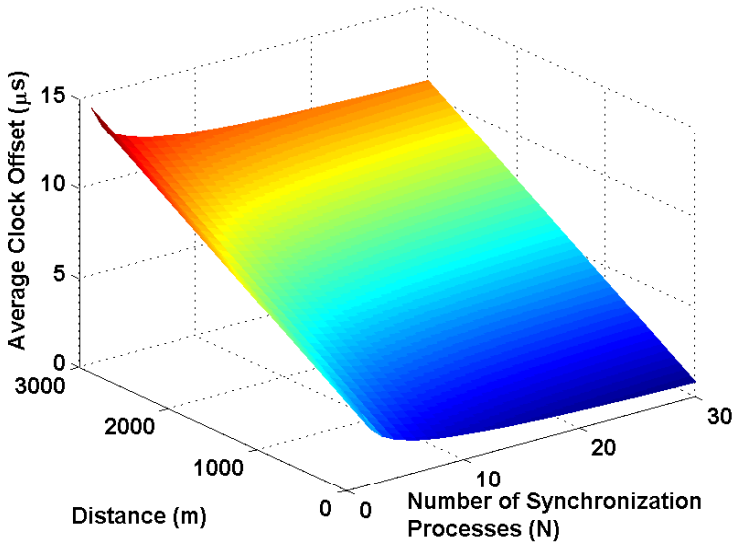

Figure 5.8: Average clock offset for RBS in a Macrocell after N synchronization processes.

5.6 Summary

In this chapter, two RRS based synchronization schemes are proposed for femtocells. Both schemes are carefully designed for respective synchronization scenarios. Compared with RBS, both schemes remove the requirement of having a fixed super node in the network. In both schemes, all nodes can synchronize to an accurate clock. This is different from RBS where all nodes are synchronized to an 'averaged time', and that makes the synchronization more reliable. In addition, Scheme 2 significantly reduces the number of overall timing messages compared to RBS. From analysis and simulation results, it is demonstrated that both of the schemes provide satisfactory performance for femtocells in term of synchronization accuracy.

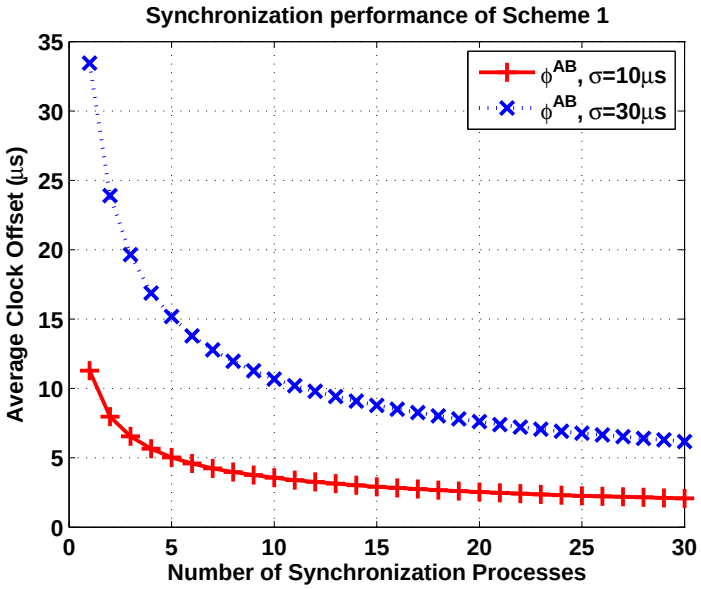

Figure 5.9: Average clock offset after N synchronization processes in Scheme 1, parameterized on different receive time standard deviations.

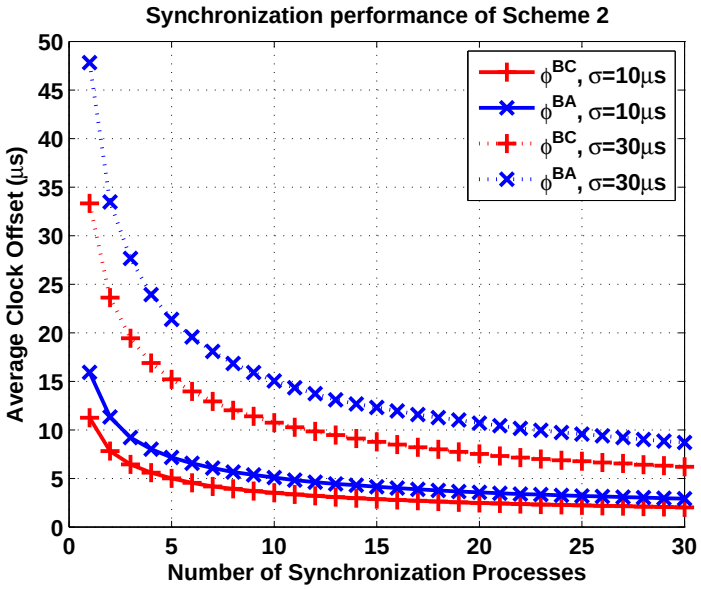

Figure 5.10: Average clock offset after N synchronization processes in Scheme 2, parameterized on different receive time standard deviations.

6 A Hybrid Synchronization Scheme Based on Wireless IEEE 1588 and Receiver-Receiver Synchronization

6.1 Introduction

In realistic deployment of femtocell networks, for example the femtocells installed on the lampposts along the Kensington Street in London during the 2012 Olympics, only a few lampposts have good visibility to the GPS satellite and due to cost and restriction from the London council, it is impossible to dig the ground for every femtocell to connect to the core network by wired backhaul. So other femtocells without GPS and backhaul need to resort to other methods, such as wireless IEEE 1588 and receiver-receiver synchronization (RRS), for their clock synchronization.

A hybrid synchronization scheme based on wireless IEEE 1588 and RRS is proposed for this scenario. The IEEE 1588 standard is widely used in and investigated for many wireless systems. [88] examines potential accuracy limitations of wireless IEEE 1588 introduced by the physical layer of the IEEE 802.11b wireless local area network (WLAN). In [89], the time stamping related problem of IEEE 1588 used in WLAN was studied. [47] proposes an enhanced IEEE 1588 scheme for asymmetric wireless links. In [90], a

method of precise time synchronization of wireless sensors employing an IEEE 802.15.4 protocol was developed. Other works such as [91, 92, 93, 94, 95, 96, 97] also investigated IEEE 1588 for wireless networks.

RRS has been investigated in Chapter 5. The principle of RRS is to compare the receiving times of one timing reference at different receivers. Considering the broadcast nature of wireless networks, the timing messages transmitted in wireless IEEE 1588 can potentially act as the timing references in RRS. The hybrid scheme proposes a way to combine both wireless IEEE 1588 and RRS, and make the best use of the advantages of these two synchronization methods. Analysis shows that this hybrid scheme can provide better synchronization accuracy with less exchanged messages than conventional wireless IEEE 1588, especially when there are a large number of 'slave' femtocells in the network. It is also shown that the proposed hybrid scheme is more robust than conventional wireless IEEE 1588 and RBS against the packet loss in the network.

So the contributions of this chapter are as follows. First, a hybrid synchronization scheme based on wireless IEEE 1588 and receiver-receiver synchronization is proposed. Second, the hybrid scheme is evaluated in terms of the number of required timing messages, the robustness against packet loss and the synchronization accuracy in comparison with both wireless IEEE 1588 and RBS through theoretical analysis and experimental simulations.

The rest of the chapter is organized as follows. In Section 6.2, the synchronization scenario is introduced. In Section 6.3, the hybrid synchronization scheme is proposed. Then, the number of required timing messages and the robustness against packet loss of the hybrid scheme are evaluated in Section 6.4 and Section 6.5, respectively. In Section 6.6, the synchronization performance of the hybrid scheme is evaluated using Monte Carlo simulations. Finally, Section 6.7 concludes this chapter.

6.2 Synchronization Scenario

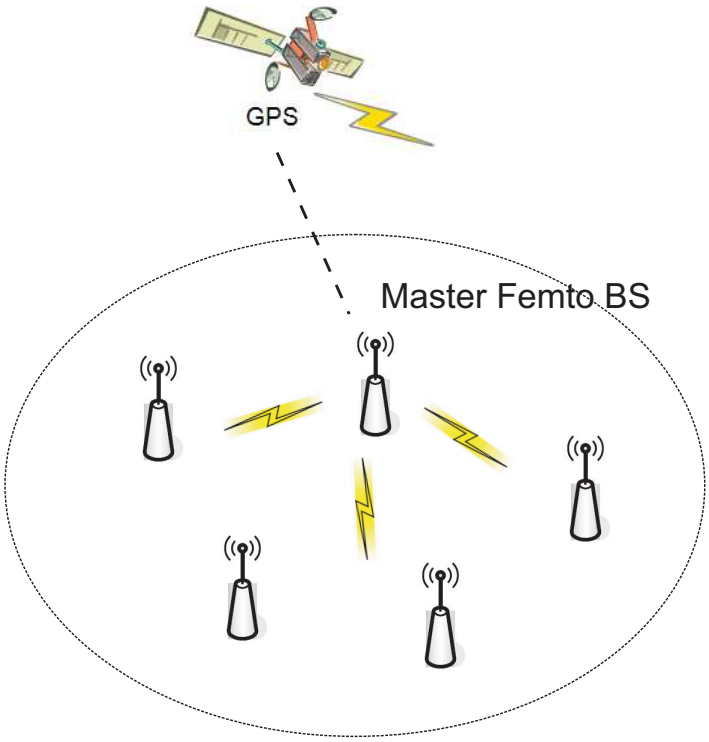

Figure 6.1: The femtocell wireless network synchronization scenario.

Fig. 6.1 shows a femtocell synchronization scenario with several femtocells in a wireless network. Only one femtocell is able to receive accurate timing references via GPS or the wired backhaul, and so is referred to as the 'Master' femtocell. Other femtocells can only be synchronized to the 'Master' via wireless techniques, and are referred to as 'Slave' femtocells. Assume that the number of 'Slave' femtocells is M.

For simplicity, a small single-hop network is studied, which means that every femtocell can receive messages from any other femtocells. Multi-hop synchronization can be derived based on the single-hop case and this will be the subject of future work.

6.3 Hybrid Wireless IEEE 1588 and Receiver-Receiver Synchronization

In this section, the conventional way that IEEE 1588 (PTP) is applied in a wireless network scenario in Fig. 6.1 is firstly introduced. And then a hybrid synchronization scheme based on wireless IEEE 1588 and receiver-receiver synchronization is proposed.

6.3.1 Conventional Wireless IEEE 1588

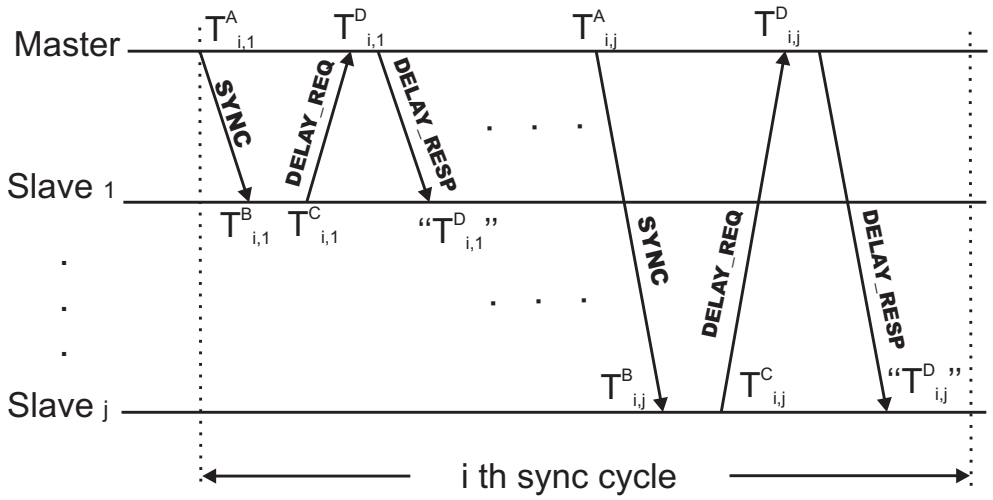

Figure 6.2: Message exchanging of the conventional wireless IEEE 1588 in the *i*th synchronization cycle.

Since the Master femtocell needs to synchronize M Slave femtocells in this scenario, it is defined that the message exchanging process introduced in Fig. 3.2 between the Master and a Slave is an IEEE 1588 synchronization process, and that the whole process of the Master femtocell completing one synchronization process with every Slave femtocell is an IEEE 1588 synchronization cycle. Similar to (4.1), the clock offset of Slave j in the ith synchronization cycle can be expressed as:

$$\phi_j(t_i) = \phi_{0,j} + \rho_j t_i. \tag{6.1}$$

where $\phi_{0,j}$ is the initial clock offset of Slave j, ρ_j is the constant clock skew of Slave j and t_i is the ending time of the ith synchronization cycle. It is assumed that the master has an accurate clock. Then Slave j's clock at the ending time of the ith synchronization cycle, $T_j(t_i)$, can be written as:

$$T_j(t_i) = t_i + \phi_j(t_i). \tag{6.2}$$

Fig. 6.2 shows that how wireless IEEE 1588 was executed conventionally in the scenario shown in Fig. 6.1. In every synchronization cycle, the Master gets the Slaves synchronized by a three message exchanging synchronization process one after another. In the synchronization process with Slave j of the ith cycle, the Master triggers the process by sending a *SYNC* message to Slave j with the time $T^A_{i,\cdot j}$ at which the message is sent. Slave j receives the *SYNC* message and stores the message arrival time $T^B_{i,j}$, according to its own clock. An optional *FOLLOW_UP* message is sometimes sent by the Master after the *SYNC* message as in Fig. 3.2, however that is not the case in this scenario. Slave j sends a *DELAY_REQ* message and stores the transmission time as $T^C_{i,j}$. When the Master receives the *DELAY_REQ* message, it sends a *DELAY_RESP* message, which contains the arrival time of *DELAY_REQ* denoted as $T^D_{i,j}$. Similar to Chapter 3 and Chapter 4, the overall communication delay can be modeled as the sum of a fixed delay and a random delay. Then the downlink delay observation ($U_{i,j}$) and the uplink delay observation ($V_{i,j}$) of Slave j in the ith cycle can be recorded as:

$$U_{i,j} \triangleq T^B_{i,j} - T^A_{i,\cdot j} = d + \phi_j(t_i) + X_{i,j} \tag{6.3}$$

$$V_{i,j} \triangleq T^D_{i,j} - T^C_{i,j} = d - \phi_j(t_i) + Y_{i,j} \tag{6.4}$$

where $\phi_j(t_i)$ is the clock offset of Slave j in the ith synchronization process. The fixed delay is assumed to be symmetric for uplink and downlink, because the uplink and down-

link transmission rates are the same and the propagation time difference is negligible in a small wireless network. The fixed delay is modeled as a constant time d. On the other hand, the random delays are assumed to follow Gaussian distributions with mean μ and variance σ^2. The IEEE 1588 (PTP) clock offset estimator can be derived as

$$\hat{\phi}_j^{PTP}(t_i) = \frac{U_{i,j} - V_{i,j}}{2}. \tag{6.5}$$

Every Slave can be synchronized to the Master by applying (6.5). The synchronization cycle can be repeated many times to achieve a better accuracy. However, there are several problems for this conventional method. Firstly, the number of timing messages exchanged between nodes is large, since every master-slave synchronization process needs to exchange three messages. Secondly, all these three messages are required to be successfully received; otherwise the corresponding synchronization process will fail. This makes it vulnerable to packet loss in the network.

6.3.2 The Hybrid Synchronization Scheme Based on Wireless IEEE 1588 and RRS

A hybrid synchronization scheme based on wireless IEEE 1588 and receiver-receiver synchronization is proposed for the wireless femtocell network scenario shown in Fig. 6.1. The principle of RRS is to compare the receiving times of one timing reference at different receivers. Since it is a single-hop area, every broadcast message, either from the Master or a Slave, can be received by many receivers. Then it can be potentially used as a timing reference.

Fig. 6.3 shows the message exchanging of the proposed hybrid scheme in the ith synchronization cycle. All messages are transmitted in 'broadcast' mode, which is supported in wireless IEEE 1588 and is applicable in a single-hop wireless network. In the ith syn-

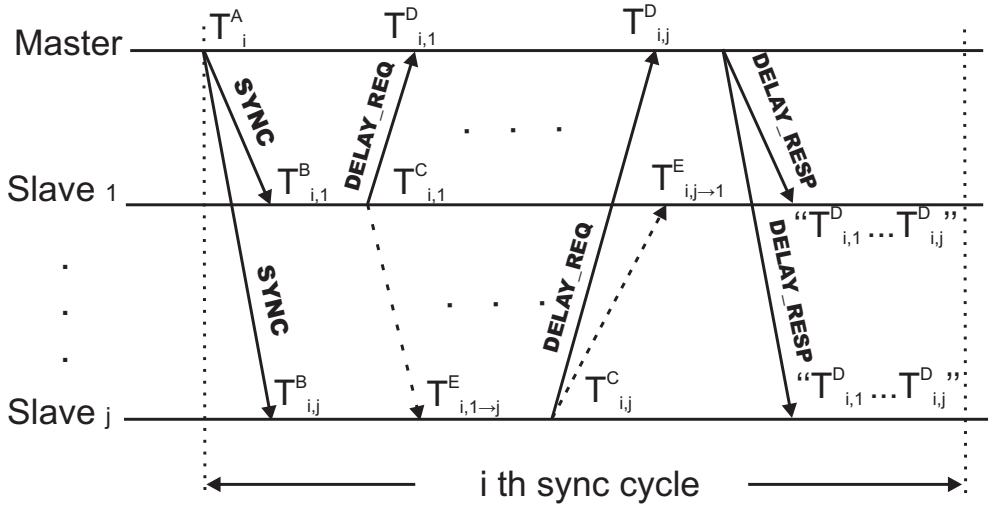

Figure 6.3: Message exchanging of the proposed hybrid scheme in the *i*th synchronization cycle.

chronization cycle, the Master firstly broadcasts a *SYNC* message containing the sending time T_i^A to all the Slaves (the *FOLLOW_UP* message is neglected). The Slaves receive the *SYNC* message and record the receiving times as $T_{i,1}^B$, $T_{i,2}^B$, ... , $T_{i,j}^B$, respectively. Then, they send *DELAY_REQ* messages back to the Master containing timestamps $T_{i,1}^C$, $T_{i,2}^C$, ... , $T_{i,j}^C$, respectively. At last, the Master broadcasts a *DELAY_RESP* message to all Slaves, which contains the arrival times of *DELAY_REQ* from all Slaves, $T_{i,1}^D$, $T_{i,2}^D$, ... , $T_{i,j}^D$. Note that this is different from the conventional wireless IEEE 1588, where the Master sends $T_{i,j}^D$ to Slave j in unicast mode. Since all femtocells are in a single-hop area, the *DELAY_REQ* messages sent by any Slave can also be received by other Slaves. Slave j can record the arrival time of Slave k's *DELAY_REQ* message as $T_{i,k\to j}^E$, and then calculate the path delay from Slave k to Slave j as:

$$W_{i,k\to j} \triangleq T_{i,k\to j}^E - T_{i,k}^C = d + \phi_j(t_i) - \phi_k(t_i) + Z_{i,k\to j} \tag{6.6}$$

where $\phi_k(t_i)$ is the real clock offset of Slave k in the ith cycle and $Z_{i,k\to j}$ is the corresponding random delay. After receiving the *DELAY_RESP* message, Slave j firstly uses $T_{i,j}^D$ to

calculate the PTP clock offset estimator as:

$$\begin{aligned}\hat{\phi}_j^{PTP}(t_i) &= \frac{U_{i,j}-V_{i,j}}{2} \\ &= \phi_j(t_i)+\frac{1}{2}(Y_{i,j}-X_{i,j}) \end{aligned} \tag{6.7}$$

where $\varepsilon_{j,i}^{PTP}=\frac{1}{2}(Y_{i,j}-X_{i,j})$ is the IEEE 1588 estimation noise added to $\phi_j(t_i)$, which also follows a Gaussian distribution with $\varepsilon_{j,i}^{PTP}\sim(0,\frac{\sigma^2}{2})$.

Then, Slave j uses $T_{i,k}^D$ $(k\neq j)$ to derive a RRS estimator. Now, similar to RBS, we assume that the Slave k's *DELAY_REQ* message arrives at Slave j and the Master at the same time. So, an RRS based clock offset estimator for Slave j can be derived as:

$$\hat{\phi}_j(t_i)=T_{i,k\rightarrow j}^E-T_{i,k}^D. \tag{6.8}$$

In each synchronization cycle, Slave j can calculate $M-1$ such clock offset estimates. Averaging these estimates and the RRS estimator can be obtained:

$$\hat{\phi}_j^{RRS}(t_i)=\frac{1}{M-1}\sum_{k=1}^{M,k\neq j}(T_{i,k\rightarrow j}^E-T_{i,k}^D). \tag{6.9}$$

Substituting both the $T_{i,k\rightarrow j}^E$ from (6.6) and the $T_{i,k}^D$ from (6.4) into (6.9) yields:

$$\hat{\phi}_j^{RRS}(t_i)=\phi_j(t_i)+\frac{1}{M-1}\sum_{k=1}^{M,k\neq j}(Z_{i,k\rightarrow j}-Y_{i,k}) \tag{6.10}$$

where $\varepsilon_{j,i}^{RRS}=\frac{1}{M-1}\sum_{k=1}^{M,k\neq j}(Z_{i,k\rightarrow j}-Y_{i,k})$ is the RRS estimation noise added to $\phi_j(t_i)$, which follows a Gaussian distribution with $\varepsilon_{j,i}^{RRS}\sim(0,\frac{2\sigma^2}{M-1})$. As introduced in the last chapter, in RBS, all slaves exchange their recorded times and calculate a universal time by simply averaging. This synchronizes all the slaves to a common time, but not necessarily an accurate time. The Master in RBS only broadcasts 'beacons' to the slaves, while

not synchronizing the slaves to its own clock. However, in the proposed hybrid scheme every slave broadcasts the *DELAY_RESP* message to other slaves and the Master, which allows every other slave to synchronize to the Master and derive an unbiased clock offset estimator (6.10), and thus provide better synchronization accuracy than RBS.

The two estimations obtained in the proposed hybrid scheme using IEEE 1588 mechanism and RBS mechanism are combined using linear combination technique:

$$\hat{\phi}_j^{Hyb}(t_i) = \alpha\hat{\phi}_j^{PTP}(t_i) + (1-\alpha)\hat{\phi}_j^{RRS}(t_i) \tag{6.11}$$

where α and $1-\alpha$ are the weights of $\hat{\phi}_j^{PTP}(t_i)$ and $\hat{\phi}_j^{RRS}(t_i)$, respectively. Since both estimators (6.5) and (6.9) are unbiased, the MSE (mean squared error) of (6.11) is:

$$\begin{aligned} var(\hat{\phi}_j^{Hyb}(t_i)) &= \alpha^2 var(\varepsilon_{j,i}^{PTP}) + (1-\alpha)^2 var(\varepsilon_{j,i}^{RRS}) \\ &= \alpha^2 \times \frac{1}{2}\sigma^2 + (1-\alpha)^2 \times \frac{2}{M-1}\sigma^2. \end{aligned} \tag{6.12}$$

Then the optimum estimator of $\phi_j(t_i)$ can be calculated by choosing the appropriate α. Differentiating (6.12) with respect to α gives:

$$\frac{\partial var(\hat{\phi}_j^{Hyb}(t_i))}{\partial\alpha} = \left(\sigma^2 + \frac{4\sigma^2}{M-1}\right) \times \alpha - \frac{4\sigma^2}{M-1} = 0 \tag{6.13}$$

$$\Rightarrow \alpha = \arg\min_{\alpha} var(\hat{\phi}_j^{Hyb}(t_i)) = \frac{4}{M+3}. \tag{6.14}$$

Thus the optimum combination of the two estimators can be written as:

$$\hat{\phi}_j^{Hyb}(t_i) = \frac{4}{M+3}\hat{\phi}_j^{PTP}(t_i) + \frac{M-1}{M+3}\hat{\phi}_j^{RRS}(t_i). \tag{6.15}$$

Then substituting (6.7) and (6.10) into (6.15) gives:

$$\begin{aligned}\hat{\phi}_j^{Hyb}(t_i) &= \phi_j(t_i) + \frac{2}{M+3}(Y_{i,j} - X_{i,j}) \\ &\quad + \frac{1}{M+3}\sum_{k=1}^{M,k\neq j}(Z_{i,k\to j} - Y_{i,k}) \end{aligned} \tag{6.16}$$

where $\varepsilon_{j,i}^{Hyb} = \frac{2(Y_{i,j}-X_{i,j})}{M+3} + \frac{1}{M+3}\sum_{k=1}^{M,k\neq j}(Z_{i,k\to j} - Y_{i,k})$ is the MMSE (minimum mean squared error) estimation noise of $\phi_j(t_i)$, which also follows a Gaussian distribution with $\varepsilon_{j,i}^{Hyb} \sim (0, \frac{2\sigma^2}{M+3})$.

After N synchronization cycles, substitute (6.16) into (6.1):

$$\hat{\phi}_j^{Hyb}(t_i) = \phi_{0,j} + \rho_j t_i + \varepsilon_{j,i}^{Hyb},\ i = 1,2,...,N. \tag{6.17}$$

Considering that a Slave can only be aware of the time on the clock of itself, substituting (6.1) and (6.2) into (6.17) produces:

$$\begin{aligned}\hat{\phi}_j^{Hyb}(t_i) &= \phi_{0,j} + \rho_j \cdot \frac{T_j(t_i) - \phi_{0,j}}{1+\rho_j} + \varepsilon_{j,i}^{Hyb} \\ &= \frac{\phi_{0,j}}{1+\rho_j} + \frac{\rho_j}{1+\rho_j}T_j(t_i) + \varepsilon_{j,i}^{Hyb}, \\ &\quad i = 1,2,...,N. \end{aligned} \tag{6.18}$$

So, the observed data can be written in matrix notation as:

$$\hat{\phi}_{\mathbf{j}}^{\mathbf{Hyb}} = \mathbf{H}\theta + \varepsilon \tag{6.19}$$

where

$$\hat{\phi}_{\mathbf{j}}^{\mathbf{Hyb}} = [\hat{\phi}_j^{Hyb}(t_1), \hat{\phi}_j^{Hyb}(t_2), ..., \hat{\phi}_j^{Hyb}(t_N)]^T \tag{6.20}$$

$$\theta = [\theta_0, \theta_1]^T = [\frac{\phi_{0,j}}{1+\rho_j}, \frac{\rho_j}{1+\rho_j}]^T \tag{6.21}$$

$$\varepsilon = [\varepsilon_{j,1}^{Hyb}, \varepsilon_{j,2}^{Hyb}, ..., \varepsilon_{j,N}^{Hyb}]^T \tag{6.22}$$

$$\mathbf{H} = [1, 1, ..., 1; T_j(t_1), T_j(t_2), ..., T_j(t_N)]^T. \tag{6.23}$$

Then the least squares estimate of θ is given by:

$$\hat{\theta} = (\mathbf{H}^T \mathbf{H})^{-1} \mathbf{H}^T \hat{\phi}_{\mathbf{j}}^{\mathbf{Hyb}}. \tag{6.24}$$

And then the clock skew and the initial clock offset can be derived from (6.21) as:

$$\hat{\rho}_j = \frac{1}{1 - \hat{\theta}_1} - 1 \tag{6.25}$$

$$\hat{\phi_{0,j}} = \frac{\hat{\theta}_0}{1 - \hat{\rho}_j}. \tag{6.26}$$

Then this scheme can be applied to all slave femtocells to get them synchronized to the master femtocell using the estimated initial clock offset and clock skew.

6.4 Number of Transmitted Timing Messages

The number of transmitted timing messages is an important metric for the evaluation of a synchronization scheme. Less required timing messages mean less energy consumption and lighter traffic load of the network. The numbers of overall transmitted packets in a single synchronization cycle in wireless IEEE 1588, RBS and the proposed hybrid scheme are compared in Table 6.1.

It is shown from the table that normally a lot more packets are transmitted in IEEE 1588 than in RBS or the proposed hybrid scheme. The proposed hybrid scheme requires one more packet to be transmitted than in RBS, however it can provide much better robustness, which will be shown in the next section, and has an unbiased clock offset estimation other than RBS as previously explained.

Table 6.1: Number of Required Timing Messages for the Three Schemes for the Scenario in Fig. 6.1.

Synchronization Method	Number of Required Timing Messages in Single Cycle
IEEE 1588	$3 \times M$
RBS	$M+1$
The Proposed Hybrid Scheme	$M+2$

Now, the number of required synchronization cycles for these schemes will be compared. The number of required synchronization cycles is determined by the synchronization performance of the scheme. In the scenario in Fig. 6.1, the more accurate is the clock offset estimator, the less synchronization processes are needed to maintain the network synchronization at a certain level. One important indicator of the network synchronization is the probability of that the synchronization error ε lies within $[-\varepsilon_{\max}, \varepsilon_{\max}]$, $\Pr(|\varepsilon| \leq \varepsilon_{\max})$, must be larger than a specific value [98, 99]. When the synchronization error follows the Gaussian distribution as in this case, the p.d.f of the synchronization error ε (i.e. clock offset) is:

$$f(\varepsilon) = \frac{1}{\sqrt{2\pi}\sigma_{sync}} \exp[-\frac{1}{2}(\frac{\varepsilon}{\sigma_{sync}})^2] \tag{6.27}$$

where σ_{sync} is the standard deviation of an unbiased clock offset estimator in this scenario. And then the probability that the synchronization error (i.e. clock offset), ε lies within $[-\varepsilon_{\max}, \varepsilon_{\max}]$ is given by:

$$\begin{aligned} \Pr(|\varepsilon| &\leq \varepsilon_{\max}) = \frac{1}{\sqrt{2\pi}\sigma_{sync}} \int_{-\varepsilon_{\max}}^{\varepsilon_{\max}} \exp[-\frac{1}{2}(\frac{x}{\sigma_{sync}})^2]dx \\ &= \frac{2}{\sqrt{2\pi}\sigma_{sync}} \int_{0}^{\varepsilon_{\max}} \exp[-\frac{1}{2}(\frac{x}{\sigma_{sync}})^2]dx. \end{aligned} \tag{6.28}$$

Substituting $y = \frac{x}{\sqrt{2}\sigma_{sync}}$ into (6.28):

$$\begin{aligned} \Pr(|\varepsilon| &\leq \varepsilon_{\max}) = \frac{2 \times \sqrt{2}\sigma_{sync}}{\sqrt{2\pi}\sigma_{sync}} \int_0^{\frac{\varepsilon_{\max}}{\sqrt{2}\sigma_{Sync}}} \exp(-y^2)dy \\ &= \frac{2}{\sqrt{\pi}} \int_0^{\frac{\varepsilon_{\max}}{\sqrt{2}\sigma_{sync}}} \exp(-y^2)dy \\ &= erf(\frac{\varepsilon_{\max}}{\sqrt{2}\sigma_{sync}}) \end{aligned} \tag{6.29}$$

where $erf(x) = \frac{2}{\sqrt{\pi}} \int_0^x \exp(-t^2)dt$. Neglecting the clock skew impact in a relatively short period, the average number of required synchronization cycles is decided by σ_{sync}. In IEEE 1588, assuming N_{PTP} synchronization cycles are needed to achieve the requirement, then $\sigma_{sync} = var(\varepsilon_{j,i}^{Hyb})^{\frac{1}{2}} = \frac{\sigma}{\sqrt{2N_{PTP}}}$, and N_{PTP} can be obtained as:

$$N_{PTP} = [erf^{-1}(\Pr(|\varepsilon| \leq \varepsilon_{\max})) \times R]^2 \tag{6.30}$$

where $R = \frac{\sigma}{\varepsilon_{max}}$ is the ratio between the standard variance of the random delay and the maximum error.

In the proposed hybrid scheme, $\sigma_{sync} = var(\varepsilon_{j,i}^{Hyb})^{\frac{1}{2}} = \sqrt{\frac{2}{N_{PTP-RR} \times (M+3)}}\sigma$. The corresponding required number of synchronization cycles can be derived as

$$N_{Hyb} = [erf^{-1}(\Pr(|\varepsilon| \leq \varepsilon_{\max})) \times \frac{2R}{\sqrt{M+3}}]^2. \tag{6.31}$$

The comparison between (6.30) and (6.31) is shown in Fig. 6.4 in terms of the number of required synchronization cycles (N_{PTP} and N_{Hyb}) against the number of slave femtocells (M) in the network, with different values of R (marked as $R1 = 1$ and $R2 = 2$) and different required synchronization performance $\Pr(|\varepsilon| \leq \varepsilon_{\max}) \geq P1$ and $\Pr(|\varepsilon| \leq \varepsilon_{\max}) \geq P2$, where $P1 = 0.95$ and $P2 = 0.99$.

It can be seen in Fig. 6.4 that N_{Hyb} decreases as M increases. When M increases,

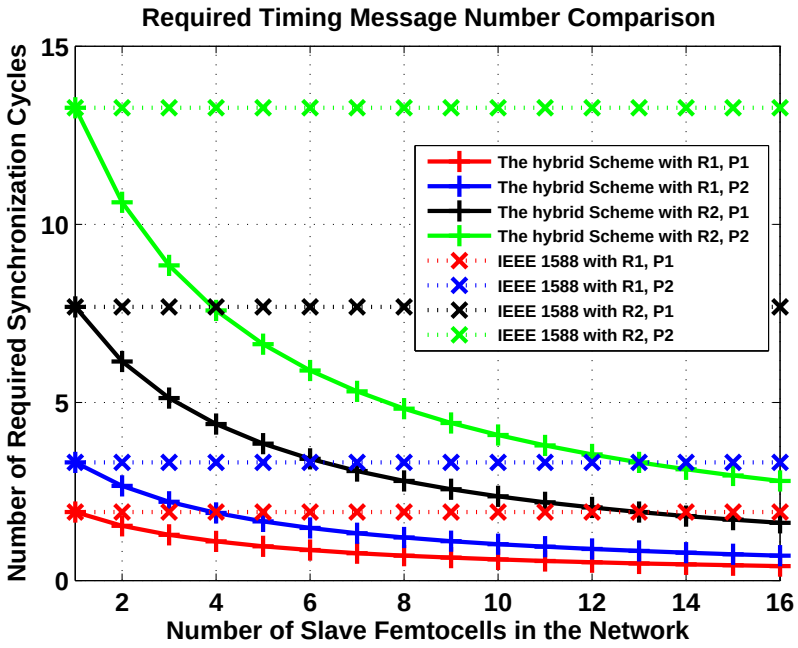

Figure 6.4: Comparison of the required synchronization cycles (per femtocell) for the proposed hybrid scheme and the conventional wireless IEEE 1588 with $R1 = 1$, $R2 = 2$, $P1 = 0.95$, $P2 = 0.99$.

the variance of (6.16) gets smaller and the synchronization performance is improved. So the required number of synchronization cycles of the proposed hybrid scheme N_{Hyb} decreases. However N_{PTP} is irrelevant to M, because the synchronization performance of wireless IEEE 1588 is irrelevant to M. The values of N_{Hyb} and N_{PTP} are equal when $M = 1$, which means only one slave femtocell in the network and no RRS estimator can be obtained. The larger values of $\Pr(|\varepsilon| \leq \varepsilon_{\max})$ and R both lead to larger number of required synchronization cycles for both wireless IEEE 1588 and the proposed hybrid scheme. The proposed hybrid scheme significantly reduces energy consumption and eases the synchronization traffic load in the network, especially when there are a large number of slave femtocells.

The numbers of overall required synchronization messages are compared in Fig. 6.5. They are calculated as the number of required synchronization cycles ((6.31) for the proposed hybrid scheme and (6.30) for wireless IEEE 1588) multiplied by the number of

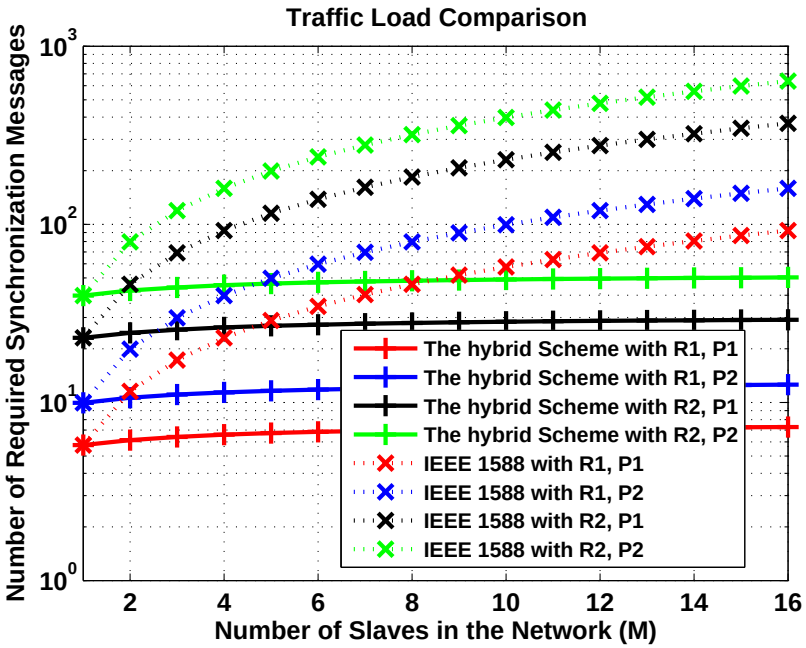

Figure 6.5: Comparison of the overall required synchronization messages for the proposed hybrid scheme and the conventional wireless IEEE 1588 with $R1 = 1$, $R2 = 2$, $P1 = 0.95$, $P2 = 0.99$.

transmitted packets in a single synchronization cycle (shown in Table 6.1), of the proposed hybrid scheme and the conventional wireless IEEE 1588. As can be seen in Fig. 6.5, the proposed hybrid scheme needs many fewer messages than the conventional wireless IEEE 1588.

6.5 Robustness Study

In this section, the robustness of wireless IEEE 1588, RBS and the proposed hybrid scheme is evaluated by means of the synchronization failure rate (FR) against the packet loss rate (PLR). The synchronization failure rate (FR) is defined as the probability that a target femtocell fails to receive the required packets to derive either an IEEE 1588 estimator or a RRS estimator, on the condition of a certain PLR in the network.

Assuming that the PLR is p, for the conventional wireless IEEE 1588, all three packets

in Fig.2 (i.e. *SYNC*, *DELAY_REQ* and *DELAY_RESP*) need to be successfully received in order to calculate (6.5) for a femtocell. Thus, the FR for the conventional wireless IEEE 1588 as a function of PLR is

$$P_{f,PTP} = 1 - (1-p)^3. \tag{6.32}$$

For RBS in Fig. 5.2, the beacon from the Master and at least one broadcast from the peer slaves are necessary. So the FR of RBS can be calculated as:

$$P_{f,RBS} = p + (1-p) \times p^{M-1}, \tag{6.33}$$

where the first term, p, is the failure probability of the master broadcasted beacon and the second term is the probability of that the Master broadcasted beacon is successfully transmitted $(1-p)$, but all messages from the other $M-1$ slaves are lost in the transmission (p^{M-1}).

For the proposed hybrid scheme, synchronization fails when IEEE 1588 synchronization and RRS synchronization are all not viable, and the FR can be written as:

$$P_{f,Hyb} = p + (1-p) \times p^{M-1} \times (1-(1-p)^2). \tag{6.34}$$

Here the first term, p, is the failure probability of the master broadcasted *DELAY_RESP* message; the second term is the probability that *DELAY_RESP* is successfully transmitted $(1-p)$ but all the peer slaves broadcast *DELAY_REQ* messages failed (p^{M-1}) and at least one message out of *SYNC* message and *DELAY_REQ* message sent by itself has failed, $(1-(1-p)^2)$. The FRs of these three schemes ((6.32), (6.33) and (6.34)) vs. PLR are compared in Fig. 6.6.

As the FRs of both RBS and the proposed hybrid scheme depend on M, the FRs with both $M = 2$ and $M = 16$ are simulated and the results are plotted in Fig. 6.6. It is shown

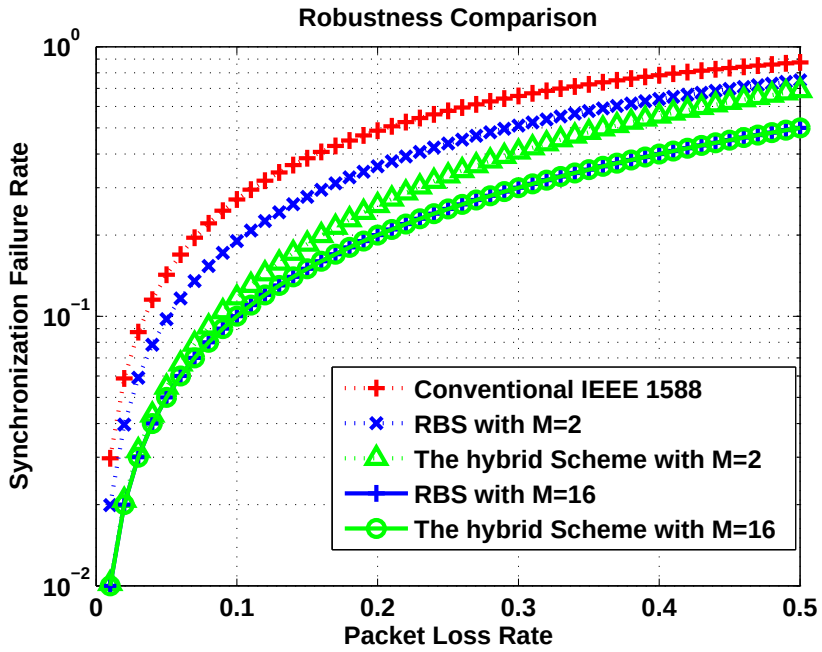

Figure 6.6: Robustness comparison between different schemes in terms of the synchronization failure rate vs. packet loss rate (from 0 to 0.5) with $M = 2$ and $M = 16$.

in Fig. 6.6 that the conventional wireless IEEE 1588 is the most vulnerable to packet loss as the FR is always the highest. The FRs of both RBS and the proposed hybrid scheme decrease when M increases. However, the proposed hybrid scheme is more robust than RBS with either value of M. The advantage is more obvious when $M = 2$. Because p^{M-1} is very small when M is big, and then both (6.33) and (6.34) will be dominated by the first term p, thus the two synchronization failure rates will be approximately the same.

6.6 Synchronization Accuracy

In this section, the synchronization accuracy performance of the proposed hybrid scheme is evaluated using Monte Carlo simulations. The performance of the proposed hybrid scheme is compared with the conventional wireless IEEE 1588. RBS is not in the comparison because the estimation of RBS is not unbiased as previously explained. The synchronization accuracy is evaluated in term of the RMSEs (Root Mean Squared Errors)

of the clock offset estimation and the clock skew estimation as shown in Fig. 6.7 and Fig. 6.8, respectively. As the performance of the proposed hybrid scheme relies on the number of the slave femtocells in the network, the slave femtocell numbers $M = 4$ and $M = 16$ are both simulated. The number of Monte Carlo simulation trials for each point is 10000. The initial clock offset $\phi_0 = 1$ sec. The clock skew $\rho = 100$ ppm (parts per million). The random delays are Gaussian random variables with $\mu = 100\mu$ sec and $\sigma = 20\mu$ sec.

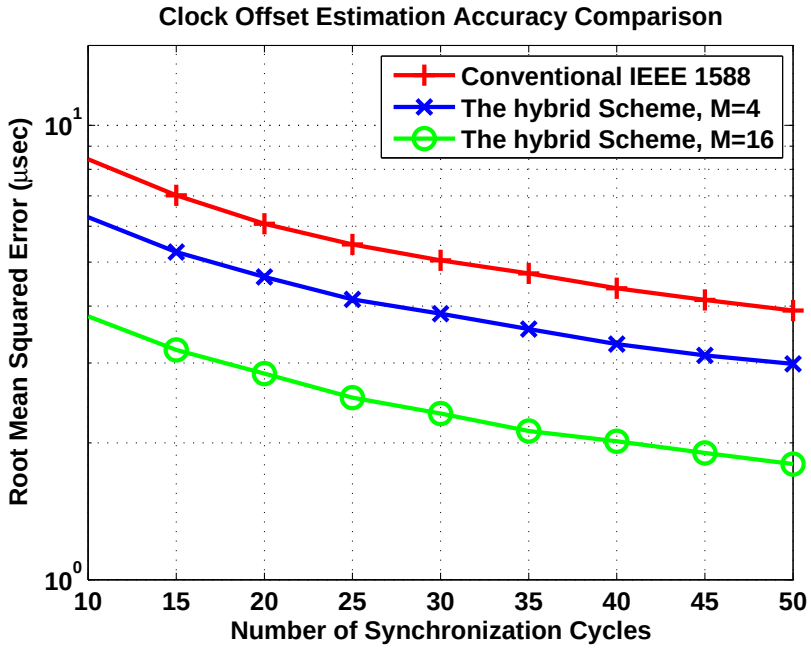

Figure 6.7: RMSEs of the clock offset estimations of the proposed hybrid scheme in comparison with the conventional wireless IEEE 1588.

Fig. 6.7 and Fig. 6.8 show that the synchronization performance of the proposed hybrid scheme is better than that of the conventional wireless IEEE 1588. The performances of both schemes improve with the increase of N. In addition, as M increases, the synchronization performance of the proposed hybrid scheme improves. For instance, the RMSE of the clock offset estimation in the proposed hybrid scheme with $M = 16$ is $2\mu s$ smaller than that of the $M = 4$ scenario and $4\mu s$ smaller than that of the conventional wireless IEEE 1588 when $N = 10$.

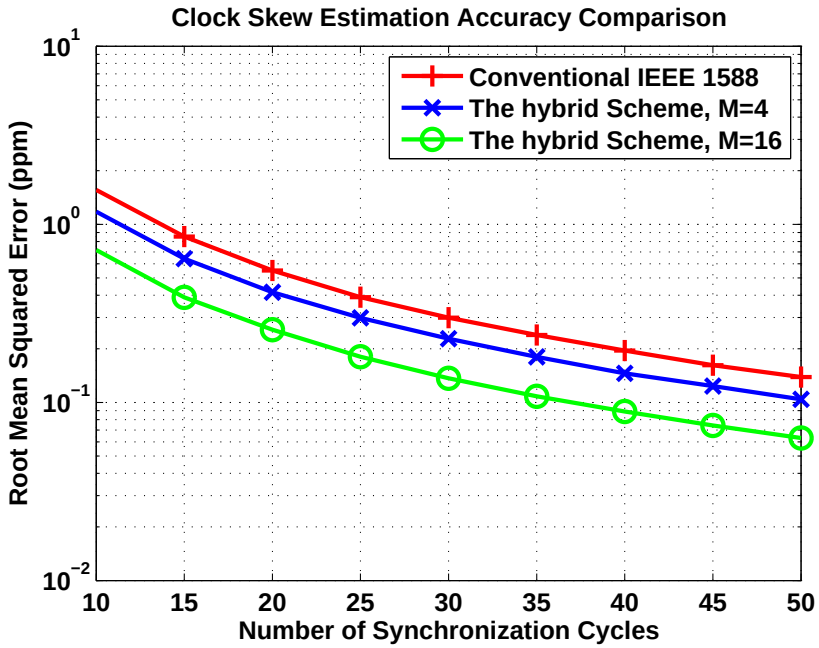

Figure 6.8: RMSEs of the clock skew estimations of the proposed hybrid scheme in comparison with the conventional wireless IEEE 1588.

6.7 Summary

This chapter proposed a hybrid synchronization scheme based on wireless IEEE 1588 and receiver-receiver synchronization. The proposed hybrid scheme makes the best use of the advantages of both wireless IEEE 1588 and RBS. The proposed hybrid scheme can provide better synchronization accuracy with less exchanged messages when compared to wireless IEEE 1588, especially when there are a large number of slave femtocells in the network. It has also been proven that the proposed hybrid scheme is much more robust against the packet loss in the network than the conventional wireless IEEE 1588 and RBS.

7 Dual Sources Synchronization for Femtocells

7.1 Introduction

As discussed in the previous chapters, a femtocell can get synchronization via GPS, backhaul and listening to neighbouring cells. On some occasions, there may be more than one synchronization sources to provide timing references. In such cases, the simplest way is to select the best one. In [43], two hybrid synchronization solutions for femtocells, Hybrid AGPS - PTP and Hybrid AGPS - Femto Sniff (i.e. neighbouring cells listening), are recommended for different femtocell deployments. In both hybrid synchronization solutions, AGPS is selected as the preference. However, when AGPS goes into holdover due to lack of satellite signal or poor signal quality, both solutions switch over to the reference of the other synchronization source, either PTP packets or neighbouring cells listening, so that it keeps timing and frequency in good quality.

However, both hybrid synchronization solutions simply uses PTP or neighbouring cells listening as the backup for GPS and they would not provide optimal performance when the different synchronization sources have comparable performance – for example the femtocell synchronization scenario where the femtocell is viable to both IEEE 1588 and neighbouring cells listening. Both methods have their own relative advantages and dis-

advantages. The backhaul based IEEE 1588 synchronization is usually more stable than neighbouring cells listening. However IEEE 1588 often suffers from the asymmetric link problem as introduced in Chapter 3, which is not a problem for neighbouring cells listening. Thus, it is desirable if the advantages of both synchronization sources can be exploited so as to achieve a better combined performance.

In this chapter, a typical femtocell synchronization scenario with two comparable synchronization sources, IEEE 1588 via backhaul and neighbouring cells listening, is studied. A two-step weighted multiple linear regression (WMLR) based synchronization scheme is proposed for the scenario. The proposed scheme can also be extended to other similar dual sources synchronization scenarios. Using this scheme, the femtocell synchronization can achieve:

1. Better accuracy: the synchronization accuracy of the proposed scheme is better than any of the two synchronization sources.

2. Better stability: the fixed bias error between these two synchronization sources, which is mainly due to the IEEE 1588 asymmetric link problem, can be accurately estimated. This is particularly important when one of the synchronization sources becomes unavailable and the femtocell switches over to the other source. Unknown bias error could lead to instability for the femtocell system or even break down the on-going communication in the worst case.

The rest of this chapter is organized as follows. In Section 7.2, the dual sources synchronization scenario is introduced. In Section 7.3, the two-step WMLR based synchronization scheme is proposed for this synchronization scenario. In the first step, a conventional normal linear regression (NLR) based estimation method is developed for coarse synchronization and noise variance estimation. Then a WMLR based estimation method is executed for fine synchronization in the second step. The synchronization performance of

the proposed scheme is evaluated using Monte Carlo simulations in Section 7.4. Finally, Section 7.5 concludes this chapter.

7.2 Synchronization Scenario

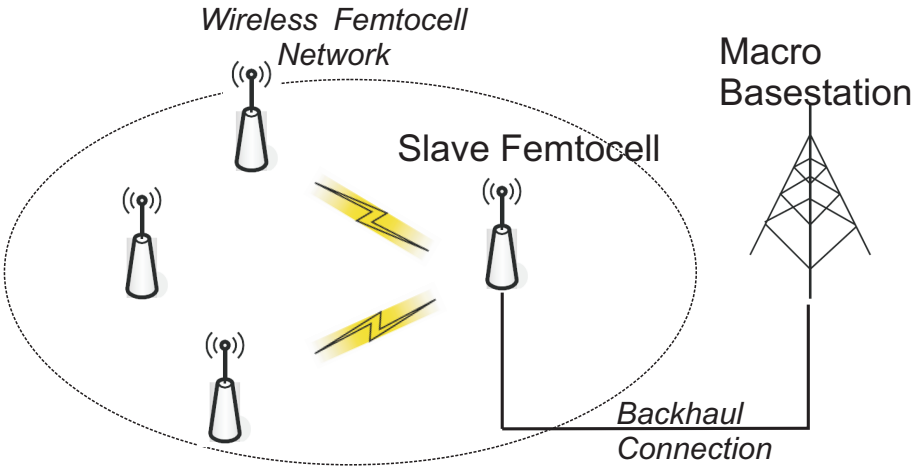

Figure 7.1: Dual Synchronization Sources Scenario.

Fig. 7.1 shows a femtocell network with two synchronization sources. The femtocell requiring synchronization is referred to as the 'Slave' femtocell. The 'Slave' femtocell is connected to the Macro base station via backhaul and the wireless femtocell network. Thus, the femtocell is able to receive timing references from two synchronization sources: neighbouring cells listening, which is referred to as Source A, and IEEE 1588 via backhaul, referred to as Source B. The timing references from these two synchronization sources can be modeled as two groups of clock offset observations, similar as in (3.7). After receiving N_A clock offset observations from Source A, the ith observation can be written as :

$$\hat{\phi}_A(t_i) = \phi(t_i) + \varepsilon_{1,i}, i = 1,2,...,N_A, \tag{7.1}$$

where t_i is the observing time of the ith clock offset observation of Source A, $\phi(t_i)$ is the true value of the femtocell clock offset at time t_i, and $\varepsilon_{1,i}$ is the ith observation noise of

Source A, following a Gaussian distribution with zero mean and variance σ_A^2. Similarly, after receiving N_B clock offset observations from Source B, the jth observation from IEEE 1588 can be written as:

$$\hat{\phi}_B(t_j^{'}) = \phi(t_j^{'}) + d_{asym} + \varepsilon_{2,j},\ j = 1,2,...,N_B, \tag{7.2}$$

where $t_j^{'}$ is the observing time of the jth clock offset observation of Source B, $\phi(t_j^{'})$ is the true value of the clock offset at time $t_j^{'}$, d_{asym} is the IEEE 1588 bias error introduced by the asymmetric communication links, and $\varepsilon_{2,j}$ is the jth observation noise of Source B, following a Gaussian distribution with zero mean and variance σ_B^2.

7.3 A Two-Step Weighted Multiple Linear Regression Based Synchronization Scheme for Femtocells

Similar to (4.1), the femtocell clock skew is assumed to be constant. The femtocell clock offset $\phi(t)$ at time t can be expressed as:

$$\phi(t) = \phi_0 + \rho t, \tag{7.3}$$

where ϕ_0 is the initial clock offset, ρ is the constant clock skew. Then the femtocell clock ($T_s(t)$) at time t can be written as:

$$T_s(t) = t + \phi(t) = \phi_0 + (1+\rho)t. \tag{7.4}$$

The goal of the proposed two-step WMLR based synchronization scheme is to accurately estimate the initial clock offset (ϕ_0), clock skew (ρ) of the femtocell and the IEEE 1588 bias error (d_{asym}) from the received timing references. In Step 1, the conventional normal

linear regression estimation is used for coarse synchronization and variance (of the observation noise) estimation. In Step 2, based on the estimated noise variance in Step 1, a WMLR based estimation method is proposed to accurately estimate the aforementioned three unknowns.

7.3.1 Step 1: Normal Linear Regression Based Coarse Synchronization and Noise Variance Estimation

Considering the femtocell can only be aware of the time on its own clock, substituting (7.4) into (7.1) and (7.2) produces:

$$\begin{aligned}\hat{\phi}_A(t_i) &= \phi_0 + \rho\frac{T_s(t_i)-\phi_0}{1+\rho} + \varepsilon_{1,i} \\ &= \frac{\phi_0}{1+\rho} + \frac{\rho}{1+\rho}T_s(t_i) + \varepsilon_{1,i}, i = 1,2,...,N_A, \end{aligned} \tag{7.5}$$

$$\begin{aligned}\hat{\phi}_B(t_j^{'}) &= \phi_0 + d_{asym} + \rho\cdot\frac{T_s(t_j^{'})-\phi_0}{1+\rho} + \varepsilon_{2,j} \\ &= \frac{\phi_0}{1+\rho} + d_{asym} + \frac{\rho}{1+\rho}T_s(t_j^{'}) + \varepsilon_{2,j}, j = 1,2,...,N_B. \end{aligned} \tag{7.6}$$

Apply the linear regression technique, (7.5) can be written in matrix notation as:

$$\hat{\phi}_{\mathbf{A}} = \mathbf{H_A}\theta_{\mathbf{A}} + \varepsilon_{\mathbf{1}}, \tag{7.7}$$

where $\hat{\phi}_{\mathbf{A}} = [\phi_A(t_1), \phi_A(t_2), ..., \phi_A(t_{N_A})]^T$, $\theta_{\mathbf{A}} = [\theta_{A,0}, \theta_{A,1}]^T = [\frac{\phi_0}{1+\rho}, \frac{\rho}{1+\rho}]^T$, $\varepsilon_1 = [\varepsilon_{1,1}, \varepsilon_{1,2}, ..., \varepsilon_{1,N_A}]^T$ and $\mathbf{H_A} = [1,1,...,1; T_s(t_1), T_s(t_2), ..., T_s(t_{N_A})]^T$. Then the least square estimation of $\theta_{\mathbf{A}}$ is given by:

$$\hat{\theta}_{\mathbf{A}} = (\mathbf{H_A^T H_A})^{-1}\mathbf{H_A^T}\hat{\phi}_{\mathbf{A}}, \tag{7.8}$$

and then ρ and ϕ_0 can be derived from (7.8) as:

$$\hat{\rho} = \frac{1}{1-\hat{\theta}_{A,1}} - 1, \tag{7.9}$$

$$\hat{\phi}_0 = \frac{\hat{\theta}_{A,0}}{1-\hat{\theta}_{A,1}}. \tag{7.10}$$

The estimated clock offset and clock skew can then be applied to compensate the femtocell clock for coarse synchronization.

In addition, assuming $N_A \geq 3$, then according to [71], σ_A^2 can be estimated as:

$$\hat{\sigma_A^2} = \frac{1}{N_A - 2} \times (\hat{\phi}_\mathbf{A} - \mathbf{H_A}\hat{\theta}_\mathbf{A})^T(\hat{\phi}_\mathbf{A} - \mathbf{H_A}\hat{\theta}_\mathbf{A}). \tag{7.11}$$

Similarly, the observations from Source B in (7.6) can be written in matrix notation as:

$$\hat{\phi}_\mathbf{B} = \mathbf{H_B}\theta_\mathbf{B} + \varepsilon_\mathbf{2}, \tag{7.12}$$

where $\hat{\phi}_\mathbf{B} = [\phi_B(t_1^{'}), \phi_B(t_2^{'}), ..., \phi_B(t_{N_B}^{'})]^T$, $\theta_\mathbf{B} = [\theta_{B,0}, \theta_{B,1}]^T = [\frac{\phi_0}{1+\rho} - d_{asym}, \frac{\rho}{1+\rho}]^T$, $\varepsilon_2 = [\varepsilon_{2,1}, \varepsilon_{2,2}, ..., \varepsilon_{2,N_B}]^T$ and $\mathbf{H_B} = [1, 1, ..., 1; T_s(t_1^{'}), T_s(t_2^{'}), ..., T_s(t_{N_B}^{'})]^T$. Then the least square estimation of $\theta_\mathbf{B}$ is given by:

$$\hat{\theta}_\mathbf{B} = (\mathbf{H_B^T H_B})^{-1}\mathbf{H_B^T}\hat{\phi}_\mathbf{B}. \tag{7.13}$$

Similar to (7.9), ρ can be derived from (7.13) as:

$$\hat{\rho} = \frac{1}{1-\hat{\theta}_{B,1}} - 1. \tag{7.14}$$

Note that there are two unknowns (ϕ_0 and d_{asym}) in $\hat{\theta}_{B,0}$, so they can not be resolved.

However the observation noise variance σ_B^2 can still be estimated as ($N_B \geq 3$):

$$\hat{\sigma_B^2} = \frac{1}{N_B - 2} \times (\hat{\phi}_{\mathbf{B}} - \mathbf{H_B}\hat{\theta}_{\mathbf{B}})^T (\hat{\phi}_{\mathbf{B}} - \mathbf{H_B}\hat{\theta}_{\mathbf{B}}). \tag{7.15}$$

7.3.2 Step 2: Weighted Multiple Linear Regression Based Fine Synchronization

After receiving $N = N_A + N_B$ observations, the observation times can be rewritten as $t_k, k = 1,2,...,N$. Similar to (4.56) in Chapter 4, the clock offset observations from (7.5) and (7.6) can be written using a single formula with a new variable b_k:

$$\phi_W(t_k) = \theta_{W,0} + \theta_{W,1} T_s(t_k) + \theta_{W,2} b_k + \varepsilon_k, k = 1,2,...,N, \tag{7.16}$$

where $\phi_W(t_k)$ is the kth clock offset observation at t_k, $T_s(t_k)$ is the femtocell clock at t_k, b_k is the new variable and ε_k is the observation noise. If the kth observation is from Source A, then $b_k = 0$ and ε_k is the corresponding observation noise of Source A. If the kth observation is from Source B, then $b_k = 1$ and ε_k is the corresponding observation noise of Source B. Also

$$\theta_{W,0} = \frac{1}{\rho + 1}\phi_0, \tag{7.17}$$

$$\theta_{W,1} = \frac{\rho}{1 + \rho}, \tag{7.18}$$

$$\theta_{W,2} = d_{asym}. \tag{7.19}$$

Now (7.16) can be written in matrix form as:

$$\hat{\phi}_{\mathbf{W}} = \mathbf{H_W}\theta_{\mathbf{W}} + \varepsilon_{\mathbf{W}}, \tag{7.20}$$

where

$$\hat{\phi}_{\mathbf{W}} = [\hat{\phi}_W(t_1), \hat{\phi}_W(t_2), ..., \hat{\phi}_W(t_k), ..., \hat{\phi}_W(t_N)]^T, \tag{7.21}$$

$$\mathbf{H_W} = \begin{bmatrix} 1 & T_s(t_1) & b_1 \\ 1 & T_s(t_2) & b_2 \\ \vdots & \vdots & \vdots \\ 1 & T_s(t_N) & b_N \end{bmatrix}, \tag{7.22}$$

$$\theta_{\mathbf{W}} = [\theta_{W,0}, \theta_{W,1}, \theta_{W,2}]^T, \tag{7.23}$$

$$\varepsilon_{\mathbf{W}} = [\varepsilon_1, \varepsilon_2, ..., \varepsilon_N]^T. \tag{7.24}$$

In Section 4.4.1, a multiple linear regression (MLR) based estimation method is proposed for the 'variable-length IEEE 1588' scheme. Comparing (4.56) and (7.16), it can be seen that the observation noise in (4.56) follows the same Gaussian distribution however the variance of ε_k in (7.16) varies. Thus, the observations in (7.16) should be weighted based on their relative observation noise, leading to a weighted multiple linear regression (WMLR) based estimation method. The performances of MLR and WMLR in this scenario will be compared in Section 7.4.

In WMLR, a weighting matrix $\mathbf{W}$ is introduced, which is a $N \times N$ diagonal matrix where the kth diagonal element (w_k) equals to $\frac{1}{\hat{\sigma}_A^2}$ or $\frac{1}{\hat{\sigma}_B^2}$, corresponding to the kth observation is from Source A or Source B. And then the weighted least square estimation of $\theta_{\mathbf{W}}$ is given by:

$$\hat{\theta}_{\mathbf{W}} = (\mathbf{H_W^T W H_W})^{-1} \mathbf{H_W^T W} \hat{\phi}_{\mathbf{W}}. \tag{7.25}$$

And then the bias error, clock skew and clock offset can be estimated as:

$$\hat{d}_{asym} = \hat{\theta}_{W,2}, \tag{7.26}$$

$$\hat{\rho} = \frac{1}{1 - \hat{\theta}_{W,1}} - 1, \tag{7.27}$$

$$\hat{\phi}_0 = \frac{\hat{\theta}_{W,0}}{1 - \hat{\theta}_{W,1}}. \tag{7.28}$$

Now the estimated fixed bias error, clock offset and clock skew can be applied to compensate the femtocell clock for fine synchronization.

Fig. 7.2 shows the flow chart of the two-step WMLR based synchronization scheme.

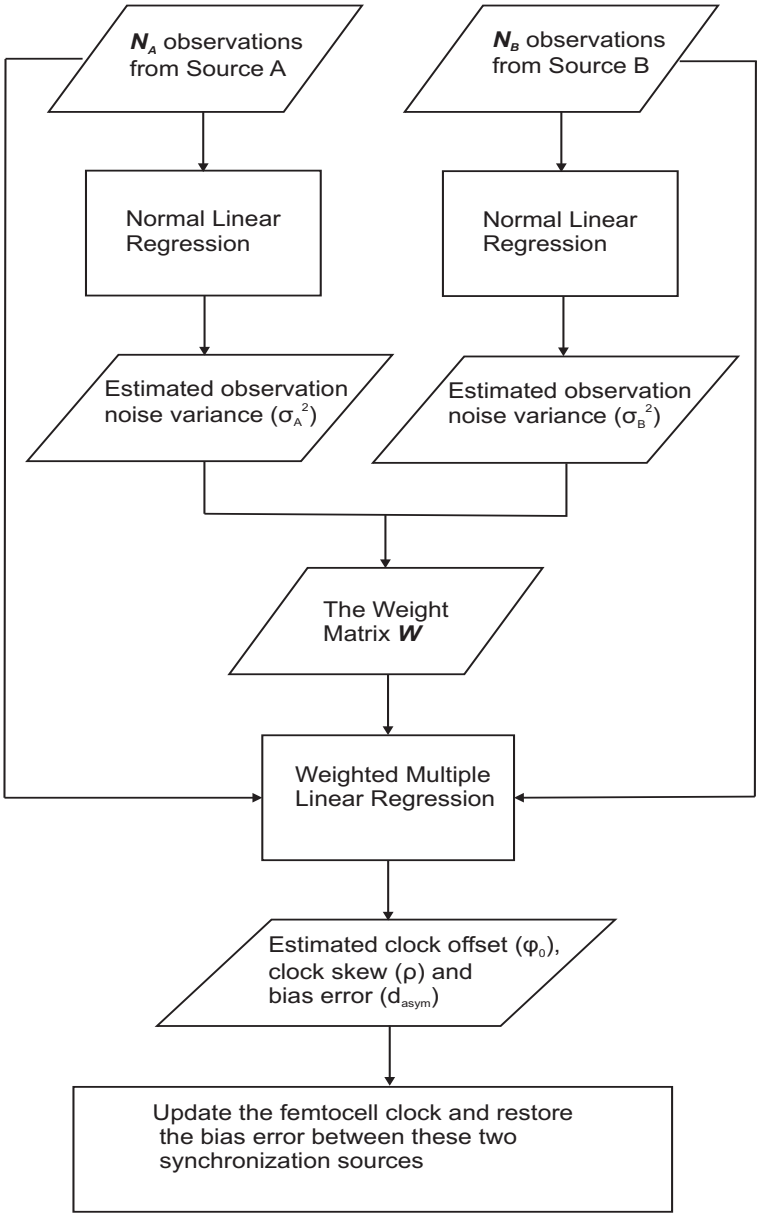

Figure 7.2: Flow chart of the proposed two-step WMLR based synchronization scheme.

7.4 Performance Evaluation

In this section, the synchronization accuracy performance of the proposed scheme is evaluated using Monte Carlo simulations. The synchronization accuracy is firstly evaluated in terms of the root mean squared errors (RMSEs) of the estimations of the initial clock offset (ϕ_0), clock skew (ρ) of the femtocell and the IEEE 1588 bias error (d_{asym}) in Fig. 7.3, Fig. 7.4 and Fig. 7.5, respectively. The number of Monte Carlo simulation trials for each point is 10000. The initial clock offset of the femtocell $\phi_0 = 1\,\text{sec}$. The clock skew $\rho = 100$ ppm (parts per million). The fixed bias error $d_{asym} = 1m\,\text{sec}$. The standard deviations of the observation noise of the two sources are $\sigma_A = 40\mu$ sec and $\sigma_B = 20\mu$ sec, respectively.

Fig. 7.3 compares the RMSEs of the initial clock offset estimation of Source A (7.10), the proposed WMLR based method (7.28) and the MLR based method ((7.28) with the weighting matrix in (7.25), $\mathbf{W} = \mathbf{I_N}$). Source B is not in the comparison, since ϕ_0 cannot be estimated from (7.13). The MLR based method is compared with the WMLR based method in order to show that the observations should be weighted based on their relative observation noise and so the derivation of the weighting matrix $\mathbf{W}$ in (7.25) is necessary. It is clearly shown in Fig. 7.3 that the WMLR based method can provide better synchronization accuracy with a smaller RMSE of the initial clock offset estimation than Source A and the MLR based method.

In Fig. 7.4, the RMSEs of the clock skew estimation of Source A (7.9), Source B (7.14), the proposed WMLR based method (7.27) and the MLR based method ((7.27) with the weighting matrix in (7.25) $\mathbf{W} = \mathbf{I_N}$) are compared. Similar to Fig. 7.3, the proposed scheme outperforms the other three methods.

Fig. 7.5 compares the RMSEs of the IEEE 1588 bias error estimation of the NLR based method, the proposed WMLR based method ((7.26)) and the MLR based method ((7.26) with the weighting matrix in (7.25) $\mathbf{W} = \mathbf{I_N}$), where the IEEE 1588 bias error in NLR

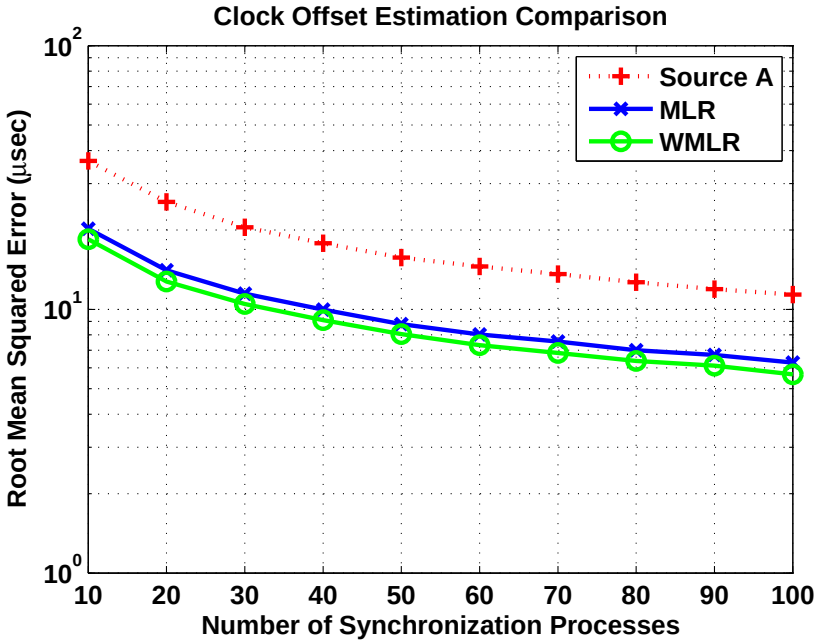

Figure 7.3: Comparison of the RMSEs of the clock offset estimations.

based method is estimated as $\hat{\theta}_{B,0} - \hat{\theta}_{A,0}$. The performance of the WMLR based method is very similar to the MLR based method but still marginally better. However, the gap between these two methods and the NLR based method is much bigger. As introduced in Section 7.1, the bias error estimation is important when one of the synchronization sources becomes unavailable and the femtocell switches over to the other source. This is because the uncompensated bias error would lead to instability for the femtocell system. In this way, the proposed scheme enhances the stability for the femtocell synchronization.

Then the impact of the observation number and the observation noise on the performance of the proposed two-step WMLR based synchronization scheme is evaluated in Fig. 7.6 and Fig. 7.7. The RMSEs of the clock skew estimation of Source A (7.9), Source B (7.14) and the proposed WMLR based method (7.27) are plotted against the observation noise variance ratio ($\frac{\sigma_A^2}{\sigma_B^2}$) are plotted in Fig. 7.6. In Fig. 7.6, $N_A = N_B = 50$, $\sigma_B = 20\mu$sec and $\frac{\sigma_A^2}{\sigma_B^2}$ ranges from 1 to 40. It can be seen in Fig. 7.6 that the proposed WMLR based method produces the biggest improvement when $\sigma_A^2 = \sigma_B^2$ and reduces the RMSE of the

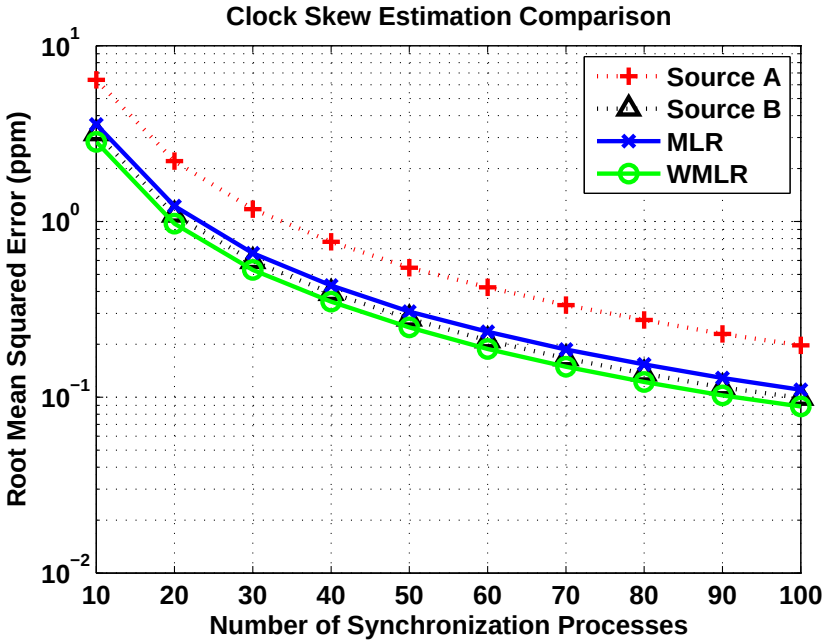

Figure 7.4: Comparison of the RMSEs of the clock skew estimations.

clock skew estimation by 29.4% compared with either Source A or Source B. This improvement on the clock skew estimation (i.e. the reduction in the RMSE compared with the better synchronization source, Source B) decreases when $\frac{\sigma_A^2}{\sigma_B^2}$ increases. When $\frac{\sigma_A^2}{\sigma_B^2} > 5$, the improvement is smaller than 10%. When $\frac{\sigma_A^2}{\sigma_B^2} = 10$, the improvement decreases to 4.6%.

Fig. 7.7 plots the RMSEs of the clock skew estimation of Source A (7.9), Source B (7.14) and the proposed WMLR based method, respectively, against the ratio of the observation numbers ($\frac{N_A}{N_B}$). Here $\sigma_A = \sigma_B = 20\mu$sec, $N_B = 10$, $\frac{N_A}{N_B}$ range from 1 to 30. Similarly, Fig. 7.7 shows that the the proposed WMLR based method produces the biggest improvement when $N_A = N_B$, reduces the RMSE of the clock skew estimation by 64.6% compared with both Source A and Source B. When $\frac{N_A}{N_B} = 10$, this improvement decreases to 13.4%. When $\frac{N_A}{N_B} > 15$, the improvement goes down to below 10%.

Both Fig. 7.6 and Fig. 7.7 illustrate that the proposed WMLR based scheme performs better when the observations from the two synchronization sources are more comparable.

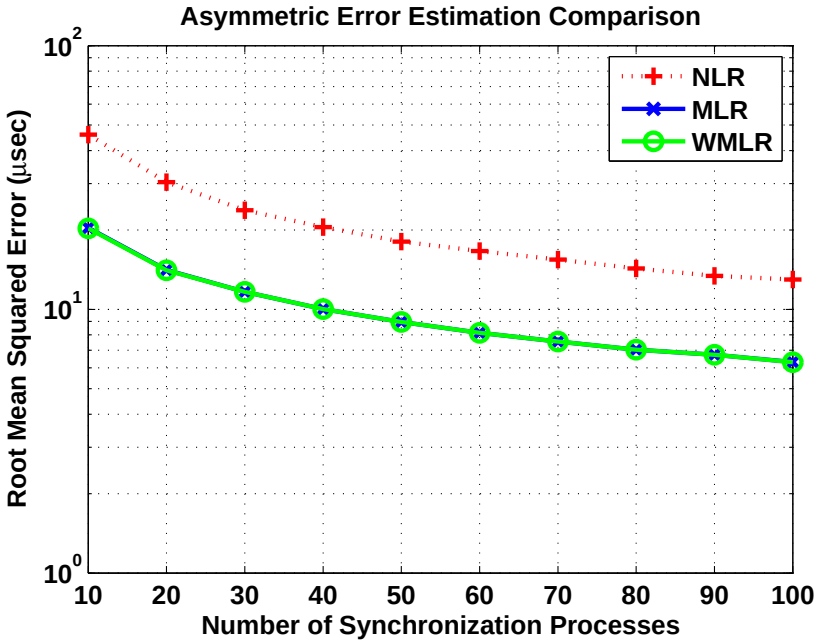

Figure 7.5: Comparison of the RMSEs of the asymmetric error estimations.

When one synchronization source is much better than another (in terms of either observation number or observation noise), the proposed method only provides a little improvement on the synchronization accuracy. In extreme circumstances, if a synchronization source offers far more observations with far lower observation noise than another, such as when GPS is available, it will then be selected as the only synchronization source.

7.5 Summary

This chapter proposed a two-step weighted multiple linear regression (WMLR) based synchronization scheme for the femtocell synchronization scenario with dual synchronization sources. A typical femtocell synchronization scenario where the femtocell is viable to both IEEE 1588 synchronization and neighbouring cells listening is studied. The WMLR base estimation is introduced to femtocell synchronization for the first time. In the first step of the scheme, a conventional normal linear regression (NLR) based estimation method is developed for coarse synchronization and noise variance estimation. In

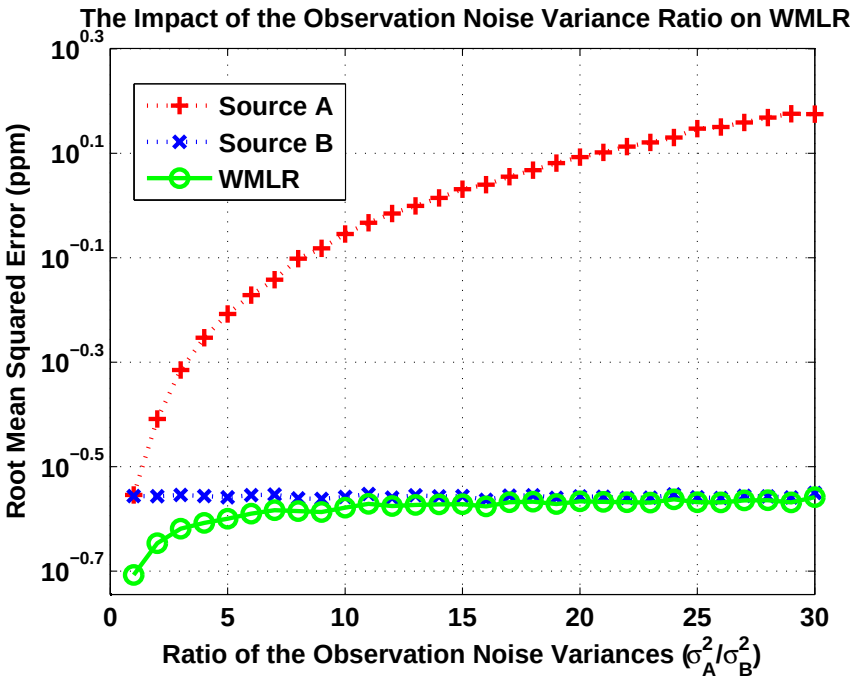

Figure 7.6: The impact of the observation noise variance ratio ($\frac{\sigma_A^2}{\sigma_B^2}$) on the performance of WMLR in terms of the RMSEs of the clock skew estimation of different methods.

the second step, a WMLR based estimation method is executed for fine synchronization. The flow chart of the proposed scheme is also given. Simulation results show that the proposed scheme provides better synchronization accuracy and better stability than any of the individual sources. It is also suggested in the simulation results that the proposed scheme performs better when the observations from the two synchronization sources are comparable.

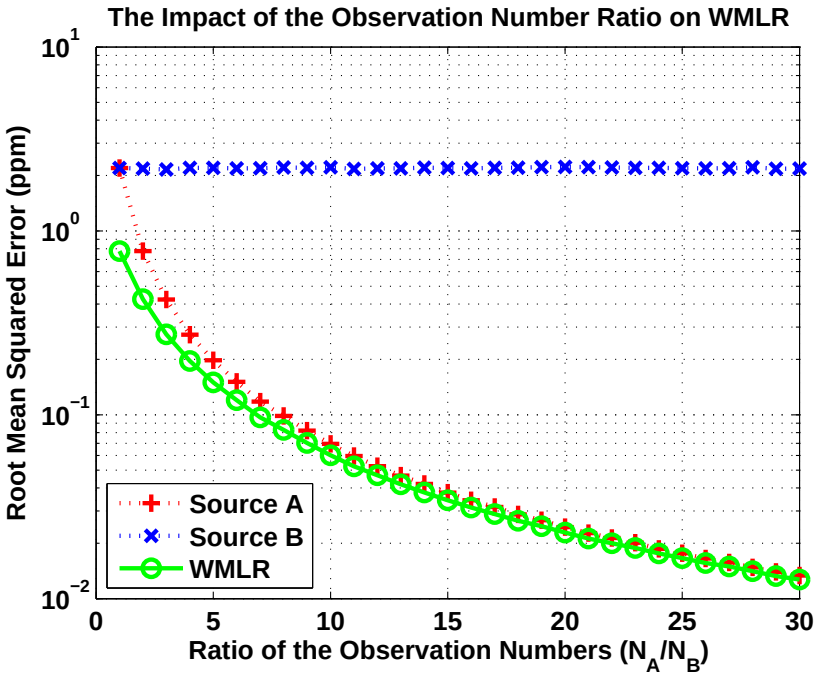

Figure 7.7: The impact of the observation number ratio ($\frac{N_A}{N_B}$) on the performance of WMLR in terms of the RMSEs of the clock skew estimation of different methods.

8 Conclusions and Future Work

8.1 Conclusions

This thesis has investigated the important issue of time synchronization problem for femtocell networks. There are a number of areas of femtocell operation that require time synchronization. These include supplying phase and frequency information to the handsets, ensuring reliable handover and interference reduction, to name but a few. As can be seen in Table 2.1, the accuracy requirements for femtocells are very strict, although they differ from one standard to another. However, most femtocells are not equipped with accurate and expensive oscillators, because of the low-cost requirement for femtocell manufacture. With a higher accuracy requirement but lower oscillator performance, the synchronization accuracy of femtocells relies more on external timing references. So other solutions with high synchronization accuracy have to be used in order to ensure the time synchronization requirements are satisfied with equipment that includes low accuracy oscillators.

According to synchronization sources, these methods can be categorized as: synchronization via GPS, synchronization via TV signals, synchronization via backhaul and synchronization via neighbouring cells listening. This thesis has focused on two of these methods: synchronization using IEEE 1588 via backhaul and synchronization via neighbouring cells listening, or more specifically, listening to other synchronized femtocells in the wireless femtocell network. A number of problems with respect to these two methods were investigated and a series of solutions were proposed.

Chapters 3 and 4 were focused on femtocell synchronization using IEEE 1588 via backhaul. However, the synchronization performance of the conventional IEEE 1588 algorithm is affected by two main problems: asymmetric link and random delays. In order to mitigate these two problems, two schemes, the 'improved IEEE 1588' synchronization scheme and the 'variable-length IEEE 1588' synchronization scheme were proposed in Chapter 3 and Chapter 4, respectively.

In Chapter 3, the basic mechanism of IEEE 1588 and the two aforementioned problems were analyzed. Then, the 'improved IEEE 1588' synchronization scheme was proposed. In this scheme, packets with different lengths are added to every IEEE 1588 synchronization process. So, two more equations can be written for every process, which can help derive the estimates of the 'fixed delays' in both the uplink and the downlink and then the asymmetric link problem will be alleviated. The simulation results have demonstrated that the 'improved IEEE 1588' scheme successfully addresses the problems of the asymmetric link and random delays. It provides significantly better performance compared to the conventional IEEE 1588 approach and an existing method [56] in terms of clock offset bias error. However, in the 'improved IEEE 1588' scheme, two more messages are transmitted in every IEEE 1588 synchronization process. This brings an additional undesirable overhead. Thus, another enhanced scheme was proposed in Chapter 4.

In Chapter 4, a 'variable-length IEEE 1588' synchronization scheme for femtocells was introduced. This scheme also solves the asymmetric link and random delay problems of IEEE 1588. Instead of adding two more packets in the 'improved IEEE 1588' scheme, the 'variable-length IEEE 1588' scheme changes the lengths of the original IEEE 1588 packets periodically. Two clock models, with no clock skew and with clock skew, were considered in Chapter 4. Through Monte Carlo simulations, the synchronization accuracy of the 'variable-length IEEE 1588' scheme was similar to the 'improved IEEE 1588' scheme but with significantly reduced transmitted messages.

Chapters 5 and 6 focus on femtocell synchronization via neighbouring cells listening. In Chapter 5, the receiver-receiver synchronization (RRS) for femtocell networks was studied. The RRS method has proved to be efficient and accurate for packet-based wireless network synchronization. However, the most widely used RRS scheme, reference broadcast synchronization (RBS), cannot be directly applied in femtocell networks. So, two new RRS based synchronization schemes were proposed to apply this mechanism in femtocell networks.

In Chapter 6, a novel hybrid synchronization scheme based on wireless IEEE 1588 and RRS was proposed for wireless femtocell networks. By slightly changing the message exchanging process and the broadcast mode of the conventional wireless IEEE 1588, the hybrid scheme makes the best use of the advantages of both wireless IEEE 1588 and RRS. Throughout the comprehensive comparison with the conventional wireless IEEE 1588 and RBS, it can be seen that this hybrid scheme can provide better synchronization accuracy with less exchanged messages compared with wireless IEEE 1588, and is much more robust than the conventional wireless IEEE 1588 and RBS against the packet loss in the network.

Chapter 7 investigated the femtocell synchronization scenario with dual synchronization sources. A typical femtocell synchronization scenario, where both IEEE 1588 synchronization and neighbouring cells listening are available, was studied. Both synchronization methods have their own relative advantages and disadvantages. It is desirable if the combination can make the best use of the advantages of these synchronization methods. A two-step weighted multiple linear regression (WMLR) based synchronization scheme was proposed. Simulation results have shown that the proposed scheme provides better synchronization accuracy and better stability than any of the individual sources. It was also suggested in the simulation results that the proposed scheme performs better when the observations from the two synchronization sources are more comparable.

8.2 Future Work

Time synchronization is a critical issue for communication systems and in particular for femtocells. A better synchronization performance is always pursued by researchers and cellular network operators, even when the present synchronization requirement is met.

The following are suggestions for future work that can further improve the femtocell synchronization performance and may lead to fruitful results:

1. For both IEEE 1588 and RRS, the random part of the link delay hugely affects the synchronization accuracy. Mostly, the random delay is assumed to follow a specific distribution which depends on the network environment. In this thesis, the random delay is modeled as either a Gaussian or an exponential random variable. However, because the random delay may follow a different distribution when the network environment changes, time synchronization schemes that are robust and adaptive to arbitrary random delay distributions are more desirable. To our knowledge, the work of Kim et al. [100] is the only one in this research area. We believe that the particle filter or advanced Kalman filter based solutions may solve the problem and lead to a better synchronization performance.

2. In Chapters 5 and 6, time synchronization for wireless femtocell networks is examined, where we only considered the time synchronization in a single-hop network. However, it is possible that the femtocells can form larger networks, especially in SOHO (Small Office and Home Office) area. Therefore, improving the schemes proposed in Chapters 5 and 6 and then adapting them for multi-hop networks will result in more practical synchronization solutions for wireless femtocell networks.

3. The macrocell listening synchronization method was introduced in Chapter 2. Although the coverage requirement is stringent for femtocells when using this method, it can provide sufficient synchronization accuracy in both frequency and phase.

However, the possibility of stronger, less predictable, and time-varying interference in femtocell networks, in particular co-channel interference (CCI), may seriously complicate the synchronization problem, particularly in OFDM based systems such as WiMAX and LTE. What is worse, the synchronization error will aggravate the interference problem in return. In [101], a pre-filter is designed to mitigate the CCI effect on cross-correlation based time synchronization. Although the system modeling in [101] and then the filter design can be further improved, the author has proved that the pre-filter based method is promising. The author also believes that the design of a joint time synchronization and interference cancellation receiver for femtocells will successfully alleviate both of these problems.

Bibliography

[1] Cisco White Paper. "Cisco Visual Networking Index: Global Mobile Data Traffic Forecast Update, 2010-2015". February 2011.

[2] Jie Zhang and Guillaume de La Roche. *Femtocells: Technologies and Deployment*. Wiley, Chichester, West Susssex, U.K., Hoboken, NJ, 2010.

[3] Vikram Chandrasekhar, Jeffrey G. Andrews, and Alan Gatherer. "Femtocell Networks: A Survey". *CoRR*, abs/0803.0952, 2008.

[4] D. Chambers. "Crystal Frequency Oscillators in Femtocells". Oct. 2007.

[5] M.-S. Alouini and A. Goldsmith. "Area Spectral Efficiency of Cellular Mobile Radio Systems". In *Vehicular Technology Conference, 1997, IEEE 47th*, volume 2, pages 652–656 vol.2, 1997.

[6] *Small Cell Forum*. [Online]. Available: www.smallcellforum.org.

[7] Small Cell Forum White Paper. "Regulatory Aspects of Femtocells". March 2011.

[8] Qualcomm. *Femtocells - The Next Performance Leap*. [Online]. Available: http://www.qualcomm.com/media/documents/femtocells-next-performance-leap.

[9] Juniper Research White Paper. "Wifi and Femtocell Integration Strategies 2011-2015". March 2011.

[10] J.G. Andrews, H. Claussen, M. Dohler, S. Rangan, and M.C. Reed. "Femtocells: Past, Present, and Future". *Selected Areas in Communications, IEEE Journal on*, 30(3):497–508, 2012.

[11] Small Cell Forum White Paper. "Interference Management in OFDMA Femtocells". March 2010.

[12] 3GPP TR 25.820. *3G Home NodeB Study Item Technical Report*, 2011.

[13] 3GPP TS 25.467. *UTRAN Architecture for Home NodeB Stage 2*, 2011.

[14] Martin Haenggi and Radha Krishna Ganti. "Interference in Large Wireless Networks". *Found. Trends Netw.*, 3(2):127–248, February 2009.

[15] Shalinee Kishore, Larry J. Greenstein, H. Vincent Poor, and Stuart C. Schwartz. "Soft Handoff and Uplink Capacity in a Two-tier CDMA System". *CoRR*, abs/cs/0503041, 2005.

[16] V. Chandrasekhar, J.G. Andrews, Tarik Muharemovict, Zukang Shen, and Alan Gatherer. "Power Control in Two-tier Femtocell Networks". *Wireless Communications, IEEE Transactions on*, 8(8):4316–4328, 2009.

[17] Mehmet Yavuz, Farhad Meshkati, Sanjiv Nanda, Akhilesh Pokhariyal, Nick Johnson, Balaji Raghothaman, and Andy Richardson. "Interference Management and Performance Analysis of UMTS/HSPA+ Femtocells". *Comm. Mag.*, 47(9):102–109, September 2009.

[18] David López-Pérez, Alvaro Valcarce, Guillaume De La Roche, and Jie Zhang. "OFDMA Femtocells: a Roadmap on Interference Avoidance". *Comm. Mag.*, 47(9):41–48, September 2009.

[19] Sundeep Rangan and Ritesh Madan. "Belief Propagation Methods for Intercell Interference Coordination". *CoRR*, abs/1008.0060, 2010.

[20] Gábor Fodor, Chrysostomos Koutsimanis, András Rácz, Norbert Reider, Arne Simonsson, and Walter Müller. "Intercell Interference Coordination in OFDMA Networks and in the 3GPP Long Term Evolution System". *JCM*, 4(7):445–453, 2009.

[21] Sang Bum Kang, Young Min Seo, Young Ki Lee, M.Z. Chowdhury, Won Sik Ko, M.N. Irlam, Sun Woong Choi, and Yeong Min Jang. "Soft QoS-based CAC Scheme for WCDMA Femtocell Networks". In *Advanced Communication Technology, 2008. ICACT 2008. 10th International Conference on*, volume 1, pages 409–412, 2008.

[22] Karthikeyan Sundaresan and Sampath Rangarajan. "Efficient Resource Management in OFDMA Femtocells". In *Proceedings of the tenth ACM international symposium on Mobile ad hoc networking and computing*, MobiHoc '09, pages 33–42, New York, NY, USA, 2009. ACM.

[23] Thomas David Novlan, Radha Krishna Ganti, Arunabha Ghosh, and Jeffrey G. Andrews. "Analytical Evaluation of Fractional Frequency Reuse for OFDMA Cellular Networks". *CoRR*, abs/1101.5130, 2011.

[24] Gary Boudreau, John Panicker, Ning Guo, Rui Chang, Neng Wang, and Sophie Vrzic. "Interference Coordination and Cancellation for 4G Networks". *Comm. Mag.*, 47(4):74–81, April 2009.

[25] 3GPP TS 25.367. *Mobility Procedures for Home NodeB; Overall Description Stage 2*, 2011.

[26] G. de la Roche, A. Valcarce, D. Lopez-Perez, and Jie Zhang. "Access Control

Mechanisms for Femtocells". *Communications Magazine, IEEE*, 48(1):33–39, 2010.

[27] L. Grokop S. Nagaraja M. Yavuz F. Meshkati, Y. Jiang and S. Nanda. "Mobility and Femtocell Discovery in 3G UMTS Networks". Technical report, Qualcomm White Paper, Feb. 2010.

[28] 3GPP TS 36.300. *Evolved Universal Terrestrial Radio Access (E-UTRA) and Evolved Universal Terrestrial Radio Access Network (E-UTRAN); Overall description; Stage 2*, 2011.

[29] 3GPP TS 36.816. *Evolved Study on Management of Evolved Universal Terrestrial Radio Access Network (E-UTRAN) and Evolved Packet Core (EPC)*, 2011.

[30] 3GPP TS 32.500. *Telecommunication Management; Self-Organizing Networks (SON); Concepts and Requirements*, 2011.

[31] 3GPP TS 36.902. *Self-Configuring and Self-Optimizing Network Use Cases and Solutions*, 2011.

[32] Donglin Hu and Shiwen Mao. "On Medium Grain Scalable Video Streaming over Femtocell Cognitive Radio Networks". *Selected Areas in Communications, IEEE Journal on*, 30(3):641–651, 2012.

[33] R. Urgaonkar and M.J. Neely. "Opportunistic Cooperation in Cognitive Femtocell Networks". *Selected Areas in Communications, IEEE Journal on*, 30(3):607–616, 2012.

[34] Yang-Yang Li, M. Macuha, E.S. Sousa, T. Sato, and M. Nanri. "Cognitive Interference Management in 3G Femtocells". In *Personal, Indoor and Mobile Radio Communications, 2009 IEEE 20th International Symposium on*, pages 1118–1122, 2009.

[35] A. Adhikary, V. Ntranos, and G. Caire. “Cognitive Femtocells: Breaking the Spatial Reuse Barrier of Cellular Systems”. In *Information Theory and Applications Workshop (ITA), 2011*, pages 1–10, 2011.

[36] 3GPP TS 33.320. *3GPP Security Aspect of Home NodeB and Home eNodeB; Release 9*, v0.2.0 edition.

[37] 3GPP2 S.S0132-0. *Femtocell Security Framework*, v1.0 edition, Jan. 2010.

[38] Jing Chen and Marcus Wong. “Security Implications and Considerations for Femtocells”. *Journal of Cyber Security and Mobility*, pages 21–35, 2012.

[39] Ravishankar Borgaonkar, Kevin Redon, and Jean-Pierre Seifert. “Security Analysis of a Femtocell Device”. In *Proceedings of the 4th international conference on Security of information and networks*, SIN ’11, pages 95–102, New York, NY, USA, 2011. ACM.

[40] Ian Poole. *Femtocell Synchronization*. [Online]. Available: http://www.radio-electronics.com/info/cellulartelecomms/femtocells/femto-cells-synchronization-synchronisation.php.

[41] Todd Humphreys Ken Pesyna, Zak Kassas. *Femtocell Synchronization and Localization*. [Online]. Available: http://radionavlab.ae.utexas.edu/opportunistic-navigation/femtocell-synchronization-and-localization.

[42] Javier DeSalas Jimmy LaMance and Jani Jarvinen. “Innovation: Assisted gps: A Low-infrastructure Approach”. *GPS World*, March 2002.

[43] Small Cell Forum White Paper. “Femtocell Synchronization and Location”. May 2012.

[44] K.M. Pesyna, K.D. Wesson, R.W. Heath, and T.E. Humphreys. "Extending the Reach of GPS-assisted Femtocell Synchronization and Localization Through Tightly-Coupled Opportunistic Navigation". In *GLOBECOM Workshops (GC Wkshps), 2011 IEEE*, pages 242–247, 2011.

[45] Dimitri Rubin and Todd Young. *Femtocells Bringing Reliable Location and Timing Indoors*. [Online]. Available: www.insidegnss.com.

[46] Nokia Siemens Networks Corporation. *Timing over Packet Technical Brief*. [Online]. Available: www.nokiasiemensnetworks.com.

[47] Sungwon Lee, SeungGwan Lee, and Choongseon Hong. "An Accuracy Enhanced IEEE 1588 Synchronization Protocol for Dynamically Changing and Asymmetric Wireless Links". *Communications Letters, IEEE*, 16(2):190–192, 2012.

[48] Shuai Lv, Yueming Lu, and Yuefeng Ji. "An Enhanced IEEE 1588 Time Synchronization for Asymmetric Communication Link in Packet Transport Network". *Communications Letters, IEEE*, 14(8):764–766, Aug. 2010.

[49] Wen long Chin and Sau gee Chen. "IEEE 1588 Clock Synchronization Using Dual Slave Clocks in a Slave". *Communications Letters, IEEE*, 13(6):456–458, June 2009.

[50] Saurabh Ganeriwal, Ram Kumar, and Mani B. Srivastava. "Timing-sync Protocol for Sensor Networks". In *Proceedings of the 1st international conference on Embedded networked sensor systems*, SenSys '03, pages 138–149, New York, NY, USA, 2003. ACM.

[51] Jeremy Elson, Lewis Girod, and Deborah Estrin. "Fine-grained Network Time Synchronization Using Reference Broadcasts". In *Proceedings of the 5th sympo-*

sium on Operating systems design and implementation, OSDI '02, pages 147–163, New York, NY, USA, 2002. ACM.

[52] Miklós Maróti, Branislav Kusy, Gyula Simon, and Ákos Lédeczi. "The Flooding Time Synchronization Protocol". In *Proceedings of the 2nd international conference on Embedded networked sensor systems*, SenSys '04, pages 39–49, New York, NY, USA, 2004. ACM.

[53] Kyoung lae Noh, E. Serpedin, and K. Qaraqe. "A New Approach for Time Synchronization in Wireless Sensor Networks: Pairwise Broadcast Synchronization". *Wireless Communications, IEEE Transactions on*, 7(9):3318–3322, 2008.

[54] F. Sivrikaya and B. Yener. "Time Synchronization in Sensor Networks: a Survey". *Network, IEEE*, 18(4):45–50, 2004.

[55] *IEEE 1588 Standard for a Precision Clock Synchronization Protocol for Networked Measurement and Control Systems*. IEEE Standard 1588, 2008.

[56] Sungwon Lee. "An Enhanced IEEE 1588 Time Synchronization Algorithm for Asymmetric Communication Link using Block Burst Transmission". *Communications Letters, IEEE*, 12(9):687–689, Sept. 2008.

[57] H.S. Abdel-Ghaffar. "Analysis of Synchronization Algorithms with Time-out Control over Networks with Exponentially Symmetric Delays". *Communications, IEEE Transactions on*, 50(10):1652–1661, Oct. 2002.

[58] D.R. Jeske. "On Maximum-likelihood Estimation of Clock Offset". *Communications, IEEE Transactions on*, 53(1):53–54, Jan. 2005.

[59] Kyoung-Lae Noh, Q.M. Chaudhari, E. Serpedin, and B.W. Suter. "Novel Clock Phase Offset and Skew Estimation Using Two-Way Timing Message Ex-

changes for Wireless Sensor Networks". *Communications, IEEE Transactions on*, 55(4):766–777, April 2007.

[60] Yik-Chung Wu, Q. Chaudhari, and E. Serpedin. "Clock Synchronization of Wireless Sensor Networks". *Signal Processing Magazine, IEEE*, 28(1):124–138, 2011.

[61] Erchin Serpedin. *Synchronization in Wireless Sensor Networks: Parameter Estimation, Performance Benchmarks and Protocols*. CAMBRIDGE UNIVERSITY PRESS, 2009.

[62] Yu-Hsiang Huang and Sau-hsuan Wu. "Time Synchronization Protocol for Small-Scale Wireless Sensor Networks". In *Wireless Communications and Networking Conference (WCNC), 2010 IEEE*, pages 1–5, 2010.

[63] Lennart Meier, Philipp Blum, and Lothar Thiele. "Internal Synchronization of Drift-constraint Clocks in Ad-Hoc Sensor Networks". In *In Fifth ACM International Symposium on Mobile Ad Hoc Networking and Computing*, pages 90–97, 2004.

[64] Kay Römer. "Time Synchronization in Ad Hoc Networks". In *Proceedings of the 2nd ACM international symposium on Mobile ad hoc networking & computing*, MobiHoc '01, pages 173–182, New York, NY, USA, 2001. ACM.

[65] M. Ouellette, Kuiwen Ji, Song Liu, and Han Li. "Using IEEE 1588 and Boundary Clocks for Clock Synchronization in Telecom Networks". *Communications Magazine, IEEE*, 49(2):164 –171, Feb. 2011.

[66] S. M. Kay. *Fundamentals of Statistical Signal Processing, Vol. I. Estimation Theory*. Englewood Cliffs, NJ: Prentice-Hall, 1993.

[67] Saralees Nadarajah and Samuel Kotz. *On The Linear Combination of Laplace Random Variables*, volume 19. 2005.

[68] *Timing and Synchronization Aspects in Packet Networks*. ITU-T G.8261/Y.1361, 2008.

[69] Liangping Ma, Hua Zhu, G. Nallamothu, Bo Ryu, and Zhensheng Zhang. "Impact of Linear Regression on Time Synchronization Accuracy and Energy Consumption for Wireless Sensor Networks". In *Military Communications Conference, 2008. MILCOM 2008. IEEE*, pages 1–7, 2008.

[70] T.I. Khandoker, Defeng Huang, and V. Sreeram. "A Low Complexity Linear Regression Approach to Time Synchronization in Underwater Networks". In *Information, Communications and Signal Processing (ICICS) 2011 8th International Conference on*, pages 1–5, 2011.

[71] S. Weisberg. *Applied Linear Regression*. Wiley Series in Probability and Statistics. Wiley, 2005.

[72] Ill-Keun Rhee, Jaehan Lee, Jangsub Kim, Erchin Serpedin, and Yik-Chung Wu. "Clock Synchronization in Wireless Sensor Networks: An Overview". *Sensors*, 9(1):56–85, 2009.

[73] M.L. Sichitiu and C. Veerarittiphan. "Simple, Accurate Time Synchronization for Wireless Sensor Networks". In *Wireless Communications and Networking, 2003. WCNC 2003. 2003 IEEE*, volume 2, pages 1266–1273 vol.2, 2003.

[74] Jana van Greunen and Jan Rabaey. "Lightweight Time Synchronization for Sensor Networks". In *Proceedings of the 2nd ACM international conference on Wireless sensor networks and applications*, WSNA '03, pages 11–19, New York, NY, USA, 2003. ACM.

[75] I. Sari, E. Serpedin, and B. Suter. "Application of Gibbs Sampler for Clock Syn-

chronization in RBS-protocol". In *Military Communications Conference, 2006. MILCOM 2006. IEEE*, pages 1–4, 2006.

[76] D. Djenouri. "Estimators for RBS-based Time Synchronization in Heterogeneous Wireless Networks". In *GLOBECOM Workshops (GC Wkshps), 2011 IEEE*, pages 298–302, 2011.

[77] I. Sari, E. Serpedin, Kyoung lae Noh, Q. Chaudhari, and B. Suter. "On the Joint Synchronization of Clock Offset and Skew in RBS-protocol". *Communications, IEEE Transactions on*, 56(5):700–703, 2008.

[78] A. Mutazono, M. Sugano, and M. Murata. "Evaluation of Robustness in Time Synchronization for Sensor Networks". In *Bio-Inspired Models of Network, Information and Computing Systems, 2007. Bionetics 2007. 2nd*, pages 89–92, 2007.

[79] Liang Tao, Junjie Chen, Wentao Ge, and Ting Lin. "Enhancement of the Security of RBS for Wireless Sensor Networks". In *Information Science and Technology (ICIST), 2011 International Conference on*, pages 500–505, 2011.

[80] D. Djenouri. "R4Syn: Relative Referenceless Receiver/Receiver Time Synchronization in Wireless Sensor Networks". *Signal Processing Letters, IEEE*, 19(4):175–178, 2012.

[81] Feng Wang and Jiangchuan Liu. "RBS: A Reliable Broadcast Service for Large-Scale Low Duty-Cycled Wireless Sensor Networks". In *Communications, 2008. ICC '08. IEEE International Conference on*, pages 2416–2420, 2008.

[82] R. Akl and Y. Saravanos. "Hybrid Energy-aware Synchronization Algorithm in Wireless Sensor Networks". In *Personal, Indoor and Mobile Radio Communications, 2007. PIMRC 2007. IEEE 18th International Symposium on*, pages 1–5, 2007.

[83] King-Yip Cheng, King-Shan Lui, Yik-Chung Wu, and V. Tam. “A Distributed Multihop Time Synchronization Protocol for Wireless Sensor Networks Using Pairwise Broadcast Synchronization”. *Wireless Communications, IEEE Transactions on*, 8(4):1764–1772, 2009.

[84] I. Guvenc. “Statistics of Macrocell-synchronous Femtocell-asynchronous Users-delays for Improved Femtocell Uplink Receiver Design”. *Communications Letters, IEEE*, 13(4):239–241, 2009.

[85] N. Patwari, R.J. O’Dea, and Yanwei Wang. “Relative Location in Wireless Networks”. In *Vehicular Technology Conference, 2001. VTC 2001 Spring. IEEE VTS 53rd*, volume 2, pages 1149–1153 vol.2, 2001.

[86] André Günther and Christian Hoene. “Measuring Round Trip Times to Determine the Distance between WLAN Nodes”. *NETWORKING 2005*, pages 768–779, 2005.

[87] Chih-Yu Wen, R.D. Morris, and W.A. Sethares. “Distance Estimation Using Bidirectional Communications without Synchronous Clocking”. *Signal Processing, IEEE Transactions on*, 55(5):1927–1939, 2007.

[88] T. Cooklev, J.C. Eidson, and A. Pakdaman. “An Implementation of IEEE 1588 Over IEEE 802.11b for Synchronization of Wireless Local Area Network Nodes”. *Instrumentation and Measurement, IEEE Transactions on*, 56(5):1632–1639, Oct. 2007.

[89] A. Mahmood and G. Gaderer. “Timestamping for IEEE 1588 based clock synchronization in wireless LAN”. In *Precision Clock Synchronization for Measurement, Control and Communication, 2009. ISPCS 2009. International Symposium on*, pages 1–6, 2009.

[90] D. Wobschall and Yuan Ma. “Synchronization of Wireless Sensor Networks Using a Modified IEEE 1588 Protocol”. In *Precision Clock Synchronization for Measurement Control and Communication (ISPCS), 2010 International IEEE Symposium on*, pages 67–70, 2010.

[91] J. Kannisto, T. Vanhatupa, M. Hannikainen, and T.D. Hamalainen. “Software and Hardware Prototypes of the IEEE 1588 Precision Time Protocol on Wireless LAN”. In *Local and Metropolitan Area Networks, 2005. LANMAN 2005. The 14th IEEE Workshop on*, pages 6 pp.–6, 2005.

[92] L. Cosart. “Precision Packet Delay Measurements Using IEEE 1588v2”. In *Precision Clock Synchronization for Measurement, Control and Communication, 2007. ISPCS 2007. IEEE International Symposium on*, pages 85 –91, Oct. 2007.

[93] H. Abubakari and S. Sastry. “IEEE 1588 Style Synchronization over Wireless Link”. In *Precision Clock Synchronization for Measurement, Control and Communication, 2008. ISPCS 2008. IEEE International Symposium on*, pages 127–130, 2008.

[94] Hyuntae Cho, Jeonsu Jung, Bongrae Cho, Youngwoo Jin, Seung-Woo Lee, and Yunju Baek. “Precision Time Synchronization Using IEEE 1588 for Wireless Sensor Networks”. In *Computational Science and Engineering, 2009. CSE ’09. International Conference on*, volume 2, pages 579–586, 2009.

[95] Li Li, Benliang Li, and Houjun Wang. “Clock Synchronization of Wireless Distributed System Based on IEEE 1588”. In *Cyber-Enabled Distributed Computing and Knowledge Discovery (CyberC), 2010 International Conference on*, pages 205–209, 2010.

[96] A. Mahmood and F. Ring. “Clock Synchronization for IEEE 802.11 Based Wired-

wireless Hybrid Networks Using PTP". In *Precision Clock Synchronization for Measurement Control and Communication (ISPCS), 2012 International IEEE Symposium on*, pages 1–6, 2012.

[97] R. Exel. "Clock Synchronization in IEEE 802.11 Wireless LANs Using Physical Layer Timestamps". In *Precision Clock Synchronization for Measurement Control and Communication (ISPCS), 2012 International IEEE Symposium on*, pages 1–6, 2012.

[98] S. PalChaudhuri, A.K. Saha, and D.B. Johnsin. "Adaptive Clock Synchronization in Sensor Networks". In *Information Processing in Sensor Networks, 2004. IPSN 2004. Third International Symposium on*, pages 340–348, 2004.

[99] Kyoung lae Noh and E. Serpedin. "Adaptive Multi-hop Timings Synchronization for Wireless Sensor Networks". In *Signal Processing and Its Applications, 2007. ISSPA 2007. 9th International Symposium on*, pages 1–6, 2007.

[100] Jang-Sub Kim, Jaehan Lee, E. Serpedin, and K. Qaraqe. "Robust Clock Synchronization in Wireless Sensor Networks Through Noise Density Estimation". *Signal Processing, IEEE Transactions on*, 59(7):3035–3047, 2011.

[101] Jinlin Peng, Pengfei Sun, Li Zhang, K. Kuber, and D. McLernon. "Timing Synchronization for OFDMA Femtocells in the Presence of Co-Channel Interference". In *Wireless Communications and Mobile Computing Conference (IWCMC), 2012 8th International*, pages 1215–1220, 2012.